PHYSICO-CHEMICAL STUDIES OF GLASS FORMING MELTS

ABSTRACT

THESIS SUBMITTED FOR THE DEGREE OF

DOCTOR OF PHILOSOPHY

IN

CHEMISTRY

BY

Ch. Abdul Maroof Khan

DEPARTMENT OF CHEMISTRY
ALIGARH MUSLIM UNIVERSITY
ALIGARH

1979

ABSTRACT

Kinematic viscosities of molten mixtures of nickel(II) chloride in tetra-n-butylammonium iodide have been measured as functions of temperature and concentration. The data of kinematic viscosity have been analysed in terms of the three parameter equations. The heat, the entropy and the free energy of activation for the viscous flow have been computed. At higher concentrations the non-Arrhenius viscous behaviour is predominant and it diminishes with decreasing concentration of nickel(II) chloride. The composition dependence of kinematic viscosity has been described in terms of the free energy of activation. The temperature and the composition dependence data of the kinematic viscosity and the specific conductance for Th_4NBr+$NiCl_2$ melts have been analyzed in the light of the Eyring's expression. The values of the heat of activation, the entropy of activation and the free energy of activation have been calculated. Positive entropy value for both the kinematic viscosity and the specific conductance has been attributed to the rupture of bonds in the associated species during the viscous flow and splitting of the associated species into simpler entities, i.e., ions in the case of conductance. The temperature dependence of kinematic viscosity and the specific conductance has been explained in terms of a modified four parameter non-linear equation. The isothermal composition dependence of the free energy of activation for the kinematic viscosity and the specific

conductance has also been discussed.

The kinematic viscosity and the specific conductance of nickel(II) chloride and tetra-n-butylammonium bromide molten salt system have been measured as functions of temperature and concentration. The temperature dependence of viscosity and conductance have been described by least-squares fitting the data to the three parameter non-linear equations, viz., the VTF and the CEM and the significance of the computed parameters, A_γ, k_γ, and T_o examined. The applicability of the above expressions has been tested for the Arrhenius and the non-Arrhenius regions of a single plot separately. Linear increase in the glass transition temperature, T_o with increase in the $[NiCl_2]$ has been attributed to an increase in the net cohesive forces. This is due to the complex formation which eventually supercools to glassy states. Isothermal concentration dependence of viscosity and specific conductance as well as those of their corresponding energies of activation have been discussed. The energy of activation for kinematic viscosity and specific conductance has been explained in the light of iso-energic concept. On the basis of this concept, the corresponding experimental temperatures were calculated at a selected value of $\theta = (T/T_o)$. Interesting relationships between the glass transition temperature, T_o and the pre-exponential parameter, A_γ and also that of the corrected energies of activation, E_{cor} with the T_o have also

been examined.

Density, viscosity, and electrical conductance measurements for molten mixtures of palladium(II) chloride and tetra-n-butylammonium bromide (TBABr) have been made as a function of temperature. The density data were least-squares fitted to the equation, $\rho = a - bT$, where ρ is the density, a and b are parameters and T is the temperature in Kelvin. The molar volumes, V were computed. The temperature dependence of fluidity and conductance data have been explained on the basis of Doolittle's expression, the free volume model, the configurational entropy model, and the environmental relaxation model. The parameters for the respective models have been computed by least-squares fitting the data of these equations and their significance has been emphasized. The values of V_o, the intrinsic molar volume and that of T_o, the glass transition temperature have been evaluated. The applicability of the above equations in understanding the temperature and the concentration dependence of the transport properties has been examined for the Arrhenius and the non-Arrhenius regions of a single plot. The energies of activation for fluidity and those for conductance have been obtained from the derivatives of the equations based on the above models and also from the tangent values of the Arrhenius plots. The values of energies of activation computed from

these models were found to be comparable. Absorption spectra were recorded in the ultraviolet, visible and the near infra red regions. The charge-transfer and the ligand-field spectra have been examined.

PHYSICO-CHEMICAL STUDIES OF GLASS FORMING MELTS

THESIS SUBMITTED FOR THE DEGREE OF

DOCTOR OF PHILOSOPHY

IN

CHEMISTRY

BY

Ch. Abdul Maroof Khan

DEPARTMENT OF CHEMISTRY
ALIGARH MUSLIM UNIVERSITY
ALIGARH

1979

ALIGARH MUSLIM UNIVERSITY
ALIGARH, U.P., INDIA

Phone : Office : 3345

Department of Chemistry

Date 2.4.79

This is to certify that the thesis entitled "Physico-Chemical Studies of Glass forming Melts" is the original work carried out by Ch. Abdul Maroof Khan under my supervision and is suitable for submission for the award of Ph.D. degree in Chemistry.

(NURUL ISLAM)
Ph.D. (New York)
R E A D E R
Department of Chemistry
Aligarh Muslim University
Aligarh

A C K N O W L E D G E M E N T

I am at a loss to find suitable words to express my deep sense of gratitude to Dr. Nurul Islam, Ph.D. (New York), who, besides being the guide and supervisor, has been a constant source of inspiration to me. I am grateful to Prof. H. Rahman, Head, Department of Chemistry for being kind enough to provide necessary research facilities. I am thankful to University Grants Commission (New Delhi) for extending the financial assistance.

I shall be failing in my duty if I do not thank my friends Dr. M.R. Islam and Dr. Ismail K whose cooperation more than made up for my limited capabilities.

(CH. ABDUL HAROOF KHAN)

CONTENTS

INTRODUCTION

One may or may not agree with Hildebrand's sweeping remark[1,2] which argues against the presence in normal liquids of 'holes', 'lattices', 'cells', 'vacancies', or 'solid like molecules'. He has got the opinion that the flow in liquids takes place through some other impressive and more natural process. But the fact remains that the problem of viscous flow in liquids is still invitingly vague and tantalisingly challenging. Several theories have been propounded but the authenticity of most of them is a suspect and their applicability sadly limited. That is why unabated interest is still being taken and much importance given to the measurements of viscosities and conductances of liquids and liquid mixtures. This problem of understanding the nature and theory of transport behaviour has been attacked by studying both the temperature and pressure dependence of viscosity and conductance. Much information has also been found to be obtainable from the study of composition dependence of viscosity and conductance in liquid mixtures.

The temperature and pressure dependence of viscosity and conductance have led to the proposal of several empirical and theoretical expressions and it will be worthwhile to make a brief survey of them. Unlike gas viscosity, in

which viscous behaviour is due to the transfer of momentum amongst gas molecules on account of collision, viscosity of liquids decreases with increasing temperature. At higher temperatures well above the freezing point of the liquid viscosity and conductance change with temperature according to the equation

$$Y = A_Y \exp\left[\pm E_Y/RT\right] \qquad (1)$$

where Y may be either viscosity or conductance, A is an empirical parameter, E_Y is the energy of activation characteristic of the process and R is the gas constant. This equation has generally been known as the Arrhenius equation. Sometimes, it is also referred to as the Andrade equation[3]. It is apparent from equation (1) that the activation energy is temperature independent in the case of Arrhenius behaviour for the transport properties. Eyring visualised the viscous flow in liquids as due to the change of initial equilibrium position of the molecule into a hole and by applying the absolute reaction rate theory to this process he arrived at an expression

$$Y = (hN/V) \exp\left[\pm \Delta G^*/RT\right] \qquad (2)$$

where h is the Planck's constant, N the Avogadro's number, V the molar volume and ΔG^* is the molar activation free energy for the viscous flow.

On the other hand, study of liquid viscosities as a function of pressure reflected on the dependence of viscosity on a new degree of freedom, namely, the free space or the free volume. Based on this view, Batschinski[5] proposed an equation which may be written in a modified form as

$$Y = \pm\, c/(v - b) \qquad (3)$$

in which v refers to the specific volume of the liquid while b and c are the empirical constants. The parameter, b is found to resemble the van der Waal's volume and (v - b) is a measure of the free volume of the liquid. In recent years, Hildebrand[6] modified this equation to

$$Y = \pm\, B\left[V_o/(V - V_o)\right] \qquad (4)$$

where V is the molar volume, B is a constant and V_o is known as the molar intrinsic volume.

All the above equations have been found to be inadequate to describe the variation in viscosity and conductance of liquids in the low temperature range, i.e., near the freezing points of the liquids. Moreover, equations (3) and (4) were applicable only to unassociated liquids even in the higher temperature region. The supercooling tendency of several liquids had added much flavour to the complexity of such studies in understanding the temperature and the concentration dependence of transport properties. Depending upon

the crystallisation kinetic constants, liquids supercool without the interference of crystallisation and in this supercooled region every liquid deviates from its Arrhenius behaviour for the flow properties like those of viscosity and conductance.

Doolittle[7] proposed for the first time an empirical equation in terms of the free volume to account for the non-Arrhenius behaviour of liquid viscosities and conductances at low temperatures which is of the form

$$Y = A_1 \exp\left[\pm B_1 V_0/V_f\right] \qquad (5)$$

where A_1 and B_1 are the empirical parameters while V_0 is the specific volume of the liquid at 0 K. The free volume, V_f is defined as

$$V_f = V - V_0 \qquad (6)$$

The V_0 was obtained by extrapolating the specific volume of the liquid to 0 K provided there was no phase change. If Doolittle's concept of V_0 is correct, the free volume can also be written as

$$V_f = V - V_0 = \alpha V_0(T - 0) = \alpha V_0 T \qquad (6a)$$

Substituting the value of the free volume from eq (6a) into eq (5), we obtain

$$Y = A_1 \exp\left[\pm B_1/\alpha T\right] \qquad (7)$$

In case there is no phase change down to 0 K, α may be assumed to vary insignificantly with temperature and it can be averaged over the temperature range of study. Equation (7) may therefore, turn out to be similar to that of the Arrhenius equation (1) and, consequently, the Doolittle's concept of V_o appears to lead to the Arrhenius type of behaviour for the viscous flow over the entire temperature range of study. The fact that equation (5) describes the non-Arrhenius viscous behaviour of liquids at low temperatures emphatically stresses that the concept of V_o suggested by Doolittle is not correct. Nevertheless, the applicability of Doolittle's expression in understanding the transport behaviour in many cases[8] is unquestionable. It may, therefore, be expressed in a slightly modified form

$$Y\ (= \phi \text{ or } \Lambda) = A_{1\phi,\Lambda} \exp\left[-B_{1\phi,\Lambda}/(V - V_o)\right] \quad (8)$$

in which A_1 and B_1 are empirical parameters, V is the molar volume at any temperature, and V_o is the intrinsic volume or the molar volume at T_o.

The discrepancy mentioned above regarding the Doolittle's view on the V_o was apparently removed by considering a phase transition in supercooled liquids above 0 K. Such a transition was termed as the glass transition and in turn the corresponding temperature was identified as the glass transition temperature. The glass transition has not

been found to be a thermodynamic phenomenon. It rather appears to be a measure of the relaxation process taking place over a temperature range instead of taking place at a particular temperature. The so-called glass transition temperature, T_g has also been found to change with the rate of cooling. The occurrence of glass transition is necessary to avert the entropy catastrophe as suggested by Kauzmann[9]. Based on this view of glass transition and considering V_o as the specific volume at T_g, Cohen and Turnbull[10] provided a theoretical basis for Doolittle's empirical equation and is known as the Free Volume Theory. Such a free volume model equation is of the form

$$Y = A_Y T^{1/2} \exp\left[\pm k_Y/(T - T_o)\right] \qquad (9)$$

A_Y and k_Y are the empirical parameters and T_o is the ideal glass transition temperature. T_o is found to be lower than the experimental glass transition temperature, T_g by about 10 K. The contribution of the preexponential temperature term to the temperature dependence of viscosity and conductance has been found to be negligible in most cases and the exponential part predominantly accounts for the non-Arrhenius viscous behaviour. Therefore, sometimes in literature equation (8) has also been employed without the pre-exponential temperature term. Equation(8) was a well established empirical equation long before the publication of the free volume model as it was applied successfully to describe the non-

Arrhenius behaviour of viscosity and conductance by several authors. This equation is also known as the Vogel-Tammann-Fulcher (VTF) equation.

Adam and Gibbs[11] proposed a similar equation as that of (8) to explain the non-Arrhenius behaviour of transport processes in polymers by presuming that the transport behaviour was due to cooperative transition or relaxation between monomer segments (configurational) of the polymer. They suggested that the configurational entropy of the system tends to become zero at T_0 instead of the free volume. They obtained an expression for the average transition probability, $W(T)$ of the form

$$W(T) = \bar{A} \exp\left(\pm \Delta \mu s_c^*/kTS_c\right)$$

where $\bar{A}$ is a frequency factor, $\Delta\mu$ is the free energy barrier per mol of particles hindering the cooperative rearrangement, s_c^* is the critical configurational entropy which a region of the liquid must possess in order to undergo cooperative rearrangement, k is the Boltzman constant and S_c is the configurational entropy of the macroscopic super system.

The development of the above equation by approximating

$$S_c \cong \Delta C_p \ln T/T_0$$

where ΔC_p is the change in the heat capacity at the glass transition, leads to an expression based on configurational

entropy model (CEM) which, near T_0, is equivalent to the well known VTF equation for the temperature dependence of relaxation processes in glass forming liquids[12]. The expression becomes

$$\bar{W}(T) = \bar{A} \exp \pm \left[\Delta\mu s_c^*/kT \Delta C_p \ln T/T_0\right]$$

which may be written in the modified form as

$$\bar{W}(T) = \bar{A} \exp \left[\pm k/T \ln T/T_0\right] \qquad (10)$$

where $k = N\Delta\mu s_c^*/R\Delta C_p$

Recently, it has been observed that in very low temperature range near T_g, the viscosity and conductance of liquids return to their Arrhenius behaviour[13]. Ultrasonic spectroscopic measurements[14] have revealed that a distribution of activation energies takes place in supercooled liquids and this led to the conclusion thtat the non-Arrhenius behaviour was due to the broadening of the distribution of activation energies at intermediate temperatures. Simmons and Macedo[15] proposed a model to account for the high temperature Arrhenius, intermediate temperature non-Arrhenius, and the low temperature Arrhenius behaviours of viscosity and conductance of liquids and is termed as the environmental relaxation model (ERM). For this purpose the expressions used in the modified form are of the type

$$\ln\eta = \ln(G_{\infty}A)_{\eta} + \left\{\bar{E} + (1/2)C_{o\eta}\left[T_o^4/(T_o^4 + \epsilon_{o\eta}^2(T-T_o)^4)\right]^{3/2}\right\}/RT \qquad (11)$$

and

$$\ln\Lambda = -\ln(G_{\infty}A)_{\Lambda} - \left\{\bar{E}_{\Lambda} + (1/2)C_{o\Lambda}\left[T_o^4/(T_o^4 + \epsilon_{o\Lambda}^2(T-T_o)^4)\right]^{3/2}\right\}/RT \qquad (12)$$

where $\ln(G_{\infty}A)_{\eta,\Lambda}$ is the logarithm of the Gaussian relaxation of transport property, $\bar{E}_{\eta,\Lambda}$ is the average distribution of energy of activation, C_o, T_o, and ϵ_o are empirical parameters (Appendix). However, a wide applicability of this model has not been recognised. The most recent measurements on the highly viscous $Ca(NO_3)_2$-KNO_3 melt[16] are inconsistent with the predictions of the environmental relaxation model.

The concentration dependence of viscosity and conductance is much more complicated to visualise as well as to interpret. Monotonous variation with concentration has not been revealed in a fairly large number of binary solutions in liquids or melts. Several equations have been proposed[17-21] to explain the concentration dependence of transport property in binary aqueous and non-aqueous solutions, but most of such equations have been found to be inadequate at very high concentrations. Theoretical expressions have also been proposed to describe the concentration dependence of transport

properties of binary liquid mixtures[22].

In binary molten mixtures an adequate expression for explaining the variation of viscosity and conductance with concentration of one of the components is still under development. Indirect approaches have been made by substituting the individual concentration-dependences of the empirical parameters into equations for examining the temperature dependence of viscosity[23,24]. Such attempts fail if the empirical parameters show irregular variations with concentration.

It may be visualized from the above brief introduction that the understanding of temperature (as well as pressure) and concentration dependence of viscosity and conductance of liquids as well as melts is inadequate and needs a rather detailed study. The development of a physically meaningful theory for explaining the transport behaviour is a challenging problem in the study of liquid properties to-date. Therefore, such studies are considered to be encouraging.

Present is, therefore, an attempt to investigate the transport behaviour of binary molten mixtures of nickel(II) and palladium(II) chlorides, MCl_2 (M = Ni or Pd) with tetra-n-butylammonium bromide (TBABr) and similarly those of nickel(II) chloride with tetra-n-butylammonium iodide (TBAI).

Anhydrous transition metal halides (MX_2) dissolve in molten tetra-alkylammonium halides, R_4AX (R is either the same or different alkyl group) very slowly and on constant heating upto about 30 mol per cent. The presence of tetrahedral geometry for the complex species, MX_2Y_2 has been established spectroscopically in such binary melts[25,26]. These molten mixtures do not supercool in the dilute region whereas they readily undergo supercooling at higher concentrations (above 20 mol%) In the supercooling region association has been reported to take place in these systems to form clusters of the type $\left[R_4A^+\right]_2\left[MX_2Y_2^{=}\right]$. Such an association in the ratio of 2:1 has accounted for the maximum solubility of metal halides upto $\sim$ 33 mol per cent in tetra-alkylammonium halides. It may, therefore, be interesting to understand the variation in transport-temperature behaviour with increasing tendency of the melts undergoing supercooling.

In the first chapter the Eyring's expression has been employed to explain the temperature dependence of kinematic viscosity of TBAI+$NiCl_2$ molten salt system. It has further been applied to explain the temperature dependence of the kinematic viscosity and the specific conductance of TBABr+ $NiCl_2$ molten salt system as well. An attempt has also been made to study the concentration dependence of kinematic viscosity in the case of the former and kinematic viscosity and specific conductance in the case of the latter.

In the second chapter, the kinematic viscosity and specific conductance of TBABr+$NiCl_2$ molten salt system have been measured as functions of temperature and concentration. The data have been least-squares fitted to the three parameter non-linear equations, the Vogel-Tammann-Fulcher (VTF) and the configurational entropy model (CEM). The concentration dependence of kinematic viscosity and that of the specific conductance has been explained in the light of the isoenergic and isentropic concepts.

Finally, in the last chapter density, viscosity and conductance measurements of TBABr+$PdCl_2$ molten salt system have been made as a function of temperature. The fluidity and the conductance data have been explained in terms of the Doolittle's expression, the Vogel-Tammann-Fulcher (VTF), the configurational entropy model (CEM), and the environmental relaxation model (ERM) equations. Spectral studies have also been made to identify and establish the structure of the complex formed.

EXPERIMENTAL

Chemicals: Tetra-n-butylammonium bromide, - iodide (Fluka, Switzerland) were used as solvents in the molten state. Anhydrous $PdCl_2$ (Johnson Mathey, London) and anhydrous $NiCl_2$ were used as solutes. Anhydrous $NiCl_2$ was prepared from the recrystallised hexahydrate of $NiCl_2$ (BDH) using purified thionyl chloride (Riedel)[27].

Commercial thionyl chloride contains traces of acids and other impurities. It is first fractionated, preferably in an all glass apparatus, from quinoline in order to remove acid impurities. The receiver is protected from moisture by a calcium chloride tube. The distillate is then refractionated as before from boiled linseed oil. The fraction at b.p. 76-78°C is collected and stored in well fitting glass stoppered bottle.

The finely powdered recrystallised nickel chloride hexahydrate is taken in a round bottom flask and freshly distilled thionyl chloride is added at room temperature. Evolution of sulphur dioxide and hydrogen chloride begins at once.

$$NiCl_2.6H_2O + 6\ SOCl_2 \longrightarrow NiCl_2 + 6\ SO_2 + 12\ HCl$$

After the bubbling ceases the flask is equipped with a reflux condenser and the slurry is refluxed for 1 to 2 hours. The condenser is then arranged for distillation and

the excess thionyl chloride is removed in vacuo using a dry nitrogen bleed. The flask containing the product is then transferred to a vacuum desiccator containing potassium hydroxide and stored for at least 12 hours to remove remaining thionyl chloride. The product is then transferred to a suitable container in a dry box.

Temperature Control: Preparation of samples and the measurements were made in a thermostated glycerol bath in order to maintain a uniform temperature. The bath consists of an immersion heater (250 W), stirrer, and check and contact thermometers [TGL 4650 NAV = 0.03 A U_n = 250 V (GDR)]. A relay [Jumo type NT 15.0, 220 V $\simeq$ 15 A (Germany)] was used to control the variations in temperature. The overall temperature stability was within $\pm$ 0.1°.

Preparation of Samples: The desired amount of solvent was allowed to melt in a weighed sample tube in an inert atmosphere. The tube was allowed to cool in a desiccator and weighed again. The second weighing gives the exact weight of the solvent thereby eliminating the weight of trapped air. This melting of the solvents before weighing serves one more purpose. When the solvent is melted and cooled rapidly it becomes compact and its capacity to absorb moisture is minimised. The calculated amount of the solute was mixed with the solvent. All the mixings and transfers were

made in a dry box. A stream of pure and dry nitrogen is passed in the box for two hours before using it. Phosphorus pentaoxide is kept exposed in the box while it is being used. This ensures that the atmosphere inside the dry box is inert and dry.

The sample tube, now containing the known amount of solvent and solute, was hanged in a jacket in the thermostated bath maintained at a temperature slightly above the melting point of the solvent. A continuous stream of pure and dry nitrogen was kept flowing in the jacket while the heating was being done. The heating continued till a clear melt was obtained.

Density measurements: Density measurements were made using a dilatometer of approximately 3.0 ml capacity with graduated stem of 0.01 ml divisions. The marks on the stem of the dilatometer were calibrated by making use of the known densities of pure and dry quinoline at test temperatures. The volume changes in quinoline during calibration were recorded as a function of temperature. The values of calculated volume of quinoline were plotted against the divisions on the stem of the dilatometer. The plots obtained with the help of least-squares fit gave the total volume of the dilatometer as well as the exact volume between the two successive divisions of the graduated stem. A known amount of the

molten salt sample was then transferred to the calibrated dilatometer with a vacuum pump and the densities were determined by recording the volume changes as a function of temperature. The accuracy of these measurements was within ± 0.3%.

Viscosity Measurements: Cannon-Ubbelohde[28] viscometers of viscometer constants 0.0355 and 0.0286 cSt/sec., respectively were used for viscosity measurements. The viscometer consists of three parallel tubes, i.e., receiving, measuring and auxiliary. The receiving tube forms a 'U' with the measuring tube through a bulb. Two fiducial bulbs were sealed to the measuring tube. Fiducial marks on these two bulbs were used for recording the efflux time. The auxiliary tube was sealed to the measuring tube through another bulb. The measuring tube also contains a capillary of appropriate length and diameter.

In order to measure viscosities the viscometer was clamped in a vertical position and filled with sufficient enough liquid so that no air bubble was let in the capillary tube while the fiducial bulb was filled. Anhydrous calcium chloride tube was attached to the open ends of the viscometer to avoid absorption of moisture. The viscometer containing the sample was allowed to stand in the thermostated bath at the desired temperature for about 30 minutes before

recording the data so that the thermal fluctuation in the viscometer was minimised. The sample was sucked into the fiducial bulb with a vacuum pump and allowed to stand there for about 5 minutes by closing the calcium chloride tubes with rubber corks. The rubber corks were then removed from the tubes and the time of fall of the melt from the upper fiducial mark to the lower one was noted three or four times and the mean of these measurements recorded. The accuracy of measurements, in this case, was within ± 0.1%. The density as well as viscosity measurements were made in a descending order of temperature.

Poiseuille's equation has been employed in computing viscosities from density and time of fall data. According to this equation viscosity, η is given as

$$\eta = \pi h \rho g r^4 t / 8 lV$$

where h is the height of the liquid column in the viscometer, ρ is the density, g is the acceleration due to gravity, r is the radius of the capillary of the viscometer, l is its length and t is the time taken for the liquid of volume V to fall through the capillary. The above expression may be written as

$$\eta = \rho \beta t$$

where $\beta = \pi h g r^4 / 8 lV$, a constant characteristic of the

viscometer and is known as viscometer constant. The unit of η is $Kgm^{-1}s^{-1}$ or poise. The kinematic viscosity is defined as

$$\nu = \eta/\rho = \beta t$$

Conductance Measurements: The conductance measurements were made using Toshniwal [Type CL 01.02A (sensitivity ± 0.2%)] conductance bridge and a standard dip type cell. The cell was constructed by sealing two platinum foils each having an area of $\sim 0.0025\ m^2$ to one end of a corning glass tube. Two platinum wires were further sealed to these two platinum foils which serve the purpose of making electrical contacts. The cell constant of the conductivity cell, determined with a decinormal KCl solution, was $0.006133\ m^{-1}$.

A corning tube containing the melt was suspended in a thermostated bath. The cell was dipped into the melt and electrical connection was made between the conductivity bridge and the cell with the help of copper wires. Care was taken to remove any air bubble sticking to the surface of the platinum electrodes. Utmost precaution was taken to avoid absorption of moisture by the sample during the conductance measurements. These measurements were made in a descending order of temperature.

Spectral Measurements: The melts were used in the form of thin films for recording the ultraviolet and the visible near infra-red spectra on Beckman DK-2A spectrophotometer, using quartz optical cell.

CHAPTER I

APPLICATION OF EYRING'S EQUATION TO THE TRANSPORT BEHAVIOUR OF TBAI + $BiCl_2$ AND TBABr + $BiCl_2$ MOLTEN SALT SYSTEMS

PART - A

Results and Discussion

The kinematic viscosities of TBAI + $NiCl_2$ molten mixtures obtained from the product of viscometer constant and the times of fall are listed in Table I as functions of temperature and concentration. The plots of logarithms of kinematic viscosities versus inverse temperature (Figure 1) have been found to be almost linear. At the higher two concentrations, i.e., 23.99 and 30.12 mol%, however, slight deviation from linearity particularly at lower temperatures have been observed. Similar plots have also been obtained with respect to absolute viscosities. The linearity of the Arrhenius plots in the case of mixtures of lower concentrations (4.62, 9.83, 14.17 and 19.31 mol%) may be visualized as due to two factors, namely, (1) higher temperature range of data measurement and (2) less association of the type $\left\{\left[C_4H_9N^+\right]_2\left[NiCl_2\,I_2^{=}\right]\right\}_x$ to form cluster like structure of the molten system. The latter factor may also be considered as the cause for solidification of the molten mixtures of lower concentrations encountered on cooling whereas the occurrence of such association let the mixtures of higher two concentrations supercool as well as deviate from Arrhenius behaviour.

Presuming that the temperature dependence of viscosity is Arrhenius in all the molten mixtures (within the experimental temperature range), an attempt has been made to

TABLE I. Kinematic Viscosities, $10^2\nu$ (m^2s^{-1}) of TBAI+$NiCl_2$ Molten Salt System

	Mol% of Ni^{2+}					
T K	4.62	9.83	14.17	19.31	23.99	30.12
418.0	0.144	0.164	0.175	0.159	0.154	0.180
413.0	0.167	0.213	0.215	0.201	0.178	0.211
408.0	0.210	0.239	0.253	0.227	0.217	0.256
403.0	0.228	0.266	0.275	0.273	0.228	0.273
398.0	0.269	0.285	0.304	0.283	0.265	0.319
393.0	0.302	0.344	0.359	0.344	0.321	0.378
388.0	0.355	0.412	0.445	0.412	0.403	0.450

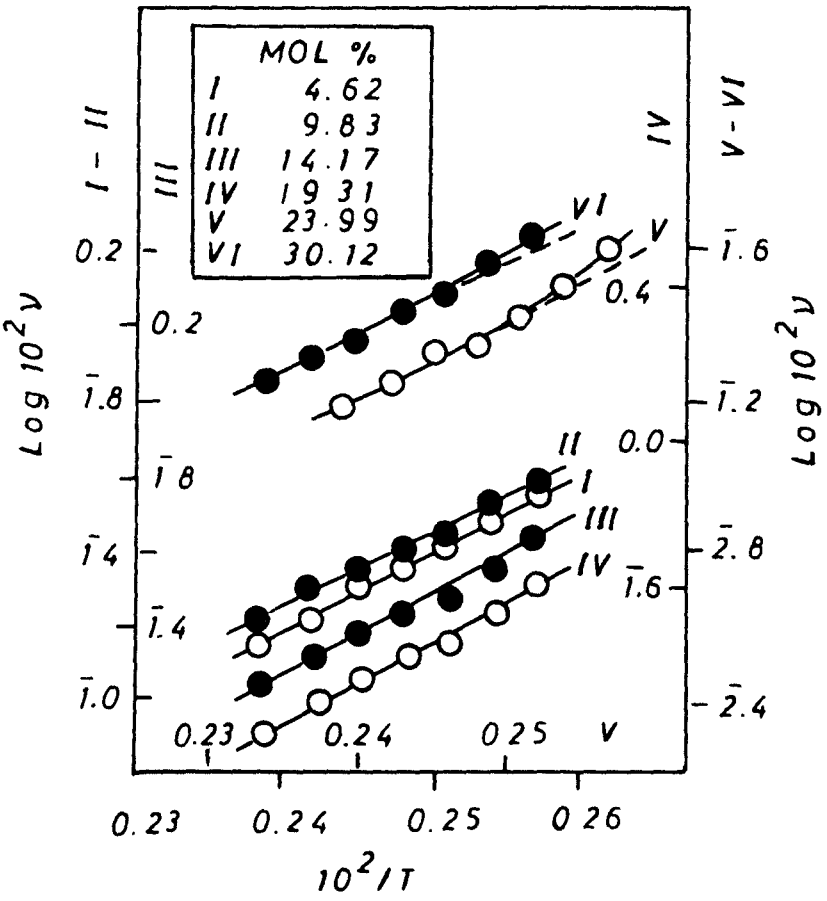

FIG. 1 ARRHENIUS PLOTS FOR THE KINEMATIC VISCOSITIES OF TBAI + $NiCl_2$ MOLTEN SALT SYSTEM

describe the viscosity data through the Eyring's expression[4]. Recently, Eyring's expression has been preferred over that of Andrade[3] equation owing to the fact that the activation free energy term in the exponential part enabled to interpret the concentration dependence of viscosity in liquid mixtures[29]. However, in the present case in order to account for the kinematic viscosity the Eyring's equation has been modified to

$$\nu = (hN/\bar{M}) \exp\left[\Delta G^*/RT\right] = A' \exp\left[\Delta H^*/RT\right] \qquad (13)$$

where $A' = (hN/\bar{M}) \exp\left[-\Delta S^*/R\right]$ and ΔS^* is the entropy of activation. $\bar{M}$ is the mean molecular weight of the molten mixture and ΔH^* is the heat of activation. The data of kinematic viscosity have accordingly been least-squares fitted to equation (13) and the computed values of the parameters A' and ΔH^* are presented in Table II. From the values of A' the entropies of activation were computed using the expression

$$\Delta S^* = R\left[\ln (hN/\bar{M}) - \ln A'\right] \qquad (14)$$

The values of ΔS^* so obtained are also included in Table II.

It is apparent from Table II that the values of ΔS^* are positive unlike the case with conductance flow where negative values have usually been reported[30,31]. Positive values of ΔS^* during the viscous flow were also reported[32]

TABLE II. Computed Parameters of Equation (13)

Mol% of Ni^{2+}	ln A'	ΔH^*/4.184 kJ mol^{-1}	Std dev in ν	ΔS^* (e.u.)
4.62	-13.67	9.7711	0.0062	4.50
9.83	-12.83	9.2176	0.0119	2.90
14.17	-13.13	9.4925	0.0125	3.56
19.31	-13.59	9.8122	0.0111	4.55
23.99	-14.05	10.1139	0.0131	5.53
30.12	-13.71	9.9672	0.0064	4.95

in the case of associated liquids. Such a trend in the values of ΔS^* reflect that the flowing species attain higher entropy after activation. It may, therefore, be visualised that the viscous flow involves simpler flowing entities and breaking up of some bonds appears to take place before the initiation of flow in order to produce these flowing entities from the associated species. In other words, the activation process for viscous flow seems to be facilitated by the increase in entropy.

Although the values of ΔH^* obtained through the least-squares fitting (Table II) appear to be temperature independent, its values derived indirectly using the expression.

$$\Delta H^* = RT \left[\ln \eta - \ln A'\right] \qquad (15)$$

have been found to vary in an irregular fashion with temperature. The least-squares fitted value of ΔH^* appears to be an average of such temperature dependent values. Therefore, in the strict sense, viscosities do not appear to show Arrhenius behaviour and when the variation of ΔH^* with temperature becomes considerably higher, particularly at low temperatures, equation of the type of that of (13) fail to explain the dependence of viscosities on temperature. In fact, in the present systems the temperature dependence of ΔH^* has not been found to be much significant.

An attempt has, however, been made to account for such a slightly non-Arrhenius viscous behaviour by least-squares fitting the kinematic viscosity data to an equation of the form

$$\nu = A''T^{n} \exp\left[B''/(T - T_o)\right] \qquad (16)$$

in which A'', n, B'', and T_o are empirical constants. This equation has been reported[33] to describe the temperature dependence of kinematic viscosities of organic liquids and was derived from the expression based on the significant liquid structure theory by some approximations. Equation (16) may also be considered as the modification of VTF equation with the power n of temperature, T in place of half accounting for the change in the temperature dependence of absolute and kinematic viscosities.

The least-squares fitted values of the parameters of equation (16) are given in Table III along with the standard deviations in ν. It is worthy to make a comparison of the fits of the data to equations (15) and (16) in terms of the standard deviations. Such a comparison reveals that the Arrhenius behaviour is more pronounced in the molten mixture of 4.62 mol%. In the cases of molten mixtures of 9.83, 14.17, and 19.31 mol%, equation (15) and (16) describe the variations in ν with temperature equally well. On the other hand, equation (16) appears to be better than equation (15) in

TABLE III. Computed Parameters of Equation (16)

Mol% of Ni^{2+}	A*	n	B*	T_0(K)	Std dev in ν
4.62	0.2238	-0.7026	649.3	249.2	0.0089
9.83	0.2348	-0.6537	624.5	247.8	0.0113
14.17	0.2292	-0.6597	637.4	248.7	0.0107
19.31	0.2241	-0.6851	650.7	249.5	0.0114
23.99	0.2181	-0.7111	658.9	251.3	0.0096
30.12	0.2195	-0.6782	652.8	250.9	0.0019

reproducing the kinematic viscosity data of mixtures of the last two concentrations, i.e., 23.99 and 30.12 mol%. Especially, in the 30.12 mol% molten mixture the fitting of the data to equation (16) is about three times better than that to equation (13) as is apparent from the significant change in the standard deviations corresponding to the two least-squares fittings. This envisages the non-Arrhenius temperature dependence of ν pertinent to 30.12 mol% and, to a lesser extent, in 23.99 mol% molten mixtures. The linearity of the plots (Figure 2) of $\log(\nu/T^n)$ vs. $1/(T - T_o)$ provides a graphical support to the applicability of equation (16).

From the above analyses it is apparent that even in molten mixtures showing Arrhenius viscosity some non-Arrhenius behaviour is embeded. The presence of such a dual viscous behaviour may be due to the overlapping of the experimental temperature range with the lower and higher temperature limits of Arrhenius and non-Arrhenius behaviour, respectively. Therefore, in the overlapping temperature region the simultaneous analyses of the data by both Arrhenius and non-Arrhenius expressions appear to be necessary to visualise the relative significances of the two behaviours. Moreover, it may be noted that in this temperature range the Arrhenius viscous behaviour diminishes as the concentration of $NiCl_2$ increases and at higher densities the non-Arrhenius

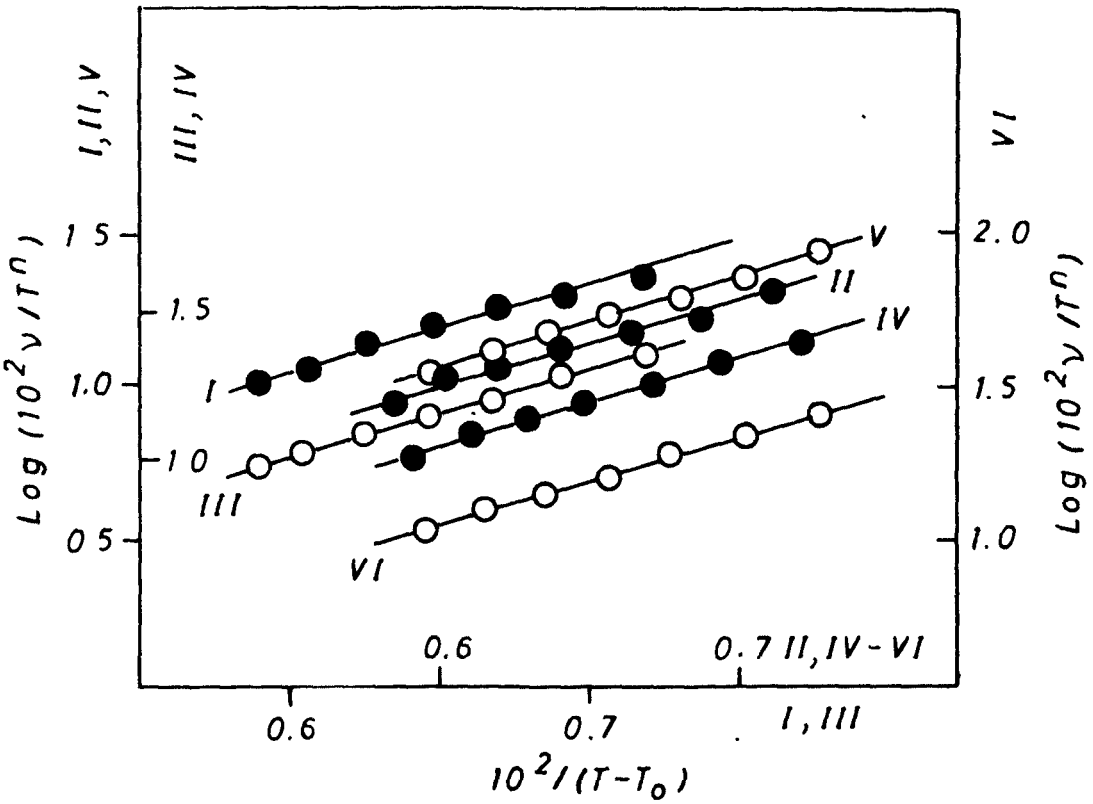

FIG 2 PLOTS OF LOG $(10^2\nu/T^n)$ VS. $1/(T-T_0)$ FOR TBABI + $NiCl_2$ MOLTEN SALT SYSTEM

behaviour becomes predominant. Such an observation has also been reported by Angell[34] in the case of binary melts of $Ca(NO_3)_2$-KNO_3. It has usually been suggested that during the transport phenomena two kinds of activation processes occur, viz., activation for the formation of hole and that for the jump or change of the equilibrium position of the moving particle. In the Arrhenius region enough holes are available and the transport is mainly guided by the activation needed for the jump of the flowing entity while in the non-Arrhenius region the activation for the hole formation dominates. In general, the dearth of some degrees of freedom in the system results into the non-Arrhenius transport behaviour. In the present binary molten mixture, therefore, some degree of freedom, may be the free volume, freezes in as the solute concentration increases.

The values of T_0 given in Table III suggest the ideal behaviour for the glass transition temperatures of the molten mixtures under investigation. These values, however, do not refer to the actual values of the ideal glass transition temperature as they depend upon the curvatures of the Arrhenius plots. In other words, the computed values of T_0 vary with the experimental temperature range of viscosity measurements. Therefore, the values presented in Table III may be considered to be lower than the actual T_0 values.

The nature of concentration dependence of kinematic viscosities of the present systems may be visualised from Figure 3. From 4.62 to 14.17 mol% an increase of $\sim$ 20% in kinematic viscosity has been observed. It decreases by about 12% from 14.17 to 23.99 mol% and then increases by $\sim$15% from 23.99 to 30.12 mol%. Accordingly, the kinematic viscosity isotherms show maxima at 14.17 mol% and minima at 23.99 mol%. It is interesting to note a similar trend in the concentration dependence of activation free energy also. These free energies of activation were computed from the values of enthalpy and entropy of activations using the expression

$$\Delta G^{*} = \Delta H^{*} - T\Delta S^{*} \qquad (17)$$

and are given in Table IV. These activation free energies which appear to increase with decreasing temperature may, however, refer to their approximate values owing to the fact that they are computed by presuming the Arrhenius viscous behaviour in all the molten mixtures. Consequently, the concentration dependence of viscosity seems to be mainly guided by the free energy of activation needed for viscous flow as suggested by Goldsack and Franchetto[29] also. This becomes more apparent through an expression obtainable by substituting equation (13) the linear variation of log ($h\bar{M}/\bar{R}$) with concentration (Figure 4 a) which is of the form

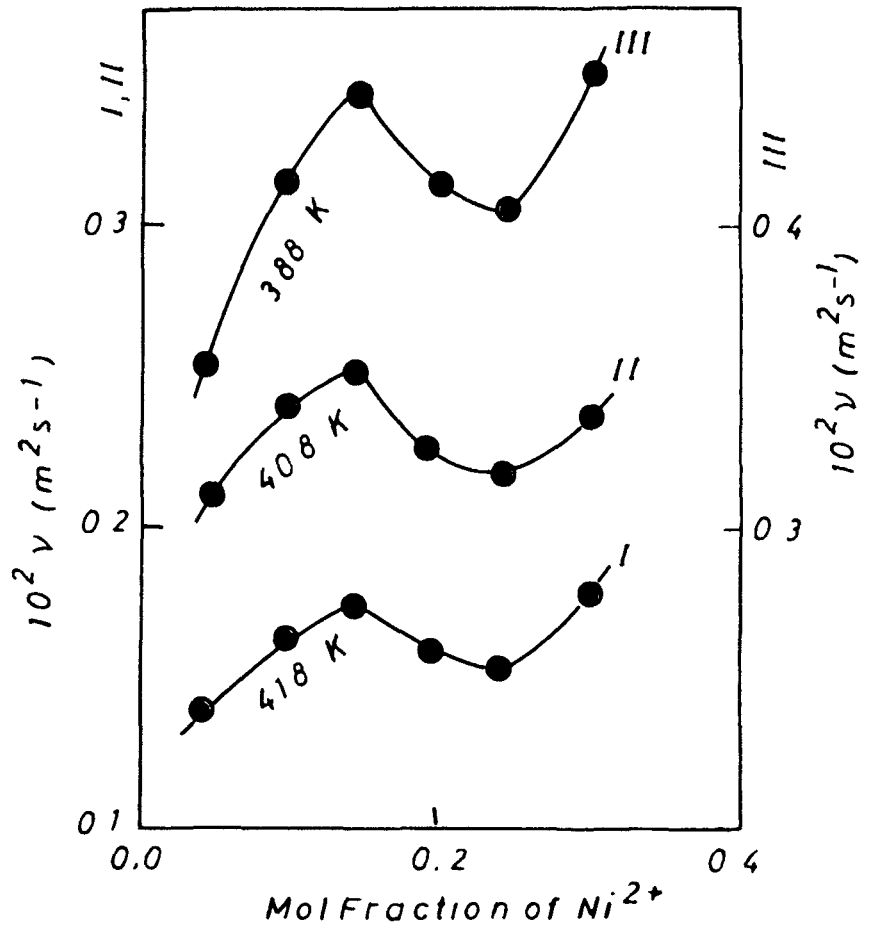

FIG 3 KINEMATIC VISCOSITY VS. COMPOSITION ISOTHERMS FOR TBAI + $NiCl_2$ MOLTEN SALT SYSTEM

TABLE IV. Free Energies of Activation ($\Delta G^{\ddagger}$/4.184 kJ mol^{-1}) for TBAI+$NiCl_2$ Molten Salt System

	Mol% of Ni^{2+}					
T K	4.62	9.83	14.17	19.31	23.99	30.12
418.0	7.9023	8.0038	8.0048	7.9108	7.8008	7.8965
413.0	7.9114	8.0183	8.0225	7.8940	7.8284	7.9212
408.0	7.9339	8.0328	8.0404	7.9564	7.8560	7.9460
403.0	7.9564	8.0474	8.0581	7.9792	7.8836	7.9709
398.0	7.9790	8.0619	8.0760	8.0019	7.9114	7.9955
393.0	8.0015	8.0764	8.0937	8.0247	7.9391	8.0203
388.0	8.0239	8.0909	8.1116	8.0474	7.9667	8.0452

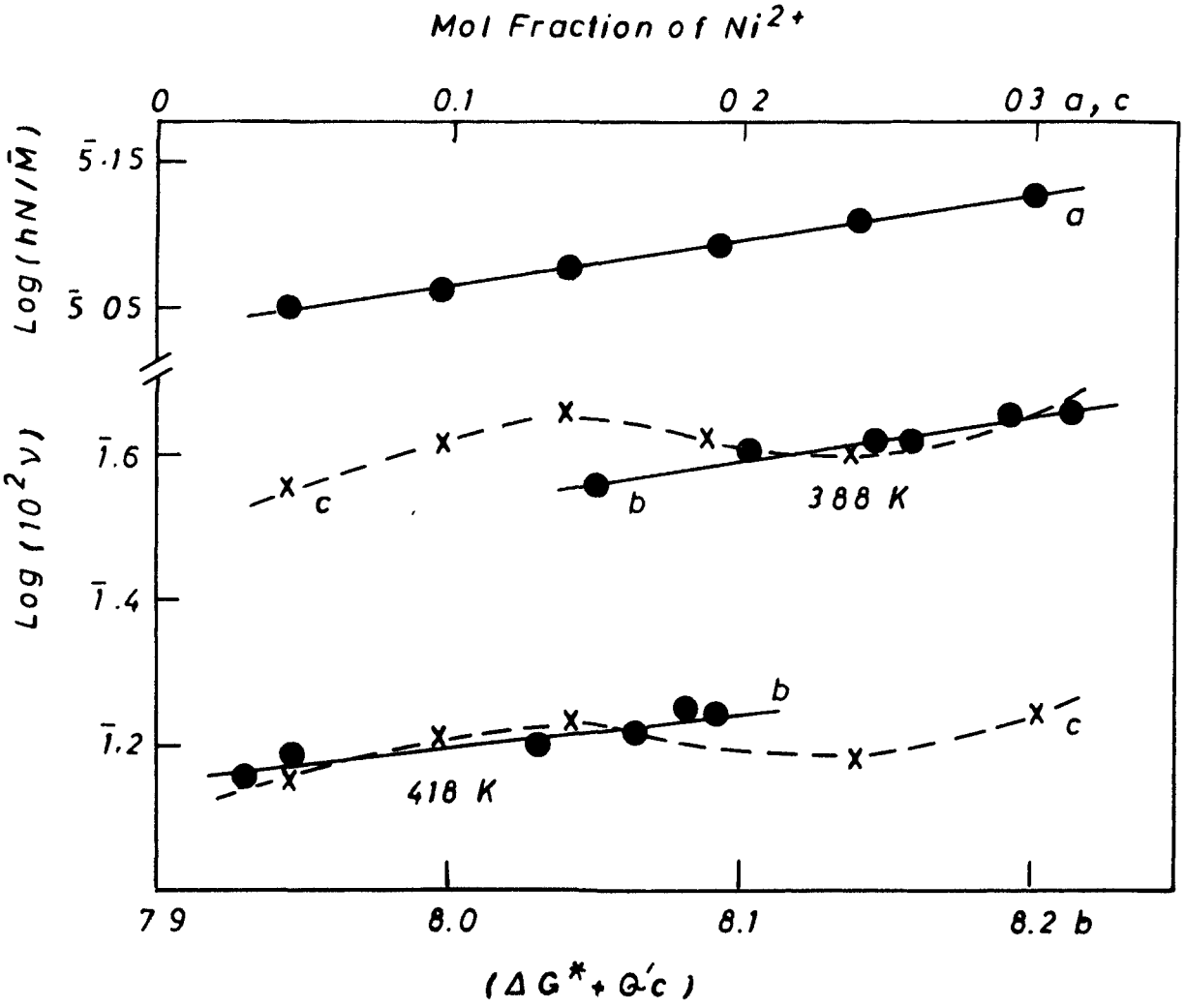

FIG. 4 (a) PLOT OF LOG (hN/M̄) VS. MOL FRACTION OF Ni^{2+}

(b) PLOT OF LOG ν VS. (ΔG* + Q'c)

(c) PLOT OF LOG ν VS. MOL FRACTION OF Ni^{2+}

$$\log \nu = \log A''_o + qc + \Delta G^*/2.303RT \qquad (18)$$

or

$$\log \nu = \log A''_o + (\Delta G^* + q'c)/2.303RT \qquad (19)$$

where q is the slope of the plot of log $(hN/\bar{M})$ versus concentration, c in mol fraction, $q' = 2.303RTq$ and A''_o is the value of $(hN/\bar{M})$ for the pure solvent. The suitability of equation (19) to describe the concentration dependence of kinematic viscosity of the system under study is apparent from the linearity of the log ν versus $(\Delta G^* + q'c)$ isotherms drawn at 418 and 388K (Figure 4b). Similar isotherms may also be obtained at other experimental temperatures. Now, by considering ΔG^* as a concentration independent factor, equation (18) may be expressed as

$$\log \nu = A''' + qc \qquad (20)$$

where $A''' = \log A''_o + \Delta G^*/2.303RT$. However, the plots of log ν versus c are non-linear (Figure 4c) which shows the inadequacy of equation (20) in describing the concentration dependence of kinematic viscosity. This suggests that such a dependence of kinematic viscosity cannot be attributed to the changes in the pre-exponential factor alone. Therefore, although the change in ΔG^* with concentration is smaller, it appears to participate, along with the changes in the pre-exponential factor, in describing the overall dependence of kinematic viscosity on concentration.

PART - B

Results and Discussion

In continuation of the earlier work described in the preceding part the temperature dependence of kinematic viscosity and specific conductance of molten mixtures of TBABr + $NiCl_2$ has been explained in terms of the Eyring's equation[4] which is modified to

$$Y = A' \exp\left[\pm\Delta H^*/RT\right] \qquad (21)$$

where Y may be either kinematic viscosity or specific conductance, $A' = hN/\bar{M} \exp\left[\pm\Delta S^*/R\right]$, ΔS^* is the entropy of activation, $\bar{M}$ is the mean molecular weight of the molten mixture and ΔH^* is the heat of activation. Therefore, the kinematic viscosity and the specific conductance data were least-squares fitted to equation (21) and the computed values of the parameters, A' and ΔH^* are given in Table I. Using the values of A' the entropies of activation, ΔS^* were computed with the help of the expression

$$\Delta S^* = R\left[\ln (hN/\bar{M}) \pm \ln A'\right] \qquad (22)$$

and are also given in Table I.

TABLE I. Computed Parameters of Equation (21)

Mol% of Ni^{2+}	ln A'_{ν}	ΔH° 4.184 kJ mol^{-1}	Std dev in ln ν	ΔS° (e.u.)	ln A'_{k}	ΔH° 4.184 kJ mol^{-1}	Std dev in ln k	ΔS° (e.u.)
2.37	-14.3751	10.2132	0.0034	6.13	4.3048	7.9648	0.006	30.98
5.88	-13.9256	9.9075	0.0063	5.26	4.3902	8.2407	0.004	31.14
8.75	-15.4653	11.1923	0.0073	8.38	3.8838	7.8817	0.008	30.07
16.28	-15.9628	11.9342	0.0202	9.47	5.0576	8.9980	0.008	32.31
21.96	-15.1480	11.3858	0.0042	7.92	4.9427	9.0584	0.011	32.00
25.92	-14.8055	11.2023	0.0055	7.30	5.4021	9.5878	0.009	32.86
28.79	-14.7194	11.4187	0.0087	7.17	5.7294	10.0032	0.009	33.47

The positive values of ΔS^* for conductance seem to be in contradiction with those reported earlier[30,31]. However, positive values of ΔS^* for the viscous flow have been observed in the cases of associated liquids[32] and TBAI + $NiCl_2$ molten salt system[35]. This may be attributed to the viscous flow of simpler species which appear to attain higher entropy of activation on account of the breaking up of some bonds in the associated species before the initiation of the flow. Consequently, the activation process for the viscous flow seems to be facilitated by the increase in entropy. The positive values of ΔS^* in the case of conductance may be ascribed to the splitting up of the associated species into simpler ions.

The computed values of heats of activation, ΔH^* for kinematic viscosities and specific conductances (Table I) are temperature independent. These values of ΔH^* appear to be the averages of the temperature dependent ΔH^* values calculated indirectly through the expression,

$$\pm \Delta H^* = RT\left[\ln\nu - \ln A'\right] \qquad (23)$$

It is evident that the evaluation of such temperature independent ΔH^* values is restricted in the case of non-Arrhenius behaviour at low temperatures. Thus equation (1) cannot be employed to explain the temperature dependence of the transport properties.

Therefore, the kinematic viscosity and the specific conductance data were least-squares fitted to the non-linear equation of the type

$$Y = A''T^{n} \exp\left[\pm B''/(T - T_o)\right] \qquad (24)$$

where A'', n, B'' and T_o are the empirical parameters. Equation (24) is based on the liquid structure theory and has recently been found to explain the temperature dependence of kinematic viscosity of TBAI + $NiCl_2$ molten salt system[35].

The best-fit values of the parameters of equation (24) along with the standard deviations in ln Y are listed in Table II. Comparison of the standard deviation values observed in the case of equation (21) (Table I) with those of equation (24) reveals that equation (21) looks more promising in explaining the transport behaviour. However, the plots of $\ln(\nu/T^{n})$ and $\ln(\kappa/T^{n})$ versus $1/(T-T_o)$ (Figures 1 &2) are linear and support the applicability of equation (24).

It is, therefore, apparent that in the present case of molten TBABr + $NiCl_2$ system both the Arrhenius and the non-Arrhenius behaviours are recognised. For this reason the treatment of data by both the Arrhenius and the non-Arrhenius methods of analysis appears to be worthwhile. Such a data-treatment helps in understanding the relative practicability of the two behaviours.

TABLE II. Computed Parameters of Equation (24)
n = -0.6

Mol% of Ni^{2+}	A''_ν	B''_ν	$T_{o,\nu}$	Std dev in $\ln \nu$	A''_K	B''_K	$T_{o,K}$	Std dev in $\ln K$
2.37	0.1063	690.0	240.0	0.04	4.7755	590.0	240.0	0.03
3.88	0.1096	685.0	243.0	0.02	4.2250	600.0	243.0	0.02
8.75	0.1120	685.0	248.0	0.06	4.0000	578.0	248.0	0.02
16.28	0.1331	700.0	250.0	0.07	3.7841	590.0	250.0	0.03
21.96	0.1521	687.0	252.0	0.03	3.3152	599.0	252.0	0.02
25.92	0.1725	680.0	255.0	0.03	2.7437	590.0	255.0	0.03
28.79	0.1832	685.0	260.0	0.05	2.5717	592.0	260.0	0.02

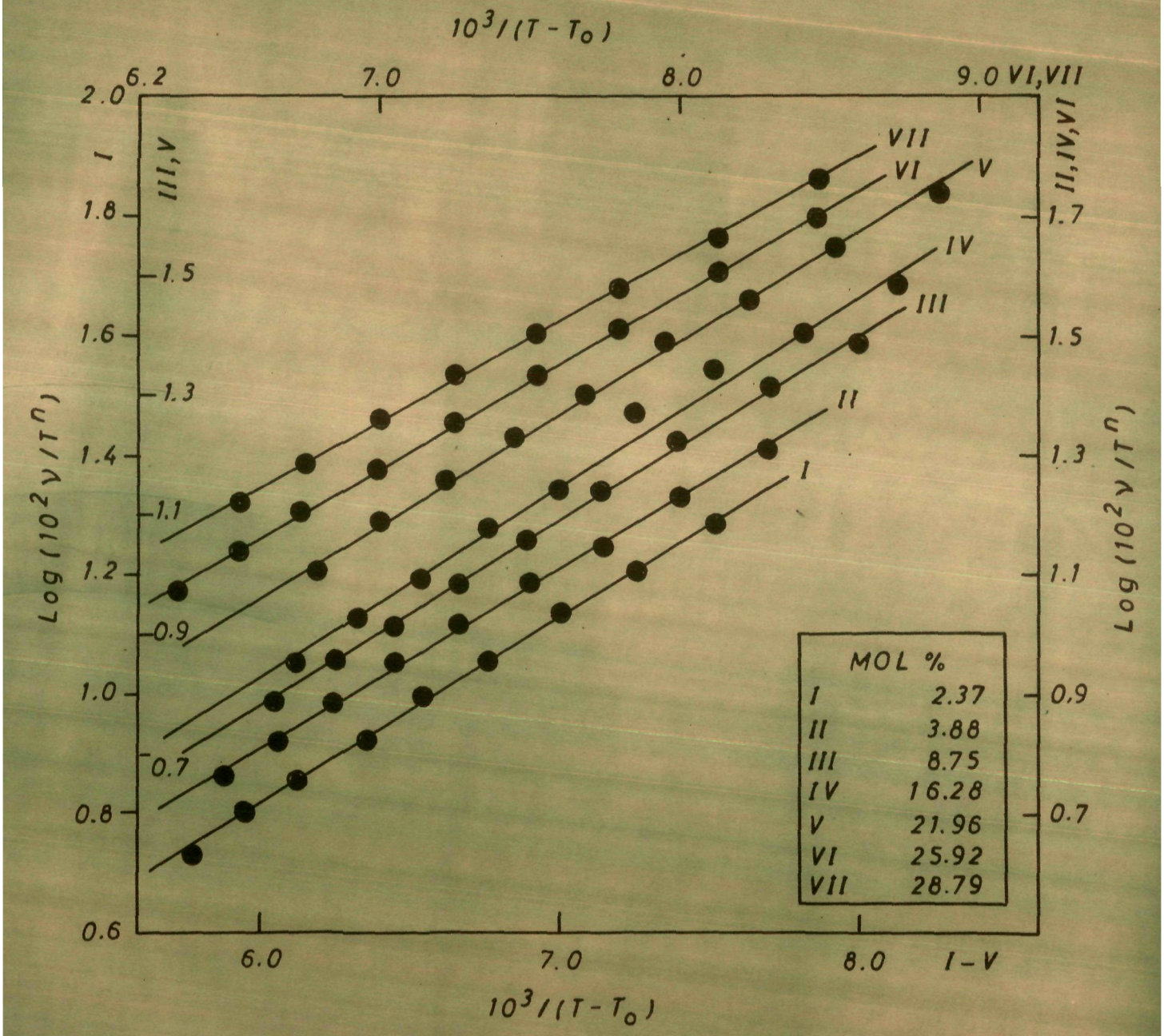

FIG. 1 PLOTS OF LOG ν/T^n VS. $1/(T-T_o)$ FOR TBABr + $NiCl_2$ MOLTEN SALT SYSTEM

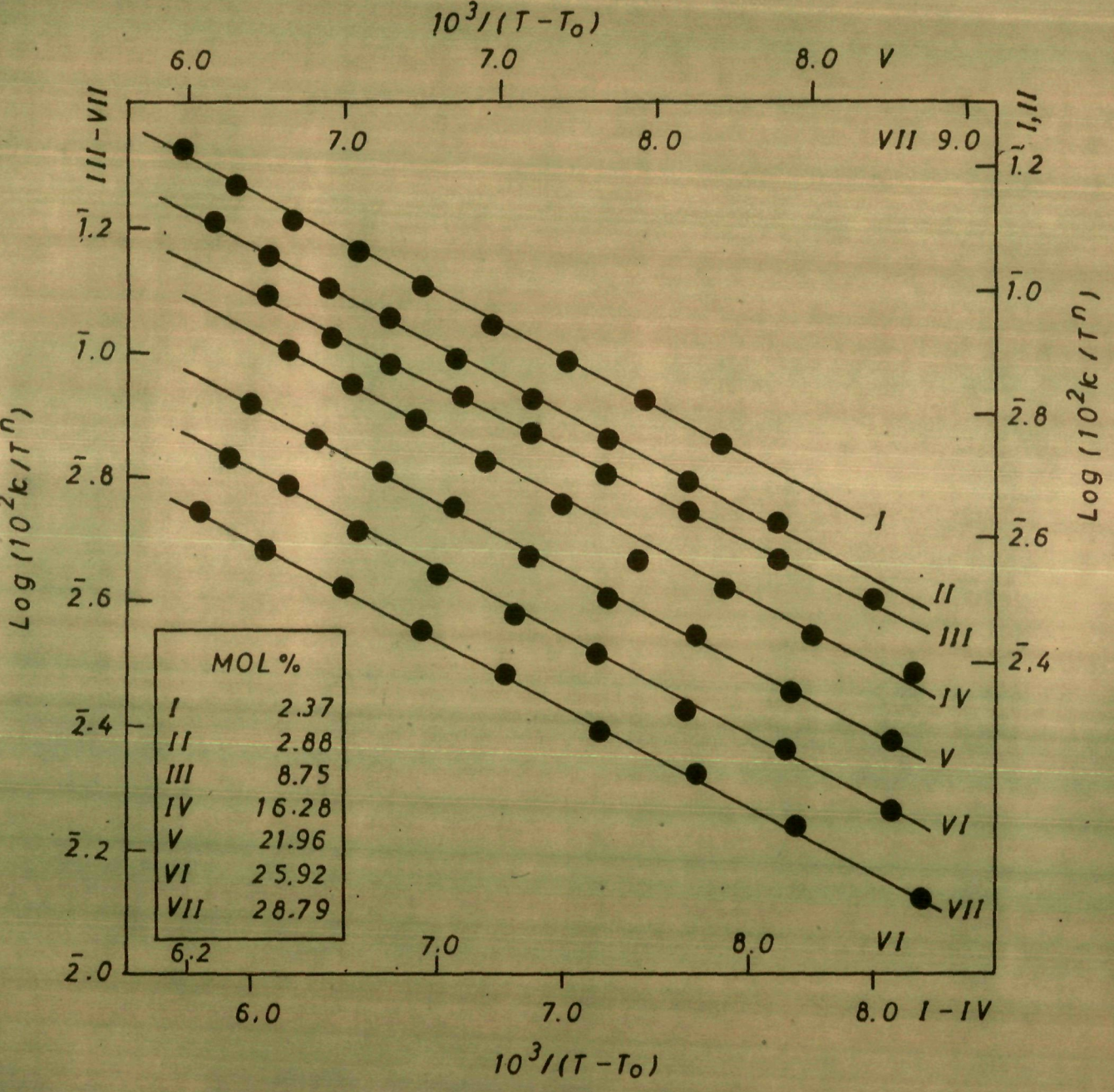

FIG. 2 PLOTS OF LOG k/T^n VS. $1/(T-T_0)$ FOR TBABr + $NiCl_2$ MOLTEN SALT SYSTEM

The concentration dependence of the kinematic viscosity and the specific conductance may be understood in terms of the 'hole' formation theory reported by Angell[23]. Therefore, in dilute mixtures of TBABr + $NiCl_2$ molten salt system the Arrhenius behaviour is prominent owing to the abundant existence of 'holes'. In such a case the transport behaviour is mainly due to the jumping of the flowing particles. In the solute-rich mixtures the transport is, therefore, guided by the activation energy for the 'hole' formation. It has been suggested[35] that the non-Arrhenius behaviour in such concentrated melts is due to the scarcity of some degree of freedom, viz., the free volume.

The values of the glass transition temperature, T_o (Table II) are found to be very close to those computed from the VTF and CKN equations in the following chapter where the significance of it has been discussed.

Further, the concentration dependence of kinematic viscosity and specific conductance may also be explained by the concentration dependent free energies of activation, ΔG^*. The values of ΔG^* were computed from those of the enthalpy and the entropy of activation by using equation (17) and are listed in Table III. It is seen from the table that the free energy of activation for the kinematic viscosity increases with the increase in the $[NiCl_2]$ while for the specific conductance it decreases. According to

TABLE III. Free Energies of Activation ($\Delta G^*/4.184$ kJ mol^{-1}) for TBABr + $NiCl_2$ molten salt system[a]

	Mol% of Ni^{2+}						
T K	2.37	3.88	8.75	16.28	21.96	25.92	28.79
413.0	7.6796 (-20.76)	7.7356 (-21.10)	7.7330 (-20.30)	8.0249 (-22.34)	8.1134 (-22.27)	8.1881 (-23.16)	8.4587 (-23.83)
408.0	7.7102 (-20.61)	7.7619 (-20.95)	7.7749 (-20.15)	8.0722 (-22.18)	8.1531 (-22.11)	8.2246 (-22.99)	8.4945 (-23.66)
403.0	7.7410 (-20.45)	7.7619 (-20.79)	7.8167 (-19.99)	8.1196 (-22.02)	8.1927 (-21.95)	8.2611 (-22.83)	8.5303 (-23.49)
398.0	7.7716 (-20.30)	7.8145 (-20.63)	7.8586 (-19.85)	8.1669 (-21.86)	8.2323 (-21.79)	8.2976 (-22.83)	8.5662 (-23.32)
393.0	7.8025 (-20.14)	7.8408 (-20.48)	7.9005 (-19.70)	8.2142 (-21.70)	8.2720 (-21.63)	8.3348 (-22.50)	8.6020 (-23.17)
388.0	7.8329 (-19.99)	7.8670 (-20.32)	7.9424 (-19.55)	8.2616 (-21.53)	8.3115 (-21.47)	8.3706 (-22.34)	8.6378 (-22.99)

(continued)

TABLE III. (continued)

T K	Mol% of Ni^{2+}						
	2.37	3.88	8.75	16.28	21.96	25.92	28.79
383.0	7.8636 (-19.83)	7.8933 (-20.17)	7.9843 (-19.40)	8.3089 (-21.37)	8.3511 (-21.31)	8.4071 (-22.17)	8.6737 (-22.82)
378.0	7.8943 (-19.52)	7.9196 (-20.01)	8.0261 (-19.25)	8.3562 (-21.21)	8.3908 (-21.15)	8.4436 (-22.01)	8.7095 (-22.66)
373.0	7.9250 (-19.52)	7.9460 (-19.86)	8.0680 (-19.10)	8.4036 (-21.05)	8.4304 (-20.99)	8.4801 (-21.85)	8.7453 (-22.49)

a The free energies obtained from specific conductance data are within parentheses.

Goldsack and Franchetto[29] the linear dependence of log ($\Delta H/\bar{H}$) on concentration (Figure 3a) may be combined with equation (15) to obtain the expression

$$\text{Log}(Y/A_0')/c = q \pm \Delta G^*/2.303\ cRT \qquad (25)$$

The value of q has been found to be negligible as compared to that of the second term on the right side of equation (25). Therefore, this equation is further approximated to the form

$$\text{Log } Y = \log A_Y' \pm \Delta G^*/2.303\ RT \qquad (26)$$

The plots of log $(Y/A_Y')/c$ versus $\Delta G^*/c$, log ν and log K versus ΔG^* are shown in Figures 3b, 3c and 3d, respectively at 393 K. The linearity in such plots shows the applicability of equations (25) and (26). Similar isotherms can also be obtained at other experimental temperatures.

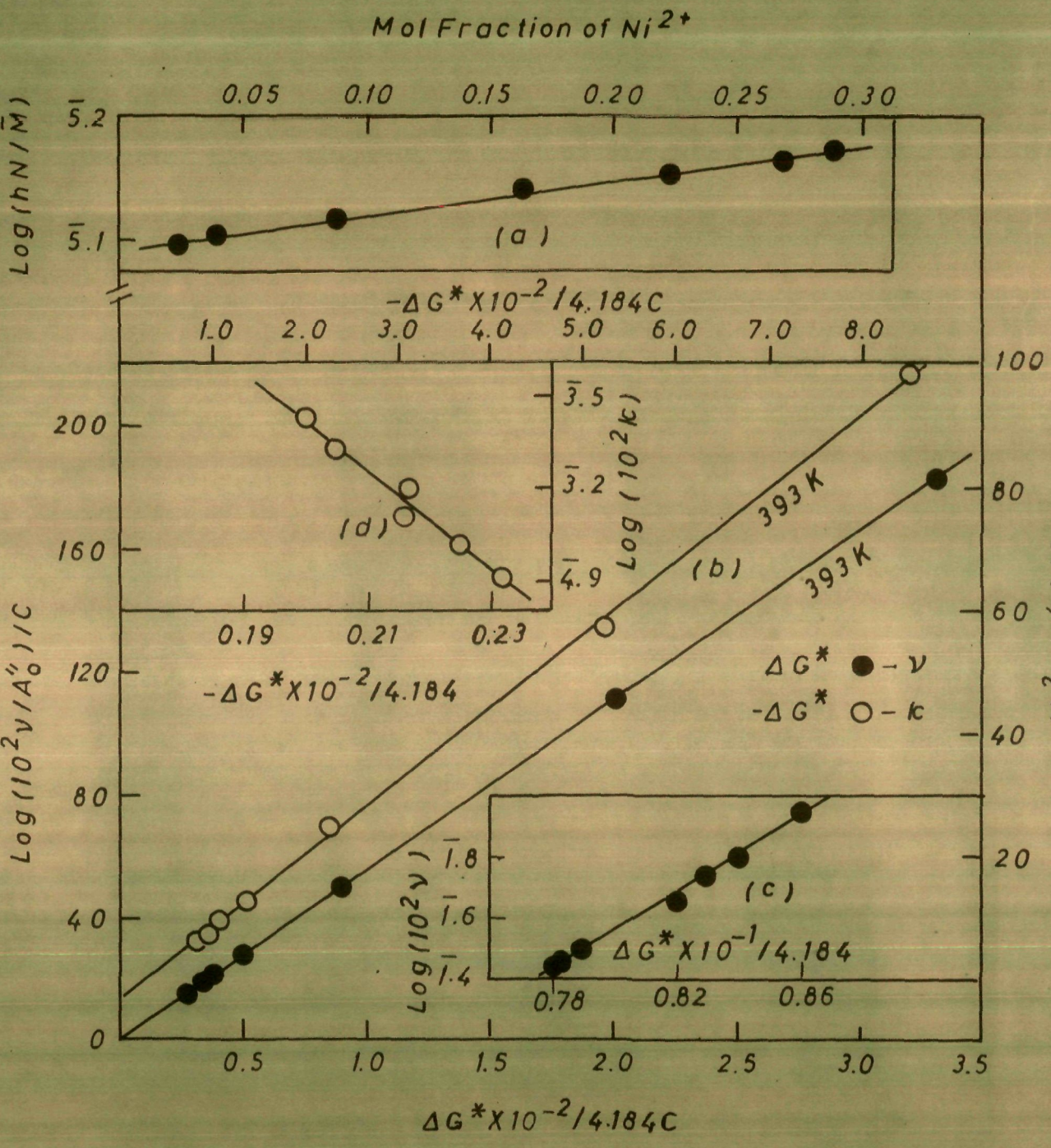

FIG. 3 (a) PLOT OF LOG ($hN/\bar{M}$) VS. MOL FRACTION OF Ni^{2+} (b) PLOTS OF LOG (V/A_0'')/C AND LOG (k/A_0'')/C VS $\Delta G^*/C$; AND (c & d) PLOTS OF LOG V AND LOG k VS. ΔG^* FOR TBABr + $NiCl_2$ MOLTEN SALT SYSTEM

CHAPTER II

KINEMATIC VISCOSITY AND SPECIFIC CONDUCTANCE OF TBABr + $NiCl_2$ MOLTEN SALT SYSTEM

Results and Discussion

The measured kinematic viscosities and specific conductances of molten mixtures of TBABr + $NiCl_2$ as functions of temperature and concentration are given in Table I. It is seen that for a given temperature the kinematic viscosity increases with the solute concentration while the specific conductance decreases. On the other hand, for a given mixture the kinematic viscosity decreases with temperature and the specific conductance increases.

The temperature dependence of kinematic viscosity and specific conductance are non-linear as is apparent from their Arrhenius plots of log ν and log κ versus the reciprocal of temperature (Figure Ia and Ib). It is also evident from these plots that the extent of curvature increases with the increase in $[NiCl_2]$, which, in turn, tends to acquire linearity when the pure ionic melt is reached. For example, in the case of 2.4 mol% $NiCl_2$ + TBABr molten mixture the Arrhenius plots for both the kinematic viscosity and the specific conductance are purely linear. Therefore, the non-linearity observed in the Arrhenius behaviour of the parent solvent, TBABr is apparently due to the addition of the solute, $NiCl_2$. Further, it may be examined that for a given mixture the non-linearity in the curve assumes linearity when the temperature reaches in the vicinity of the melting point of the solvent. One, therefore, expects such

TABLE I. Kinematic Viscosities, $10^2\nu$ ($m^2\ s^{-1}$) and Specific Conductance, $10^2\kappa$ ($S\ m^{-1}$) of TBABr + $NiCl_2$ molten salt system[a]

	Mol% of Ni^{2+}						
T K	2.368	3.875	8.748	16.280	21.959	25.924	28.792
413.0	0.1429 (0.4630)	0.1586 (0.3496)	0.1637 (0.3312)	0.2388 (0.2668)	0.2767 (0.2147)	0.3165 (0.1840)	0.4560 (0.1472)
408.0	0.1698 (0.3956)	0.1798 (0.3067)	0.1951 (0.2810)	0.2907 (0.2423)	0.3342 (0.1993)	0.3758 (0.1625)	0.5312 (0.1288)
403.0	0.1975 (0.3526)	0.2099 (0.2760)	0.2233 (0.2576)	0.3362 (0.2116)	0.3950 (0.1748)	0.4412 (0.1411)	0.6349 (0.1135)
398.0	0.2324 (0.3158)	0.2506 (0.2453)	0.2660 (0.2331)	0.4226 (0.1909)	0.4726 (0.1533)	0.5241 (0.1196)	0.7501 (0.0981)
393.0	0.2762 (0.2699)	0.2890 (0.2116)	0.3173 (0.2054)	0.4779 (0.1564)	0.5661 (0.1288)	0.6271 (0.1042)	0.8832 (0.0828)
388.0	0.3246 (0.2392)	0.3405 (0.1840)	0.3846 (0.1779)	0.6682 (0.1288)	0.6889 (0.1104)	0.7489 (0.0920)	1.0710 (0.0675)

(continued)

TABLE I. (continued)

	Mol% of Ni^{2+}						
T K	2.368	3.875	8.748	16.280	21.959	25.924	28.792
365.0	0.3862 (0.2116)	0.3931 (0.1595)	0.4713 (0.1564)	0.7962 (0.1165)	0.8192 (0.0981)	0.9047 (0.0736)	1.2983 (0.0583)
370.0	0.4549 (0.1871)	0.4768 (0.1380)	0.5887 (0.1319)	0.9247 (0.0981)	0.9963 (0.0797)	1.1053 (0.0644)	1.6425 (0.0491)
373.0	0.5487 (0.1595)	0.5847 (0.1196)	0.6861 (0.1165)	1.0840 (0.0851)	1.2540 (0.0675)	1.3979 (0.0521)	2.0456 (0.0399)

a Specific conductances are within parentheses.

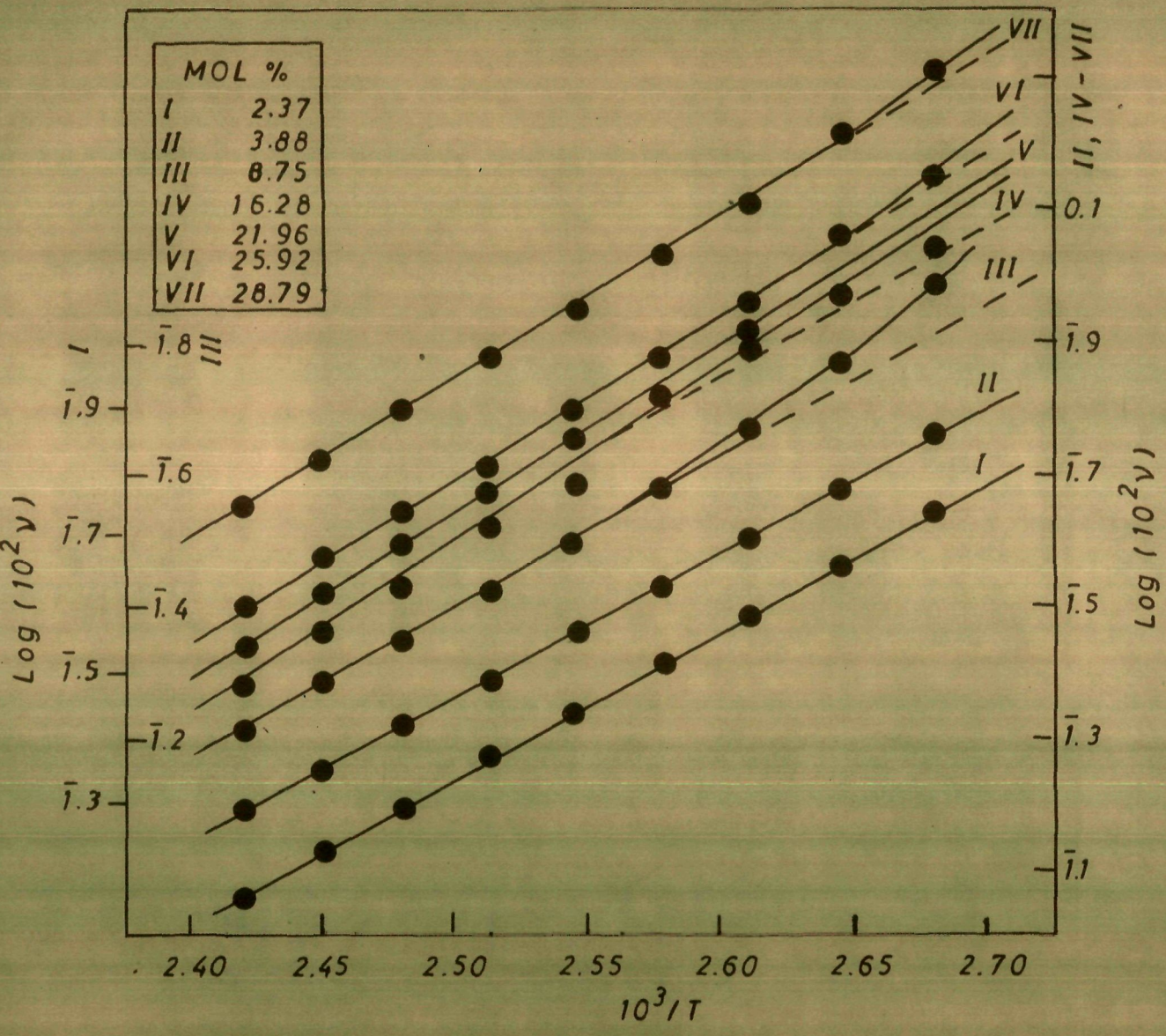

FIG. 1a ARRHENIUS PLOT FOR KINEMATIC VISCOSITY OF TBABr + $NiCl_2$ MOLTEN SALT SYSTEM

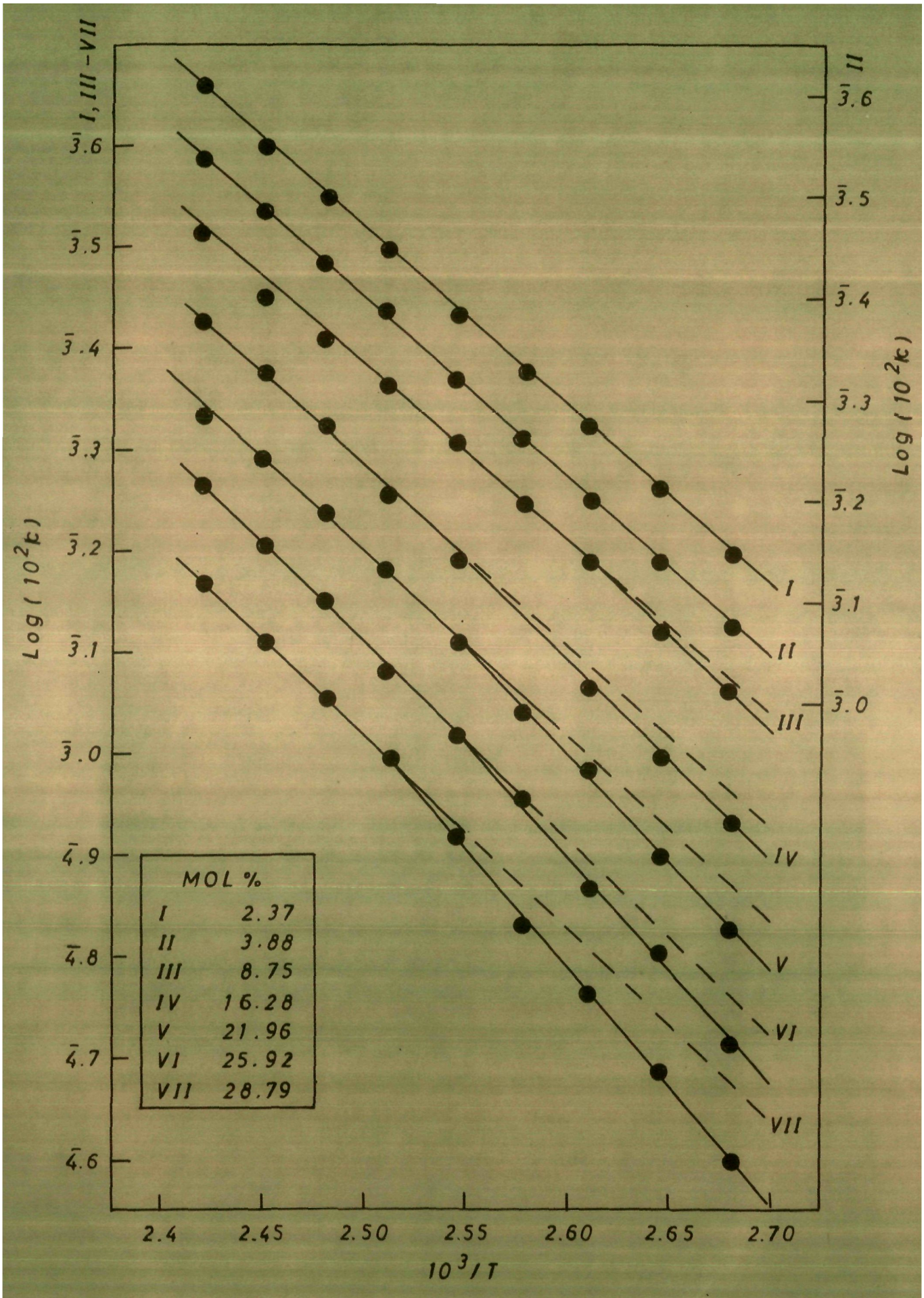

FIG. 1 b ARRHENIUS PLOTS FOR SPECIFIC CONDUCTANCE OF TBABr + $NiCl_2$ MOLTEN SALT SYSTEM

a nature in the case of supercooled region only.

In order to explain the temperature dependence of the kinematic viscosity and the specific conductance data for the molten mixtures of TBABr + $NiCl_2$ (x = 3.9, 8.75, 16.28, 21.96, 25.92 and 28.79 mol% of $NiCl_2$) were least-squares fitted to the three parameter non-linear equations, the Vogel-Tammann-Fulcher (VTF) and the configurational entropy model (CEM). The best-fit values of the parameters, A_Y, A'_Y, k_Y and T_0 along with the standard deviations in ln Y thus computed are listed in Tables IIA and IIIA. Such an analysis was made with a given set of temperature considering all the data points within the temperature range of measurement (373-413 K). The choice of best-fit was made by employing the method adopted by Moynihan et al.[36] Since each Arrhenius plot shows non-linear behaviour particularly at the melting point of the parent solvent, the temperature dependence was explained separately by least-squares fitting the same set of data considering only the non-linear portion (373-398 K) of each of these plots to the same equations in order to examine the applicability of the above models. The respective parameters thus computed through such an analysis are given in Tables IIB and IIIB. It is interesting to note that the values of standard deviation are considerably reduced. The linear plots of $\ln \nu T^{1/2}$ and $\ln \kappa T^{1/2}$ versus $1/(T-T_0)$ (Figures 2a and 2b) and $\ln \nu$ and $\ln \kappa$ versus $1/(T \ln T/T_0)$ (Figures 3a and 3b) show the applica-

TABLE IIA. Parameters of Equation (9)

Temperature Range 373 - 413 K

Mol% of Ni^{2+}	A_ν	k_ν	$T_{o,\nu}$	Std dev in ln ν	A_κ	k_κ	$T_{o,\kappa}$	Std dev in ln κ
3.88	0.05299	709.0	241.0	0.0179	2.3383	609.0	241.0	0.0248
8.75	0.06121	690.0	244.0	0.0530	2.1969	595.0	243.0	0.0198
16.28	0.07582	700.0	249.0	0.0762	1.9766	600.0	248.0	0.0378
21.96	0.08195	690.0	252.0	0.0277	1.8402	600.0	252.0	0.0191
25.92	0.09125	675.0	255.0	0.0209	1.6848	605.0	255.0	0.0210
28.79	0.10703	690.0	258.0	0.0334	1.5470	608.0	259.0	0.0209

TABLE IIIA. Parameters of Equation (11)

Temperature Range 373 - 413 K

Mol% of Ni^{2+}	$\bar{A}_\nu$	k_ν	$T_{o,\nu}$	Std dev in ln ν	$\bar{A}_K$	k_K	$T_{o,K}$	Std dev in ln K
3.88	0.00834	690.0	239.0	0.0695	0.0462	595.0	240.0	0.0422
8.75	0.00731	700.0	245.0	0.0836	0.0465	590.0	243.0	0.0228
16.28	0.00991	695.0	250.0	0.1077	0.0532	617.0	251.0	0.0317
21.96	0.00958	695.0	254.0	0.0458	0.0433	605.0	253.0	0.0191
25.92	0.00947	690.0	258.0	0.0204	0.0341	590.0	255.0	0.0292
28.79	0.01294	690.0	259.0	0.0147	0.0324	590.0	260.0	0.0202

TABLE IIB. Parameters of Equation (9)

Temperature range 373 - 398 K

Mole% of Ni^{2+}	A_ν	k_ν	$T_{o,\nu}$	Std dev in ln ν	A_K	k_K	$T_{o,K}$	Std dev in ln K
3.88	0.0609	703.0	238.0	0.0097	2.1676	600.0	241.0	0.0169
8.75	0.0586	705.0	243.0	0.0336	2.1448	595.0	243.0	0.0136
16.28	0.0786	700.0	249.0	0.0639	1.8692	590.0	249.0	0.0273
21.96	0.0828	690.0	252.0	0.0200	1.8324	600.0	252.0	0.0192
25.92	0.0827	685.0	256.0	0.0315	1.5326	596.0	254.0	0.0200
28.79	0.1117	680.0	258.0	0.0294	1.3497	600.0	257.0	0.0213

TABLE IIIB. Parameters of Equation (11)

Temperature Range 373 - 398 K

Mol% of Bi^{2+}	$\bar{A}_\nu$	k_ν	$T_{o,\nu}$	Std dev in lnν	$\bar{A}_\kappa$	k_κ	$T_{o,\kappa}$	Std dev in lnκ
3.88	0.007428	700.0	242.0	0.0171	0.0451	595.0	240.0	0.0246
8.75	0.007660	700.0	245.0	0.0546	0.0449	585.0	245.0	0.0160
16.28	0.010520	695.0	250.0	0.0706	0.0403	590.0	248.0	0.0269
21.96	0.009893	695.0	254.0	0.0123	0.0370	585.0	252.0	0.0213
25.92	0.010452	699.0	254.0	0.0060	0.0335	590.0	255.0	0.0197
28.79	0.013988	688.0	258.0	0.0070	0.0291	589.0	258.0	0.0222

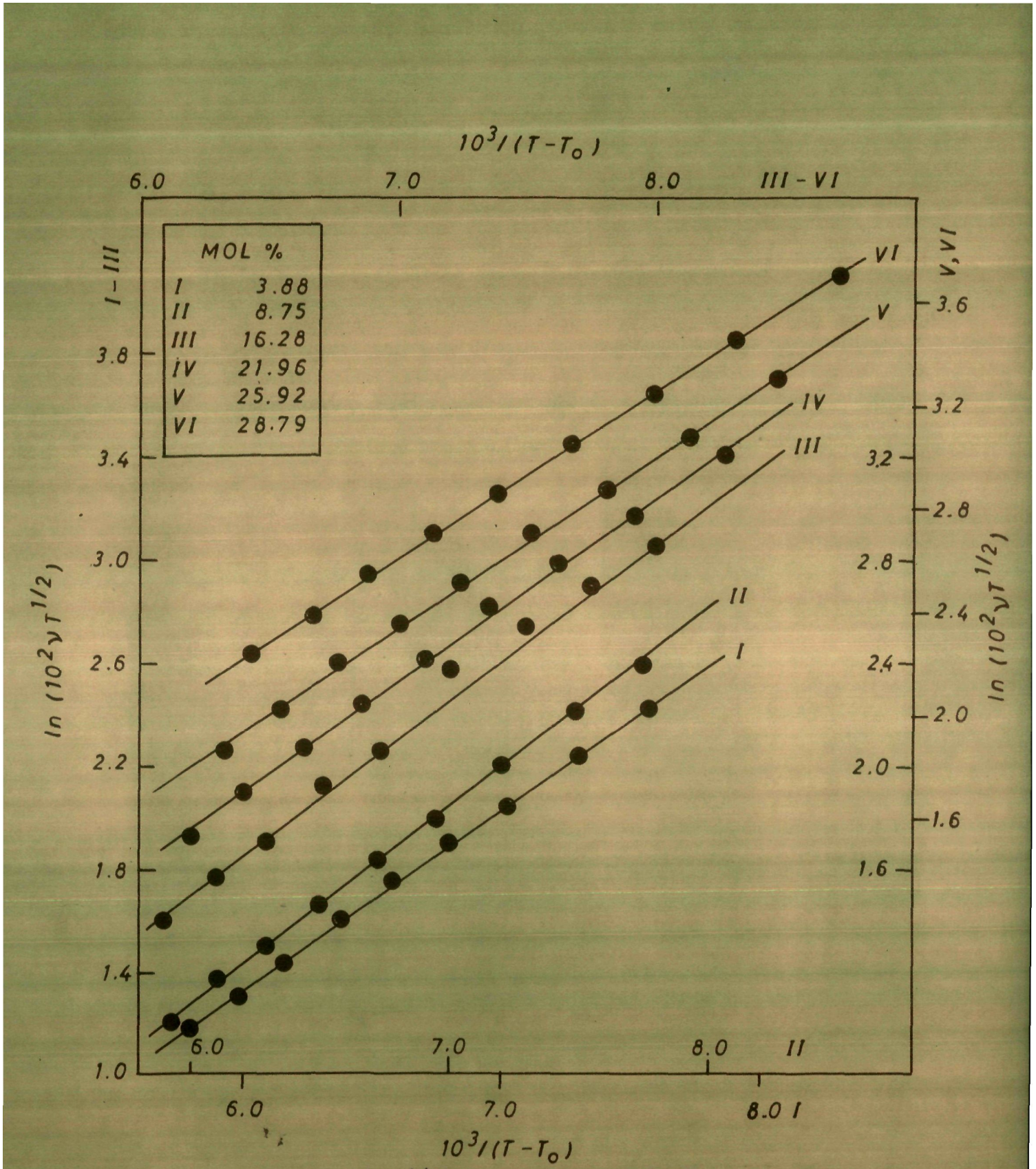

FIG. 2a PLOTS OF $\ln \nu T^{1/2}$ VS. $1/(T-T_0)$ FOR TBABr + $NiCl_2$ MOLTEN SALT SYSTEM

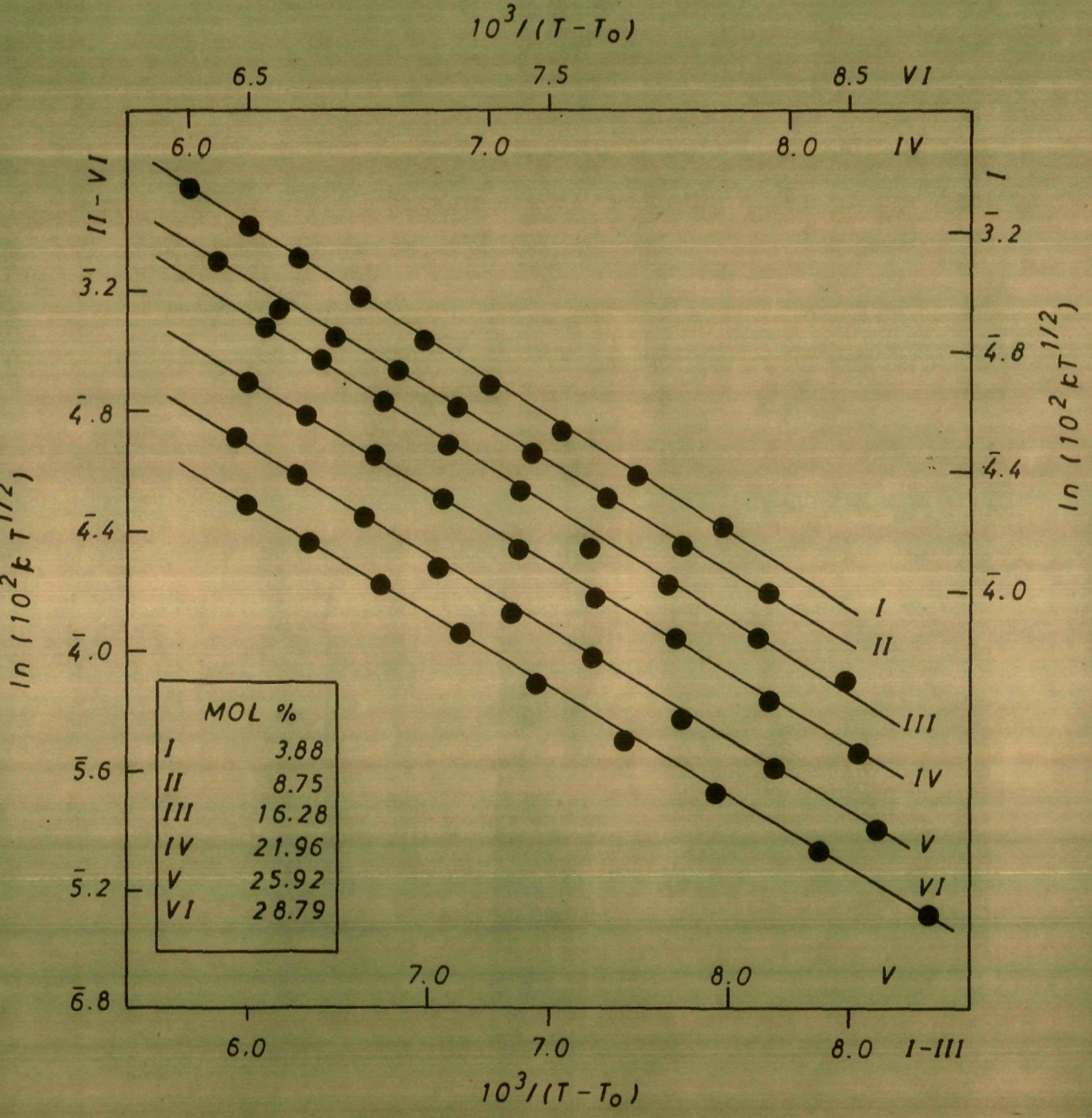

FIG. 2b PLOTS OF $\ln \kappa T^{1/2}$ VS. $1/(T-T_0)$ FOR TBABr + $NiCl_2$ MOLTEN SALT SYSTEM

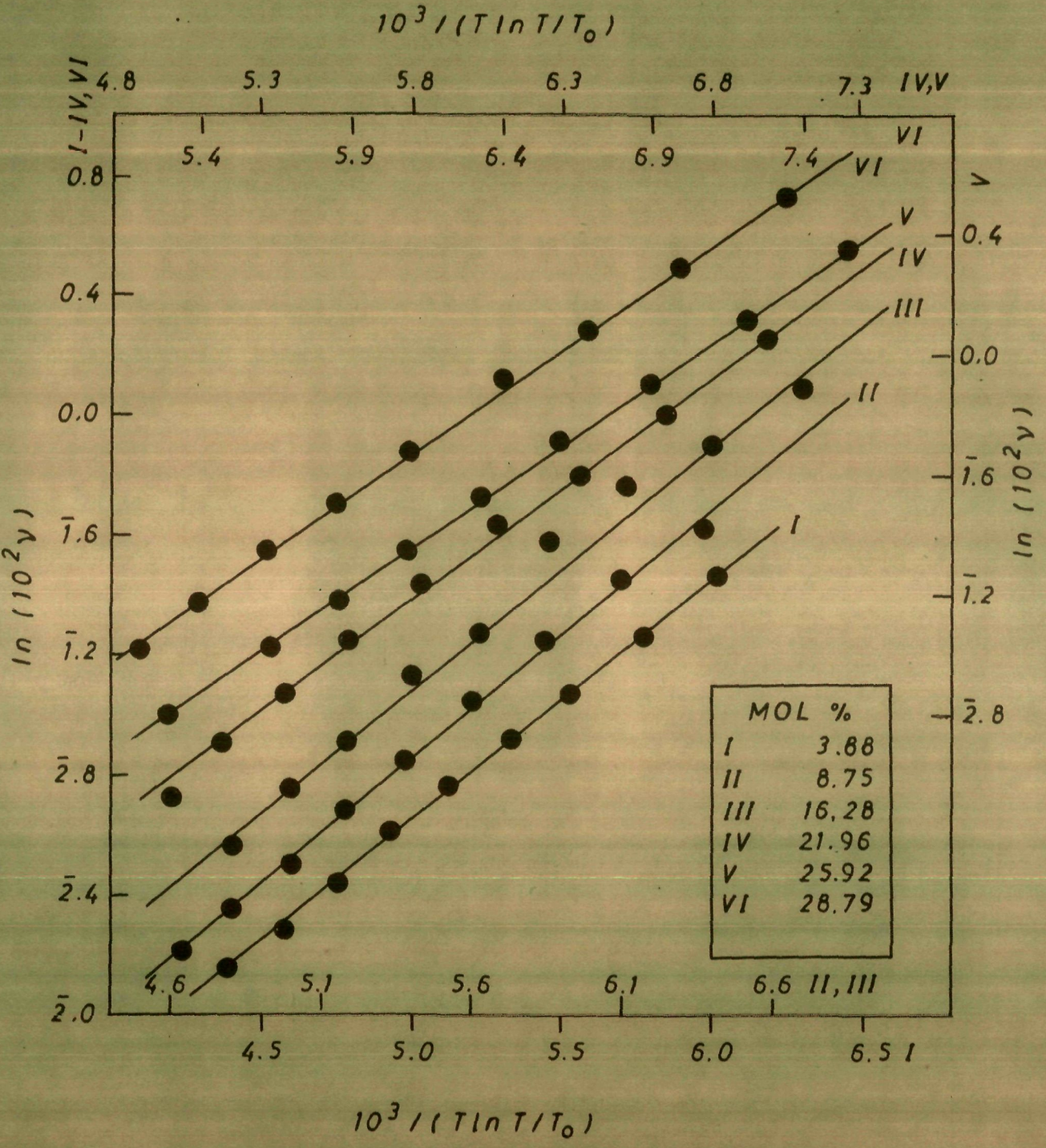

FIG. 3 a PLOTS OF $\ln \nu$ VS. $1/(T\ln T/T_0)$ FOR TBABr + $NiCl_2$ MOLTEN SALT SYSTEM

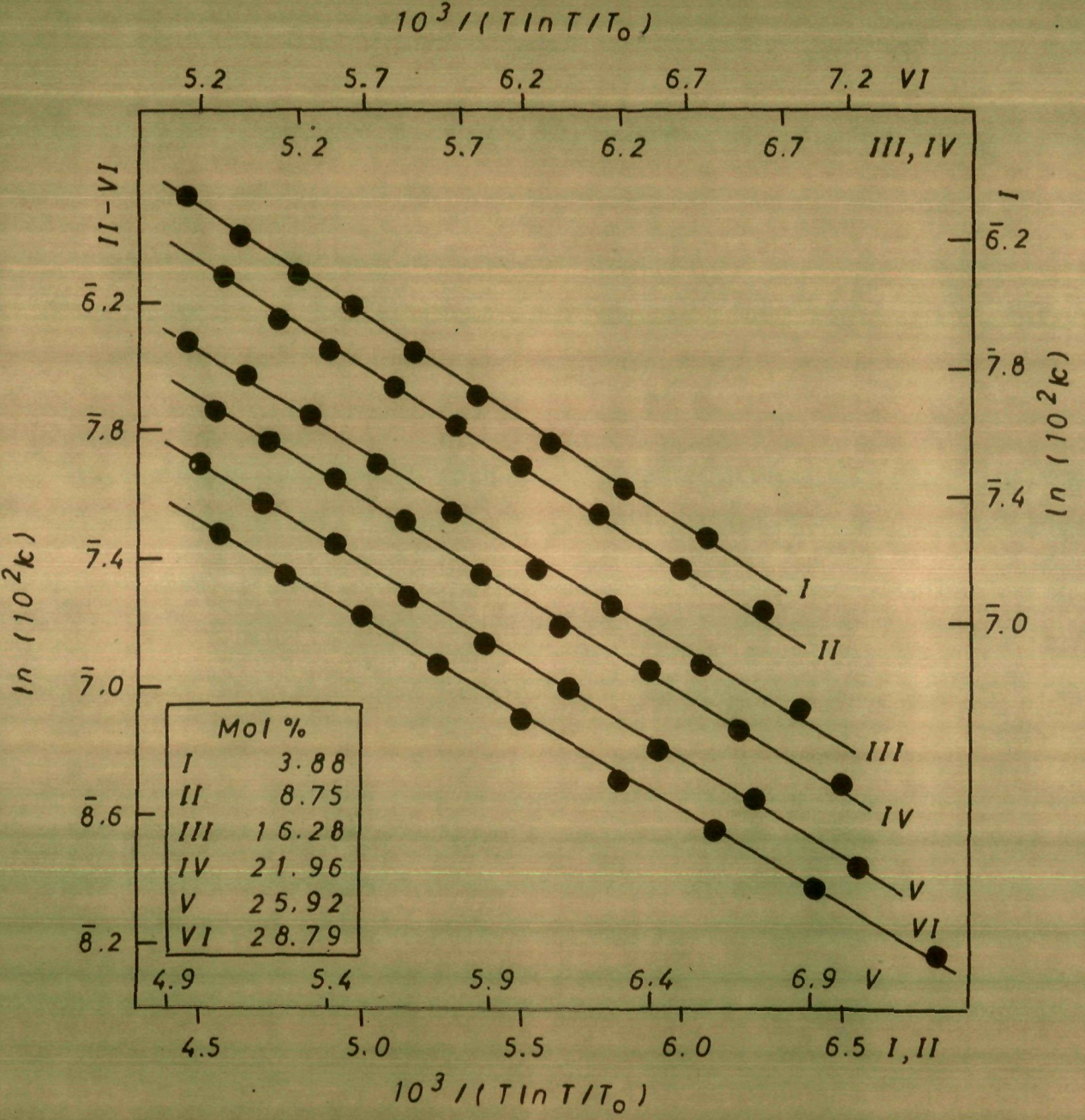

FIG. 3b PLOTS OF $\ln k$ VS. $1/(T\ln T/T_0)$ FOR TBABr + $NiCl_2$ MOLTEN SALT SYSTEM

bility of the VTF and the CHN equations, respectively. Further, the temperature dependence of the same sets of data for the Arrhenius region, viz., 393-413 K were least-squares fitted to the two parameter equation of the form

$$Y_{\nu,\kappa} = C_2 e^{-C_1/RT} \qquad (27)$$

where Y may be either kinematic viscosity or specific conductance, while C_2 and C_1 are parameters. The values of the parameters, C_2 and C_1 along with the standard deviations are listed in Table IV. The much decreased standard deviation values further support the consideration of two regions of a single plot. The energy of activation obtained from the slope of the linear portion of these plots is given in Table IV.

The values of the parameters, k_Y are found to be concentration invariant whether it is the case of kinematic viscosity or that of specific conductance. This is supported by an empirical relation[23,37,38] which states that the k term is concentration independent for systems in which the concentration changes do not alter the melt structure in too radical a fashion. Consequently, the values of the universal constant k have been suggested as $k_\eta \sim 700$ K for the viscosity and $k_\lambda \sim 600$ K for the conductance. In the present case the k values may be observed as $k_\nu = 690 \pm 2$ K and $k_\kappa = 600 \pm 3$ K in the cases of the VTF and the CHN

TABLE IV. Parameters of Arrhenius Equation (26)[a]

Mol% of Mi^{2+}	$E_{\nu,K}$/4.184 kJ mol^{-1}	$C_1/Rx10^{-4}$	log C_2	Std dev in ln(ν, K)
3.88	9.9192 (7.6027)	0.21674 (-0.1661)	-6.0518 (1.5631)	0.0056 (0.0034)
8.75	10.3310 (7.4229)	0.22570 (-0.1622)	-6.2483 (1.4379)	0.0046 (0.0101)
16.28	12.0601 (8.4868)	0.26350 (-0.1854)	-7.0012 (1.9238)	0.0081 (0.0068)
21.96	11.5087 (7.4498)	0.25150 (-0.1627)	-6.4334 (1.2804)	0.0030 (0.0072)
25.92	10.8578 (9.3456)	0.23750 (-0.2042)	-6.2420 (2.2131)	0.0017 (0.0043)
28.79	10.8561 (8.7594)	0.23720 (-0.1913)	-6.0854 (1.8026)	0.0023 (0.0016)

a The parameters obtained from specific conductance data are given within parentheses.

equations, respectively for the entire concentration range under study. On the basis of Cohen and Turnbull's "hard sphere" model[10] the constant, k is defined as $\gamma V^*/\alpha V_m$ where α is the mean molecular expansion coefficient from T_o to the measuring temperature, V^* is the critical void volume, V_m is the molar volume and γ is the geometric factor for correcting the overlap of free volume in calculating the probability of occurrence of critical void. Accordingly, one may expect a similar rate of diffusion of the solute $NiCl_2$ of smaller size as well as the solvent TBABr of greater size. Therefore, a constant value of critical void volume, V^* is evidently expected in the solvents as well as in the mixtures too though the free volumes decrease with increase in $[NiCl_2]$.

The parameters, $T_{o_{\nu,k}}$ and $A_{\nu,k}$ obtained from the VTF and the CHM equations are found to vary in a consistent manner similar to those reported earlier[8]. Since the T_o, defined as the zero mobility or the glass transition temperature, is independent of the model or any process, it is a property of the system alone and shows a linear variation with concentration.

The parameters, $A_{\nu,k}$ varies with concentration according to $m^{-1/2}$ dependence relationship as pointed out by Cohen and Turnbull[10]. Since the molecular mass is decreasing with increasing $[NiCl_2]$ the frequency factor shows an increase in

the case of viscosity while a decrease in the case of conductance.

The conventional energies of activation were computed from the derivative, $\frac{d \ln \gamma}{d(1/T)}$ of the VTF equation. The corrected energies of activation, E_{cor} for the kinematic viscosity and the conductance were computed by adding $\frac{1}{2}$ RT to the corresponding energies of activation, E_ν and E_κ and are given in Table V. The plots of E_{cor} versus $\left[T/(T-T_o)\right]^2$ for the glassy material ($\sim$ 29 mol%) for the kinematic viscosity and the specific conductance are shown in Figure 4 which exhibit the sensitivity to the appropriate choice of T_o. Similar behaviour is also found in the case of other mixtures.

The energies of activation, E_ν and E_κ computed through the VTF and the CEM equations (Tables VI and VII) viz., 368 K isotherm are comparable (Figures 5 and 6). It is seen that the energy of activation decreases with the increase in temperature due to the decrease in the cohesive energies of the entities.

The values of E_ν and E_κ were plotted as a function of solute concentration (Figures 5 and 6). From the energy of activation isotherms for the kinematic viscosity as well as the specific conductance it is evident that the energies of activation show a slow but steady increase initially with the increasing $[NiCl_2]$. The isotherms become successively

TABLE V. Corrected Energies of Activation (kJ mol^{-1}) for Kinematic Viscosity and Specific Conductance as a function of temperature[a]

	Mol% of Ni^{2+}					
T K	3.88	8.75	16.28	21.96	25.92	28.79
373.0	11.1806 (9.6626)	11.4606 (9.8616)	12.5806 (10.6156)	12.9306 (11.3326)	13.4006 (12.1106)	14.2906 (12.9326)
378.0	10.7256 (9.2116)	10.9056 (9.3876)	11.9356 (10.0796)	12.2456 (10.7326)	12.6656 (11.4436)	13.4856 (12.1896)
383.0	10.2495 (8.8025)	10.4005 (8.9565)	11.3605 (9.5955)	11.6305 (10.1935)	12.0005 (10.8445)	12.7605 (11.5245)
388.0	9.8155 (8.4295)	9.9545 (8.5655)	10.8355 (9.1565)	11.0755 (9.7065)	11.4155 (10.3065)	12.1155 (10.9285)
393.0	9.4185 (8.0885)	9.5385 (8.2085)	10.3605 (8.7576)	10.5705 (9.2645)	10.8705 (9.8185)	11.5305 (10.3915)
398.0	9.0535 (7.7765)	9.1575 (7.8615)	9.9245 (8.3925)	10.1155 (8.8615)	10.3905 (9.3755)	10.9955 (9.9045)

(continued)

TABLE V. (continued)

T K	Mol% of Ni^{2+}					
	3.88	8.75	16.28	21.96	25.92	28.79
403.0	8.7184 (7.4884)	8.8084 (7.5804)	9.5254 (8.0584)	9.6954 (8.4934)	9.9454 (8.9724)	10.5104 (9.4624)
408.0	8.4094 (7.2220)	8.4864 (7.3044)	9.1584 (7.7514)	9.3104 (8.1564)	9.5384 (8.6034)	10.0764 (9.0584)
413.0	8.1224 (6.9764)	8.1884 (7.0484)	8.8214 (7.4694)	8.9574 (7.8474)	9.1644 (8.2644)	9.6714 (8.6884)

a Corrected energies of activation for specific conductance are given within parentheses.

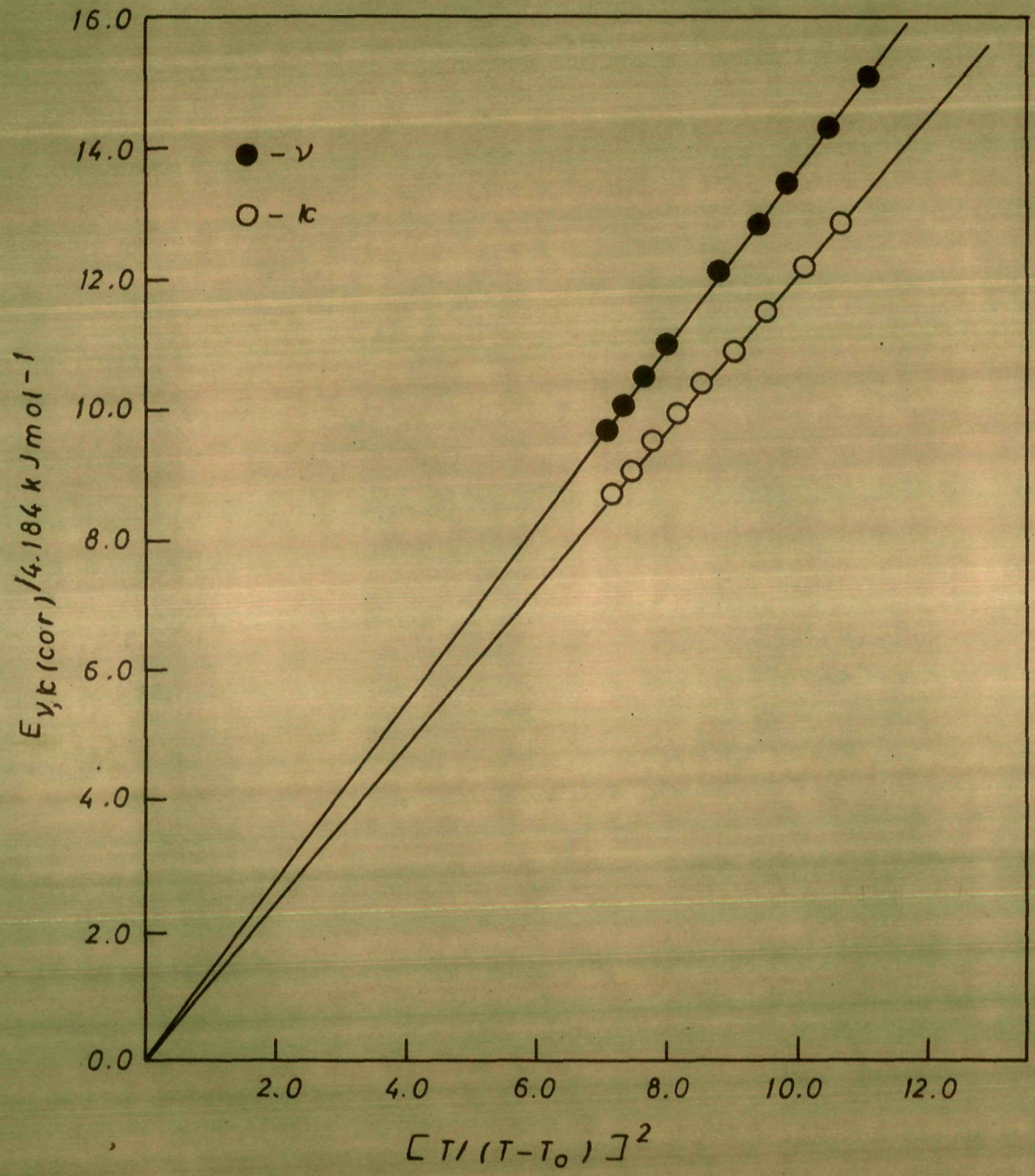

FIG. 4 PLOTS OF E_{cor} OF KINEMATIC VISCOSITY AND SPECIFIC CONDUCTANCE FOR 28.79 MOL % $NiCl_2$ IN TBABr MOLTEN SALT SYSTEM

TABLE VI. Energies of Activation (kJ mol^{-1}) computed through Equation (9) for Kinematic Viscosity and Specific Conductance as a function of temperature[a]

	Mol% of Ni^{2+}					
T K	3.88	8.75	16.28	21.96	25.92	28.79
373.0	10.810 (9.292)	11.090 (9.491)	12.210 (10.250)	12.560 (10.960)	13.030 (11.740)	13.920 (12.562)
378.0	10.350 (8.836)	10.530 (9.012)	11.560 (9.704)	11.870 (10.360)	12.290 (11.068)	13.110 (11.814)
383.0	9.869 (8.422)	10.020 (8.576)	10.980 (9.215)	11.250 (9.813)	11.620 (10.464)	12.380 (11.144)
388.0	9.430 (8.044)	9.569 (8.180)	10.450 (8.771)	10.690 (9.321)	11.030 (9.921)	11.730 (10.543)
393.0	9.028 (7.698)	9.148 (7.818)	9.970 (8.367)	10.180 (8.874)	10.480 (9.428)	11.140 (10.001)
398.0	8.658 (7.381)	8.762 (7.486)	9.529 (7.997)	9.720 (8.466)	9.995 (8.980)	10.600 (9.509)

(continued)

TABLE VI. (continued)

T K	Mol% of Ni^{2+}					
	3.88	8.75	16.28	21.96	25.92	28.79
403.0	8.318 (7.088)	8.408 (7.180)	9.125 (7.658)	9.295 (8.093)	9.545 (8.572)	10.110 (9.062)
408.0	8.004 (6.817)	8.081 (6.899)	8.753 (7.346)	8.905 (7.751)	9.133 (8.198)	9.671 (8.655)
413.0	7.712 (6.976)	7.778 (6.638)	8.411 (7.059)	8.547 (7.437)	8.754 (7.854)	9.261 (8.278)

a Energies of activation for specific conductance are given within parentheses.

TABLE VII. Energies of Activation (kJ mol^{-1}) computed through Equation (10) for Kinematic Viscosity and Specific Conductance as a function of temperature[a]

	Mol% of Ni^{2+}					
T K	5.88	8.75	16.28	21.96	25.92	28.79
373.0	10.0010 (8.7628)	11.1830 (9.1210)	12.078 (10.924)	12.948 (11.061)	13.778 (11.188)	14.106 (12.275)
378.0	9.5154 (8.3329)	10.6050 (8.6595)	11.420 (10.322)	12.212 (10.440)	12.960 (10.545)	13.257 (11.528)
383.0	9.0735 (7.9421)	10.0820 (8.2409)	10.827 (9.780)	11.550 (9.881)	12.228 (9.968)	12.498 (10.861)
388.0	8.6700 (7.5854)	9.6068 (7.8598)	10.290 (9.289)	10.954 (9.376)	11.571 (9.448)	11.816 (10.263)
393.0	8.3003 (7.2589)	9.1730 (7.5117)	9.803 (8.845)	10.413 (8.918)	10.977 (8.977)	11.202 (9.724)
398.0	7.9605 (6.9590)	8.7759 (7.1925)	9.358 (8.439)	9.922 (8.502)	10.439 (8.549)	10.646 (9.237)

(continued)

TABLE VII. (continued)

	Mol% of Ni^{2+}					
T K	3.88	8.75	16.28	21.96	25.92	28.79
405.0	7.6473 (6.6827)	8.4112 (6.8991)	8.950 (8.068)	9.474 (8.122)	9.949 (8.159)	10.140 (8.794)
408.0	7.3579 (6.4275)	8.0753 (6.6285)	8.576 (7.727)	9.065 (7.775)	9.502 (7.802)	9.679 (8.390)
413.0	7.0896 (6.1912)	7.7651 (6.3783)	8.642 (7.414)	8.686 (7.453)	9.092 (7.474)	9.257 (8.021)

a Energies of activation for specific conductance are given within parentheses.

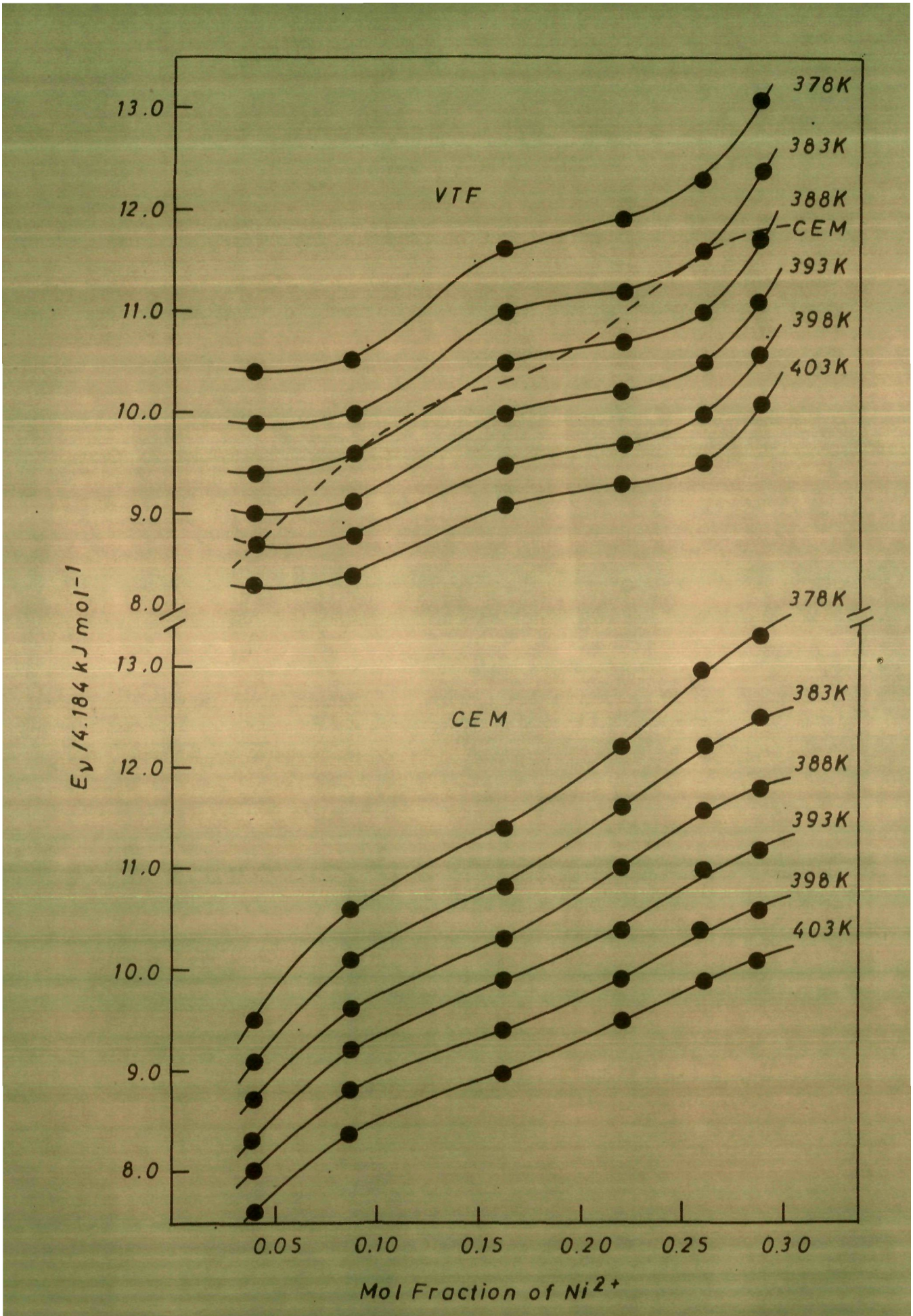

FIG. 5 PLOTS OF E_v VS. CONCENTRATION FOR TBABr + $NiCl_2$ MOLTEN SALT SYSTEM

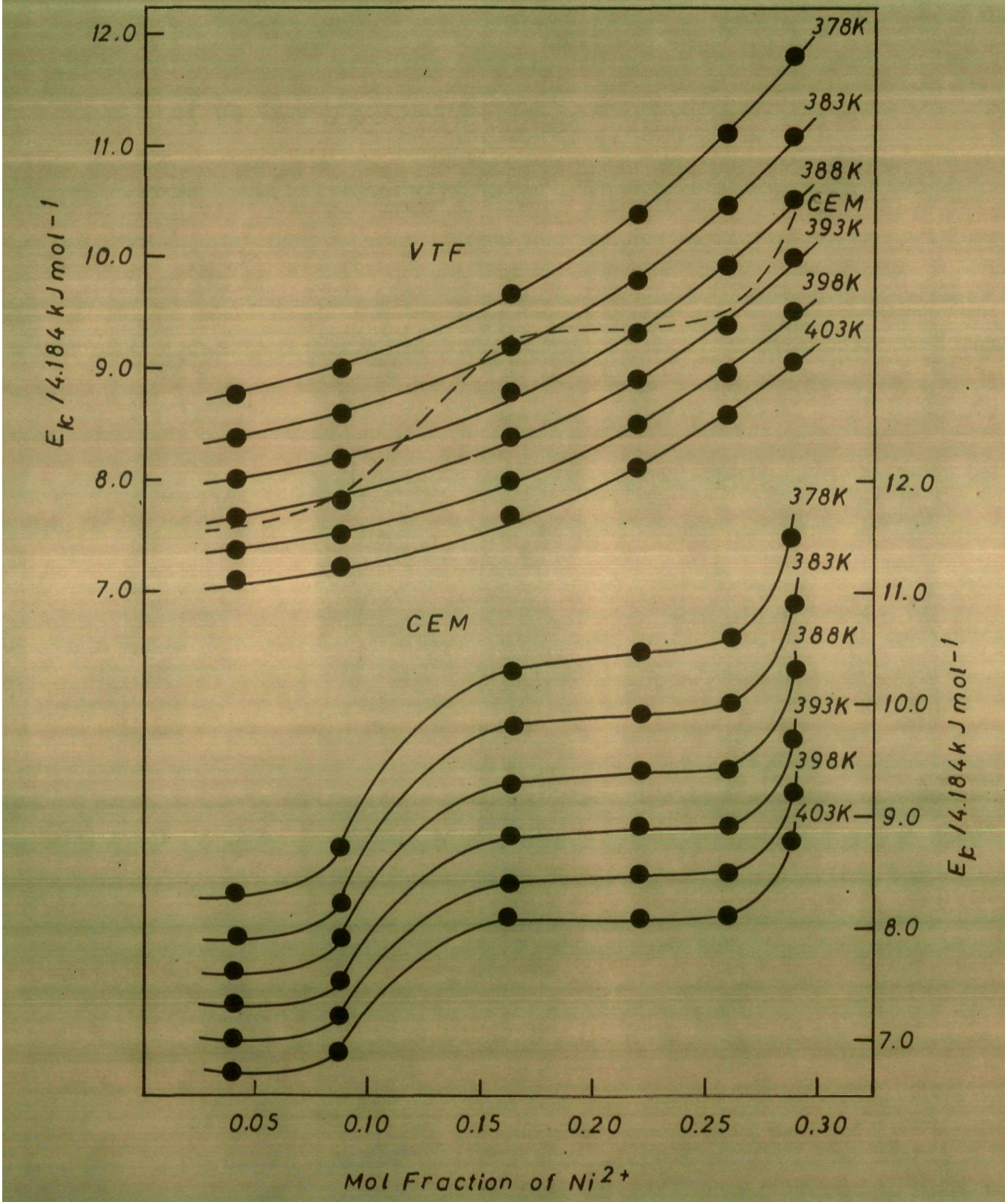

FIG. 6 PLOTS OF E_k VS. CONCENTRATION FOR TBABr + $NiCl_2$ MOLTEN SALT SYSTEM

more steep at relatively higher concentrations. A sharp increase in the energies of activation in the concentrated region may be understood in the light of the free volume model. Much increased solute concentration reduces the free volume while the moving entities evidently require high value of energy which surmounts the potential energy barrier. Such observations have been found in the cases of anhydrous[8,25] and many hydrated melts[24,39-41]. Further, the solute-rich mixture may be considered to be one with much increased intermolecular forces which facilitate the formation of a cluster that requires adequate energy for the viscous flow. On increasing the temperature the free volume increases and the entities will require comparatively less energy thereby bringing down the energy barrier. Similar explanation may also be given for the flow of ions in the case of conductance.

Concentration dependence of kinematic viscosity and specific conductance

The kinematic viscosities and the specific conductances have been plotted as a function of concentration in Figures 7a and 7b. From these isotherms it is clear that the kinematic viscosity increases slightly in the beginning with the increase in $[NiCl_2]$, but quite rapidly when the $[NiCl_2] \approx 18$ mol% and then onwards the increase is monotonous. Similar behaviour has also been observed in the case of

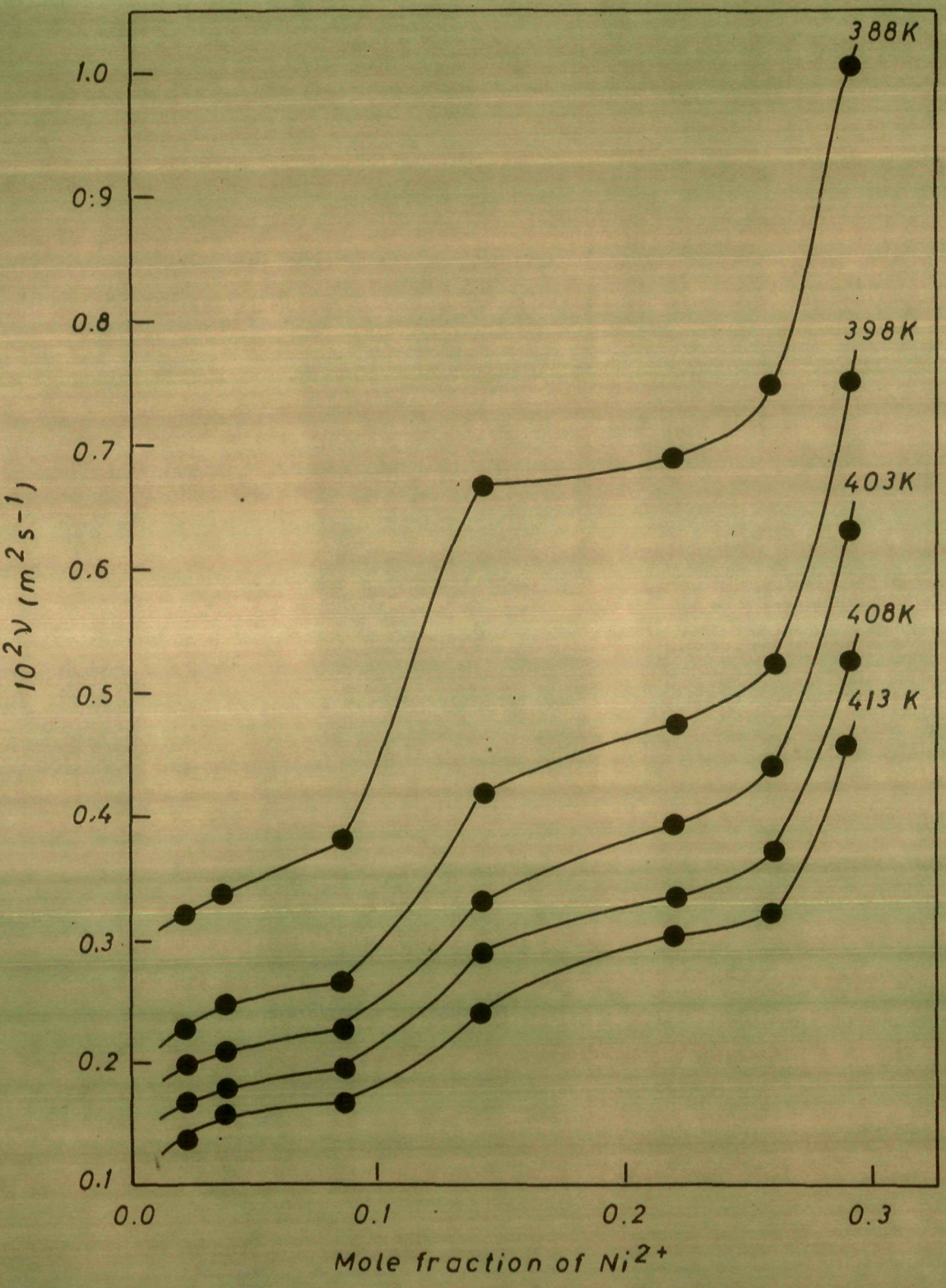

FIG. 7a KINEMATIC VISCOSITY VS. CONCENTRATION ISOTHERM FOR TBABr + $NiCl_2$ MOLTEN SALT SYSTEM

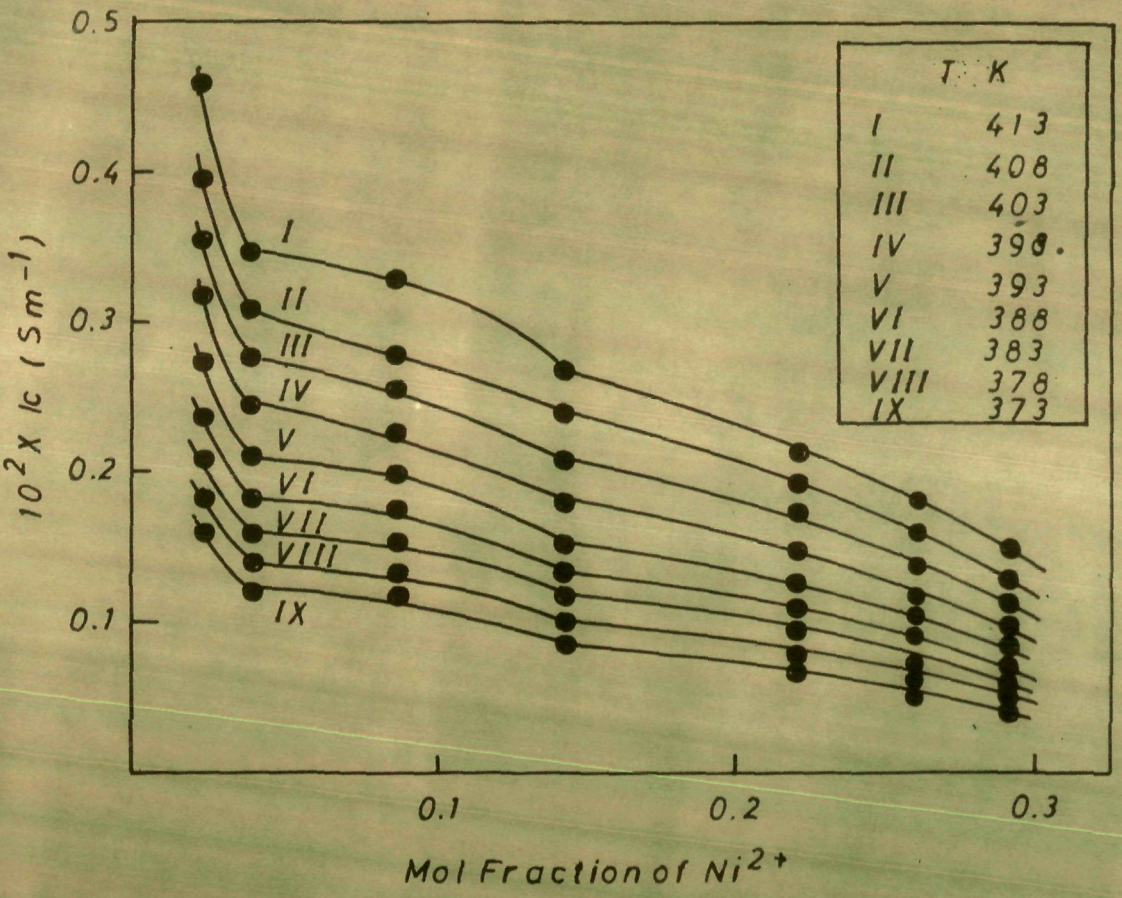

FIG. 7 b SPECIFIC CONDUCTANCES VS. COMPOSITION ISOTHERMS FOR TBABr + $NiCl_2$ MOLTEN SALT SYSTEM

specific conductance isotherms (Figure 7b), viz., 415 K isotherm. Such a variation in the concentration dependence of viscosity and conductance has also been observed in the cases of TBAI + $CoCl_2$[8] and TBAX + $MnCl_2$ (where X = Cl, Br or I)[42,43] molten systems. The sudden increase in the kinematic viscosity around the concentration range of about 18 mol% attributes to the formation of the complexes of the type $\left[(C_4H_9)_4N^+\right]_2\left[NiCl_2Br_2^=\right]$, the presence of which has already been identified by the ligand-field spectra studied earlier[7,14]. The above facts are supported by the discussion made above in the case of activation energy isotherms (Figures 5 and 6).

In order to understand the concentration dependence of kinematic viscosity and specific conductance the parameters, A_ν, A_K and $T_{o\nu,K}$ obtained from the VTF equation (Table IIA) were plotted as a function of concentration (Figure 8). All the three parameters vary linearly with concentration similar to those reported earlier[24-26,39,43]. The above plots of the parameters, A_Y and $T_{o\nu,K}$ versus concentration in mol%, x, were made through the least-squares fitting the data to the equations of the type

$$A_Y = A_{oY} \pm Q_{1Y}x \qquad (28)$$

$$T_o = T_{o(o)} + Q_{2Y}x \qquad (29)$$

where A_{oY} and $T_{o(o)}$ are the respective parameters for the

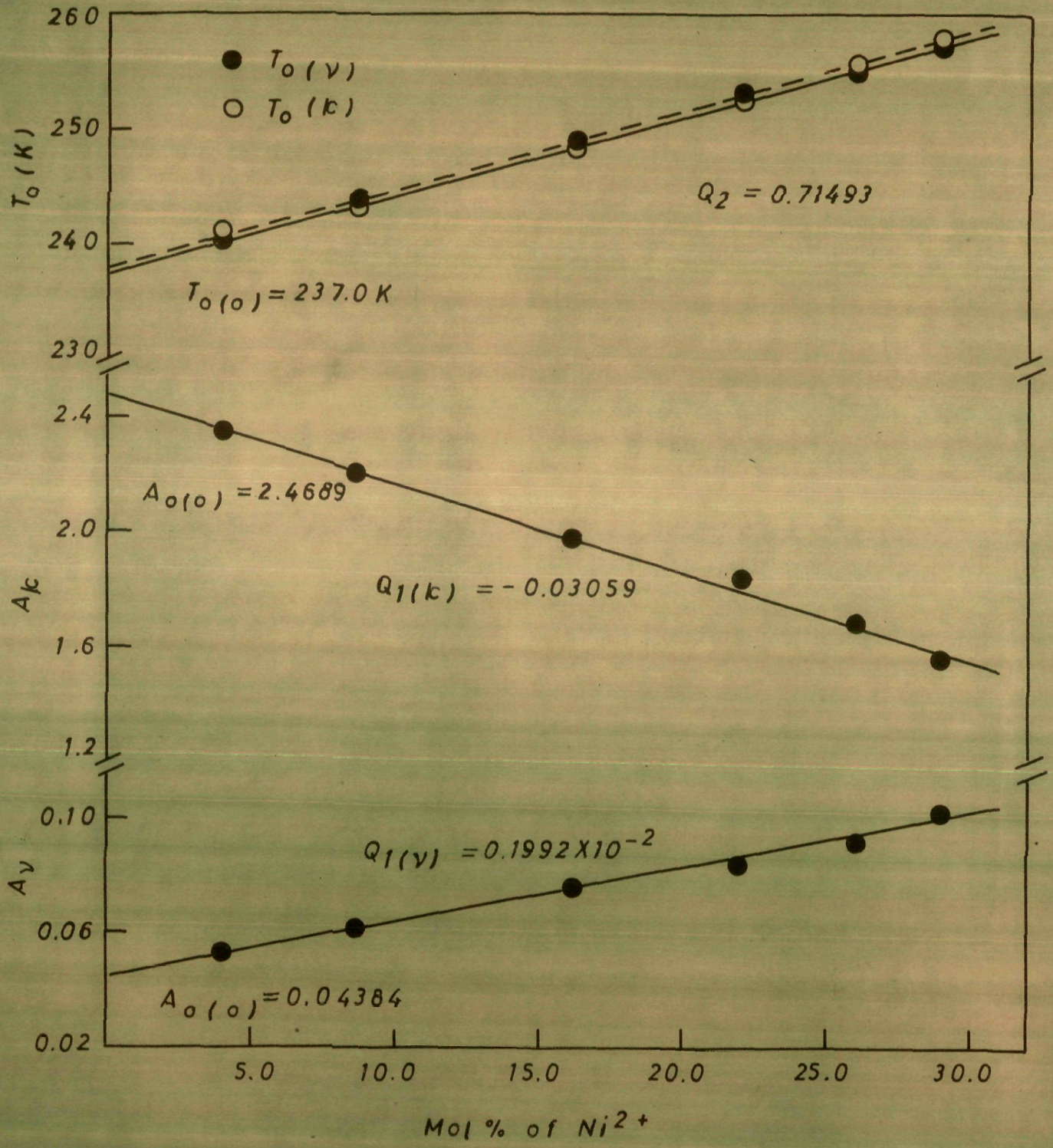

FIG. 8 PLOTS OF T_o, A_k AND A_v VS. CONCENTRATION FOR TBABr + $NiCl_2$ MOLTEN SALT SYSTEM

pure melt and Q_{1Y} and Q_{2Y} are the slopes of the A_Y and the T_o versus mole%, x plots, respectively. The values of the parameters, $A_{o\nu}$, $A_{o\kappa}$, $T_{o(o)}$, $Q_{1\nu}$, $Q_{1\kappa}$ and Q_{2Y} are 0.0438, 2.4689, 237.0, 0.002, -0.0306 and 0.7149, respectively. The values of the parameters, $A_{o\nu}$ and $A_{o\kappa}$ seem to be consistent and reproducible with the $m^{-1/2}$ dependence relation[10]. Since the parameter, A_Y is directly related to the effective masses of the component species, A_ν increases with increasing solute concentration while A_κ shows a decrease. The increase in A_ν may be understood as due to the rigidity of the system with increasing $[NiCl_2]$ and the decrease in A_κ is due to the decrease in the mean molecular masses of the component species and much increased cohesion in the system.

The linear increase of the glass transition temperature, T_o with concentration may be understood in the light of the free volume model, the cohesive energy consideration, the mean molecular masses in different mixtures, and the extent of complexation. Since the free volume decreases on adding the solute, $NiCl_2$ to the solvent, TEABr, less cooling is required to reach the glass-transition temperature, T_o. Hence, the expected increase in the T_o values with concentration is observed. In addition to that, the decrease in the free volume in the system assists the molecules in bringing them closer together, which, in turn, enhances the

cohesive energy due to high charge to radius ratio of the solute cation and the solvent anion. Furthermore, an increase in the T_o values with increasing $[NiCl_2]$ may also be ascribed to the decrease in the mean molecular masses in the mixtures, TBABr + $NiCl_2$ and to the complexation which results in a closely packed geometry. On extrapolation of the plot of T_o versus concentration to zero concentration one obtains T_o = 237 K for the pure TBABr.

The values of the parameters, A_{oY}, a_{1Y}, a_{2Y} and $T_{o(o)}$ thus computed on the basis of the linear dependences of A_Y and T_o on concentration were used to calculate the experimental values of ν and κ at several values of the constant, $c(T/T_o)$ using the VTF equation. The values of the corresponding experimental temperature, T_{corres} at a given value of c were also calculated for this purpose. The experimental values of the kinematic viscosity and the specific conductance thus calculated were then least-squares fitted to the equation of the type

$$Y = (A_{oY} \pm a_{1Y}x)e^{-1/2}\,(T_{o(o)} + a_{2Y}x)^{-1/2}$$

$$\exp\left[\pm k_Y/(T_{o(o)} + a_{2Y}x)\,(c - 1)\right] \qquad (30)$$

where Y may be either the kinematic viscosity or the specific conductance and x is the concentration of the solute in mol%. Equation (30) has been derived by the substitution of equations (28) and (29) into the VTF equation assuming $T/T_o = c$.

The values of the corresponding experimental temperature, T_{corres} for a given value of c lying in the experimental range of measurements were selected on the basis of the minimised standard deviation. The values of the parameters of equation (30) thus computed along with the standard deviations are listed in Table VIII. It may be noted that the computed values of A_{oY}, q_{1Y}, $T_{o(c)}$, q_{2Y} and k_Y are found to be very close to those obtained from their least-

TABLE VIII. Best-fit Parameters of Equation (16)[a]

c = 1.6

A_{oY}	q_{1Y}	k_Y	$T_{o(c)}$	q_{2Y}	Std dev in ln Y
0.0483	0.0014	697.0	234.0	0.70	0.07
(2.3586)	(-0.031)	(585.0)	(233.0)	(0.72)	(0.04)

a Parameters computed through conductance data are within the parentheses.

squares plots. The plots of $\ln[Y\, e^{y/2}(T_{o(c)} \pm q_{2Y}x)^{y/2}]$ versus $1/(T_{o(c)} \pm q_{2Y}x)\,(c-1)$ (Figure 9) are linear which show the applicability of equation (30).

According to equation (16) one obtains a constant energy of activation, E_{cor} for a given value of c, viz., $E_{cor} = k_Y R \left[T/(T-T_o)\right]^2 = \left[c/(c-1)\right]^2$ for the entire concentration range. On the basis of this concept the concentration dependence

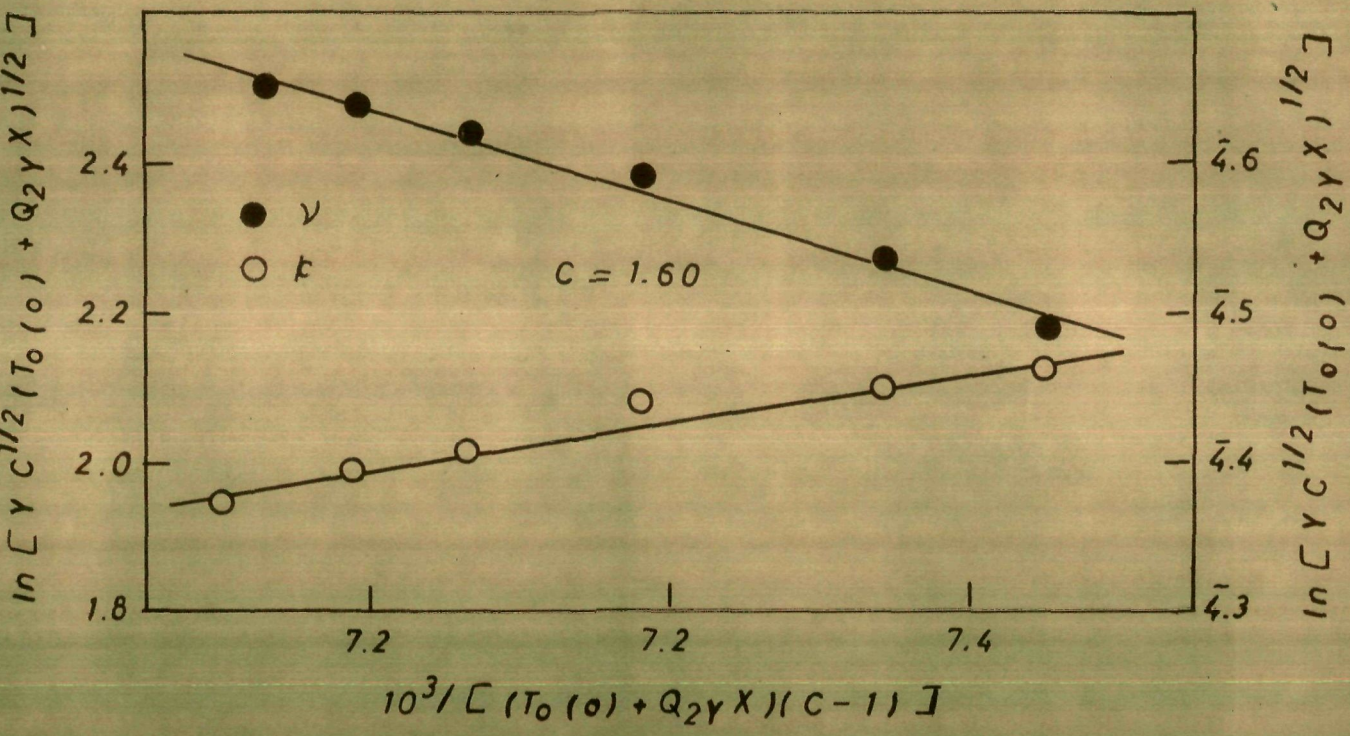

FIG. 9 COMPOSITION DEPENDENCE OF KINEMATIC VISCOSITY AND SPECIFIC CONDUCTANCE FOR TBABr + $NiCl_2$ MOLTEN SALT SYSTEM

of the kinematic viscosity and the specific conductance of TBABr + $NiCl_2$ molten system is successfully explained. Similar results[40,41] have also been observed with the isentropic concept using the CRM equation in place of VTF.

The linear dependence of A_γ on concentration is further employed to correlate the parameters A_γ and T_o. For this purpose, equation (28) was compared with equation (29) to obtain the following expression,

$$A_\gamma = A_{o\gamma} - (q_{1\gamma}/q_{2\gamma})T_{o(o)} + (q_{1\gamma}/q_{2\gamma})T_o \qquad (31)$$

The linear plots of A_γ versus T_o (Figure 10) show the applicability of equation (31).

Similarly, a relationship of E_{cor} with T_o is also imminent in view of the linear plots of E_{cor} versus concentration (Figure 11a),

$$E_{cor} = E^{\circ}_{cor} + q_{3\gamma}x \qquad (32)$$

which on combining with equation (28) gives

$$E_{cor} = E^{\circ}_{cor} - (q_{3\gamma}/q_{2\gamma})T_{o(o)} + (q_{3\gamma}/q_{2\gamma})T_o \qquad (33)$$

The computed values of E_{cor} (Table IX) by using equation (33) were plotted as a function of T_o (Figure 11 b). It is evident that the corrected energies of activation for the kinematic viscosity increase with increase in the values of T_o while those for specific conductance decrease, which

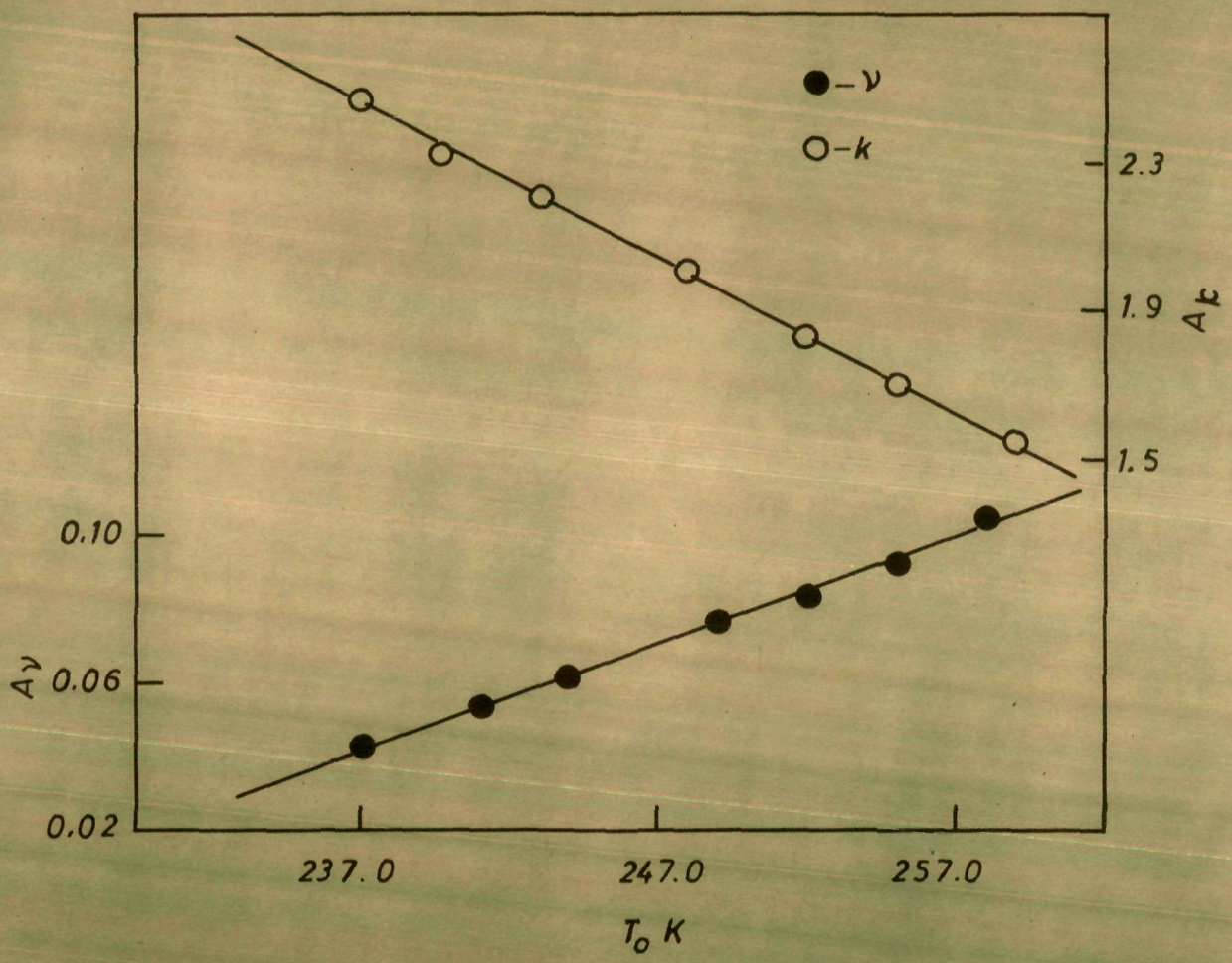

FIG. 10 PLOTS OF A_ν AND A_t VS. T_o FOR TBABr + $NiCl_2$ MOLTEN SALT SYSTEM

TABLE IX. Corrected energy of activation (E_{cor}/4.184 kJ mol^{-1}) as a function of glass transition temperature, T_o

Mol% of Ni^{2+}	E_{ν}(cor)	E_k(cor)	T_o K
3.875	11.5	9.94	240.0
8.748	11.8	10.26	243.0
16.280	12.5	10.95	249.0
21.959	12.9	11.28	253.0
25.924	13.2	11.62	255.0
28.792	13.7	12.02	258.0

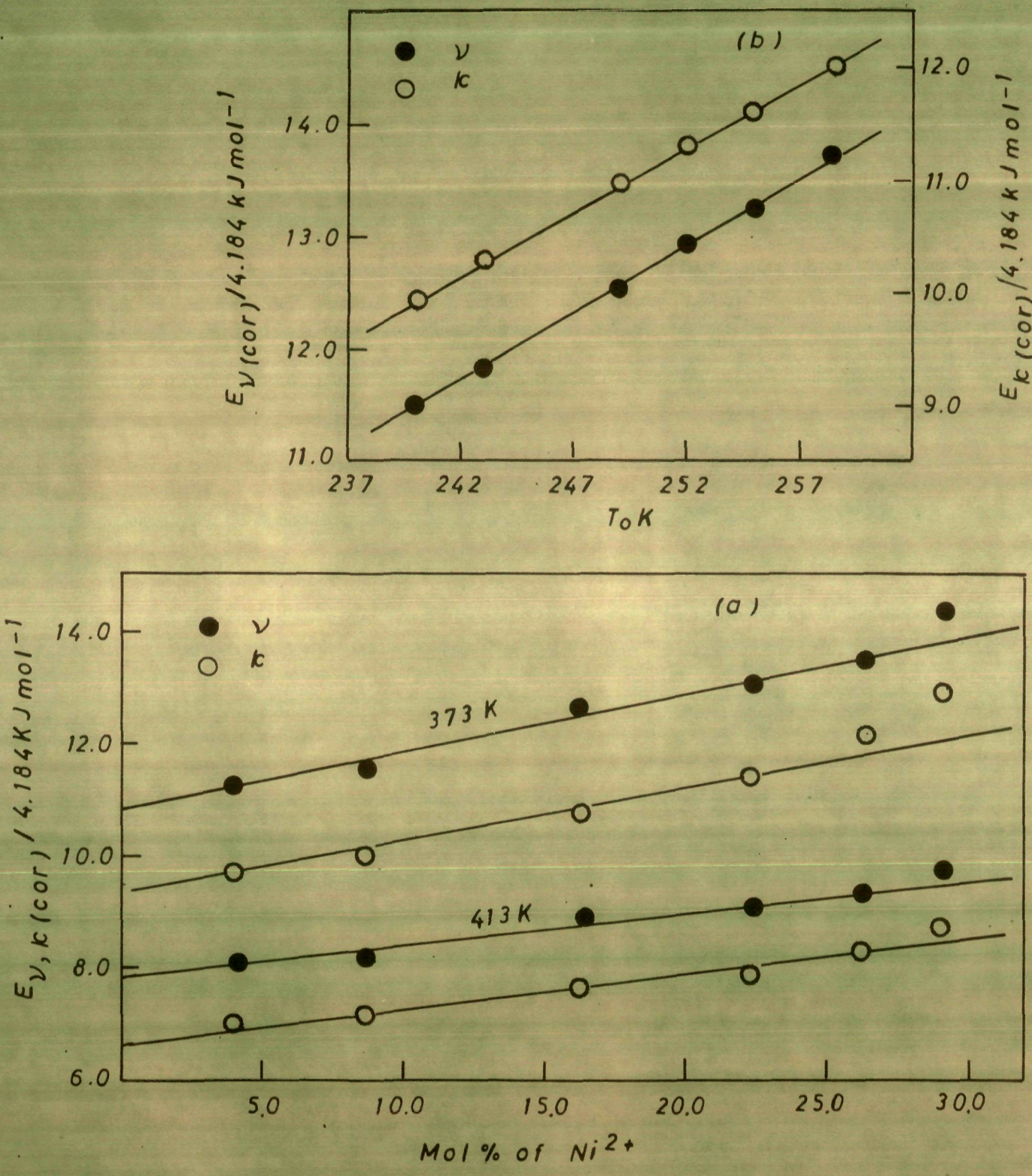

FIG. 11(a) COMPOSITION DEPENDENCE OF E_{cor} FOR TBABr + $NiCl_2$ MOLTEN SALT SYSTEM

(b) PLOTS OF E_{cor} VS. T_0 FOR TBABr + $NiCl_2$ MOLTEN SALT SYSTEM

is physically justifiable. The above correlation of E_{cor} with T_o is in good agreement with those reported earlier[44].

CHAPTER III

OPTICAL SPECTRA, FLUIDITY AND ELECTRICAL CONDUCTANCE OF TBABr + $PdCl_2$ MOLTEN SALT SYSTEM

Results and Discussion

The ability of molten organic halides of large [cation] to [anion] ratio to facilitate the formation of tetrahedral, Td, tetrahalo-metal complex ions has already been demonstrated[42,45-52]. In case the geometry is energetically not feasible for a given transition metal ion the corresponding metal halide will refuse to go into solution in such melts as is the case with Cr^{3+} ions[26]. It has also been found earlier[26,42,45,47-49,52] that the metal halide-rich mixtures of low melting organic halides of large [cation] to [anion] ratio containing $(R_4B)^+_2MX_4^{2-}$ (where R = an alkyl group, B = N or P; M = Mn^{2+}, Fe^{3+}, Co^{2+} or Ni^{2+}, and X = Cl, Br or I) supercool to glassy states. The degree of dissociation of MX_4^{2-} is negligible in pure $(R_4B^+)_{(4-n)}MX_4^{(4-n)^-}$ as is apparent from the decreases in the electrical conductances[42,52] with increase in $[MX_n]$, where n denotes the charge on M. Because of the close proximity of the species, $(R_4B^+)_{(4-n)}MX^{(4-n)^-}$ in highly concentrated solutions, they appear to be held together at low temperatures giving rise to a compact form. This consequently, results in a highly viscous liquid due to the presence of highly associated flowing entities of the form, $\left\{(R_4B^+)_{(4-n)}(MX_4)^{(4-n)^-}\right\}_x$. The optical spectra and the transport behaviour of such systems suggest a relationship between the melts on one hand and the corresponding glassy state on the other.

Tremendous amount of such studies have been made with the 3d transition metal ions while scarcely with those of the 4d metal ions. In view of this, such studies have been undertaken with palladium(II) chloride dissolved in molten organic halide of large [cation] to [anion] ratio, R_4ABr (A = ammonium). The dilute as well as concentrated solutions of MX_2 in molten R_4BX have been found to contain the same absorbing species, implying the presence of the same Td geometry. They seem to differ in their compactness, the most concentrated solution being the most compact in arrangement as evidenced by their relative viscosities and conductances. The glassy material has another advantage of providing a wider temperature range of study, i.e., from much below the melting point of the parent solvent up to the temperature of stability of the sample. Palladium(II) ion being isoelectronic with that of nickel(II), (d^8 system), has been selected for the spectral and transport studies. This will not only help in investigating the behaviour of 4d transition metals but will also provide a basis for comparing such properties with those of the 3d metal ions. The charge-transfer spectra to solvent (CTTS), the charge-transfer (C - T) spectra of the complex ion, PdI_4^{2-} and those of the ligand-field (L-F) transition bands for the intraconfigurational transitions in a T_d-field have been investigated. These bands are recorded in thin films of the glassy material. The T_d geometry has been identified

on the basis of comparison with that of nickel(II)-complex ions in the same medium. The transport properties of the glassy material have been undertaken in order to investigate either the similarity or the difference in the overall pattern of the transport properties in the same solvent. The transport properties of different concentrations are expected to follow a pattern similar to that observed in the case of nickel(II). Thus, such properties investigated at a given concentration may serve as an exemplary behaviour for that system, say nickel(II), or palladium(II) in a given solvent. For this reason, only the concentrated solution of palladium(II) chloride in molten TBABr was investigated as such systems provide a wide temperature range for the above studies.

Tetrahedral geometry has been identified for PdX_4^{2-} on the basis of that for NiX_4^{2-} reported earlier[25]. Some indications for the presence of L-F bands at about 1700 and 700 nm for $^3A_2(F) \longleftarrow {}^3T_1(F)$ and $^3T_1(P) \longleftarrow {}^3T_1(F)$ transitions are available in the thin film spectra of the corresponding glassy material. The spin forbidden band for the transition $^1G \longleftarrow {}^3T_1(F)$ appear to have borrowed its intensity from the neighbouring intense C-T bands for the complex ions, $PdCl_2Br_2^{=}$ the presence of which is based on the following considerations.

As reported earlier, the metal halide is expected

to go into solution in the molten solvent through either ionisation or complexation. In the case of dilute solutions, the proposed mechanism of dissolution suggests the presence of essentially Br^- ions of the parent solvent around the Pd^{2+} ion as $[Cl^-]$ is low. On the other hand, in relatively concentrated solutions of $PdCl_2$ in molten TBABr, the ionisation of $PdCl_2$ appears to be suppressed by successive increase in $[PdCl_2]$ and the dissolution of $PdCl_2$ may take place through complexation. This will, therefore, leave the metal ion in contact with Cl^- as well as Br^- ions arranged tetrahedrally or almost tetrahedrally and the absorbing species in $PdCl_2$-rich mixtures of molten TBABr may be given as $\left[(C_4H_9)_4N^+\right]_2\left[PdCl_2Br_2^=\right]$ which eventually supercools to a glassy material as has already been mentioned above.

A comparison of the bands in the ultraviolet region having maxima at ~ 254 and 346 nm with those of NiX_4^{2-} support the above conclusion regarding their being as due to the charge transfer processes from the nonbonding orbital of the ligand to that of the antibonding of the central metal ion. This implies a predominant covalent character in the metal-ligand bond[25].

The CT transition is attributed to an electron jump from a filled γ_4 subshell to the partially filled γ_5 subshell. The γ_4 subshell has π-type two centre symmetry

and is nonbonding in metal ligand directions in LCAO-MO model that ignores metal orbitals above 4p.

In addition to the L-F and the CT spectra of PdI_4^{2-}, still more intense band at $\sim$ 209 nm has been recorded for the solvent's Br^- ion as the ratio of $[(R_4N^+)_2PdCl_2Br_2^{2-}]$ to $[Br^-]$ increases in the $PdCl_2$-rich mixtures of $R_4N^+Br^-$ and is unaffected by the viscous medium containing the species of the type $[(R_4N^+)_2PdCl_2Br_2^{2-}]_x$. The CTTS of Br^- may be assigned either to Br^- $np^5(n+1)S \longleftarrow Brnp^6$ or (Xnp^5 + a quasi-continuum of delocalised states of one electron) $\longleftarrow Xnp^6, p^5\gamma_1 \longleftarrow p^6\gamma_4$ transitions.

Density, viscosity and equivalent conductance of TBABr + $PdCl_2$ molten mixture (24.98 mol%) have been measured as a function of temperature (Table I). The densities were found to increase linearly with temperature and were least-squares fitted to the linear equation of the type, $\rho = a - bT$ where ρ is the density of the mixture, a and b are parameters and T is the temperature in degree Kelvin. The computed values of a and b are 1.3260 and 0.6662×10^{-3}, respectively with the standard deviation, $\sigma = 0.007$. The molar volumes V_m were calculated from the density data and were found to vary linearly with temperature (Table I).

The logarithms of fluidity (i.e., reciprocal of viscosity) and equivalent conductance have been plotted against the reciprocal of temperature in Figure 1. It is

TABLE I. Density, fluidity, equivalent conductance, and molar volume as a function of temperature for TEABr + $PdCl_2$ molten salt system

T K	ρ, kg m^{-3}	ϕ, Poise^{-1}	$10^3\Lambda$, S m^2 equiv^{-1}	V_m, m^3
353.0	1.0908	0.5329	0.0838	2.6239
358.0	1.0875	0.6908	0.1034	2.6318
363.0	1.0841	0.8805	0.1259	2.6401
368.0	1.0808	1.1107	0.1626	2.6482
373.0	1.0775	1.4331	0.1956	2.6563
378.0	1.0741	1.7590	0.2288	2.6647
383.0	1.0708	2.1478	0.2689	2.6729
388.0	1.0675	2.5707	0.3092	2.6812
393.0	1.0641	2.9744	0.3565	2.6898
398.0	1.0608	3.6711	0.4040	2.6981
403.0	1.0575	4.2845	0.4783	2.7065
408.0	1.0541	4.7619	0.5331	2.7152
413.0	1.0508	5.7937	0.5884	2.7238

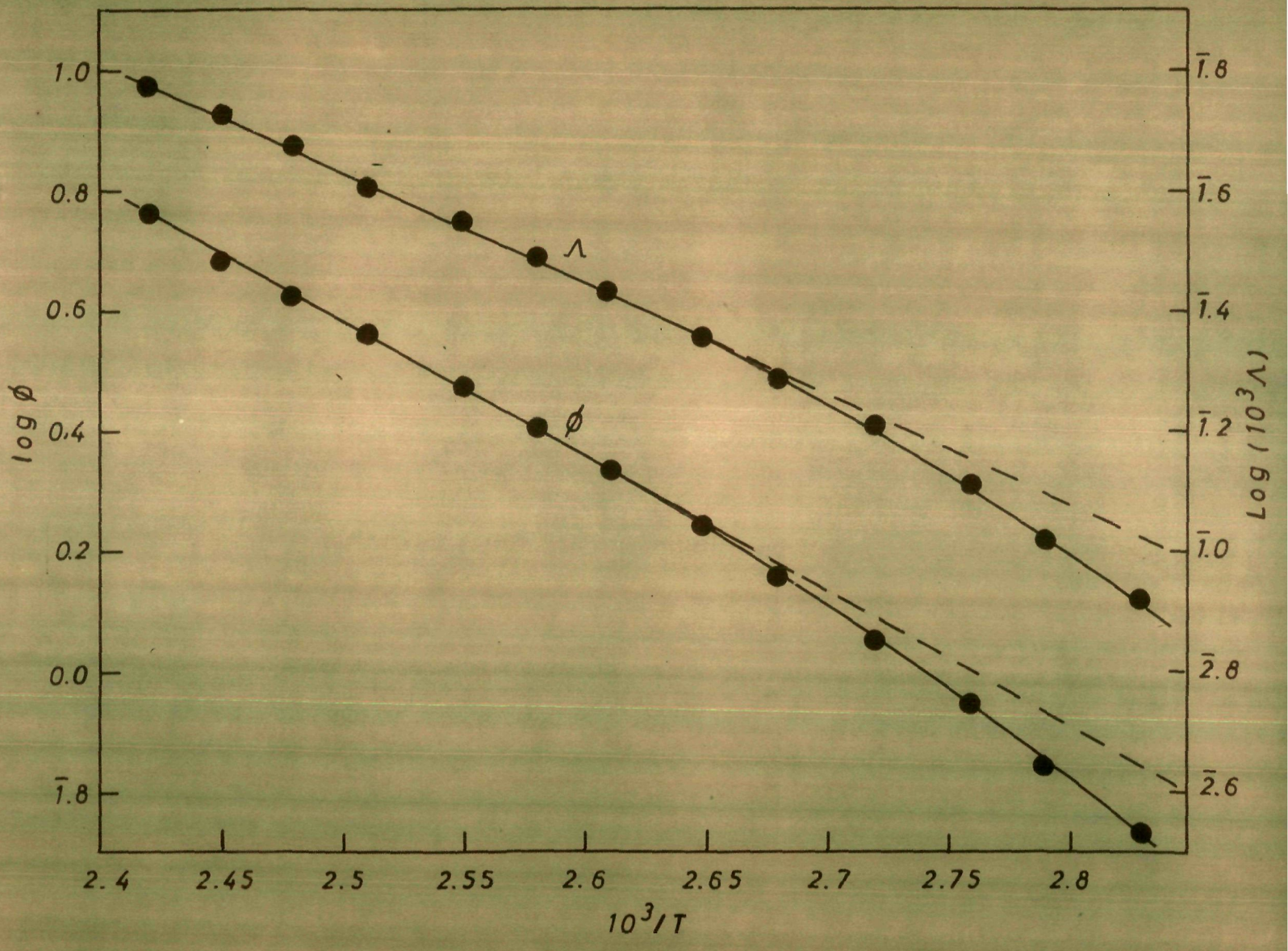

FIG. 1 ARRHENIUS PLOTS OF FLUIDITY AND EQUIVALENT CONDUCTANCE FOR TBABr + $PdCl_2$ MOLTEN SALT SYSTEM

evident that the temperature dependence of fluidity as well as equivalent conductance shows non-Arrhenius behaviour particularly in the region below the melting point of the parent solvent. Similar behaviour has also been observed in many other anhydrous melts[8,25,26,42] and explained in the light of association of species like $[Bu_4N^+]_2[MX_4^{=}]$ where M is a transition metal ion and X is the halide. This type of complex formation has already been identified by spectral studies. The non-Arrhenius behaviour was explained first by the three parameter Doolittle's equation. The fluidity and equivalent conductance data were least-squares fitted to the above equation and the values of the best-fit parameters, $A_{1\phi,\Lambda}$, $B_{1\phi,\Lambda}$ and $V_{o\phi,\Lambda}$ are listed in Table II. The choice of best-fit

TABLE II. Parameters of Doolittle's Equation[a]

$A_{1\phi,\Lambda}$	$B_{1\phi,\Lambda}$	$V_{o\phi,\Lambda}$	Std dev in $\ln(\phi,\Lambda)$
300.0	103.54	246.33	0.041
(11.88)	(75.0)	(247.45)	(0.025)

a Parameters obtained from the equivalent conductance data are given within parentheses.

has been made by the method adopted by Moynihan et al.[36] Accordingly the best-fit parameters were selected on the

basis of minimised standard deviation with the values of k_ϕ and k_Λ as $\sim$700 and $\sim$600 K, respectively, which have been presumed as universal constants[23,37,38]. The significance of these constants is given elsewhere[10,39]. The plots of ln ϕ and ln Λ versus reciprocal of $V-V_0$ (Figure 2) show the applicability of Doolittle's equation.

In view of the non-Arrhenius behaviour mentioned above the fluidity and the conductance data were least-squares fitted to the non-linear Vogel-Tammann-Fulcher (VTF) and the configurational entropy model (CEM) equations based on the free volume and the cooperative rearrangement models, respectively. The values of the best-fit parameters computed for both the equations are given in Table III. An examination of this table reveals that the best-fits obtained considering all the data points of a plot (viz., 353-413 K) lead to higher standard deviation. On the other hand, considering the two regions, i.e., the Arrhenius and the non-Arrhenius regions of a single plot separately, it may, however, be noted that the best-fit values of the non-Arrhenius region only (viz., 353-383 K) give reasonably low standard deviation. For example in the case of the VTF equation (353-413 K) the best-fit values obtained for the fluidity data gave the values of parameters as A_ϕ = 7942.2, k_ϕ = 700 and $T_{o(\phi)}$ = 249 with the standard deviation 0.05 while the fit to the same

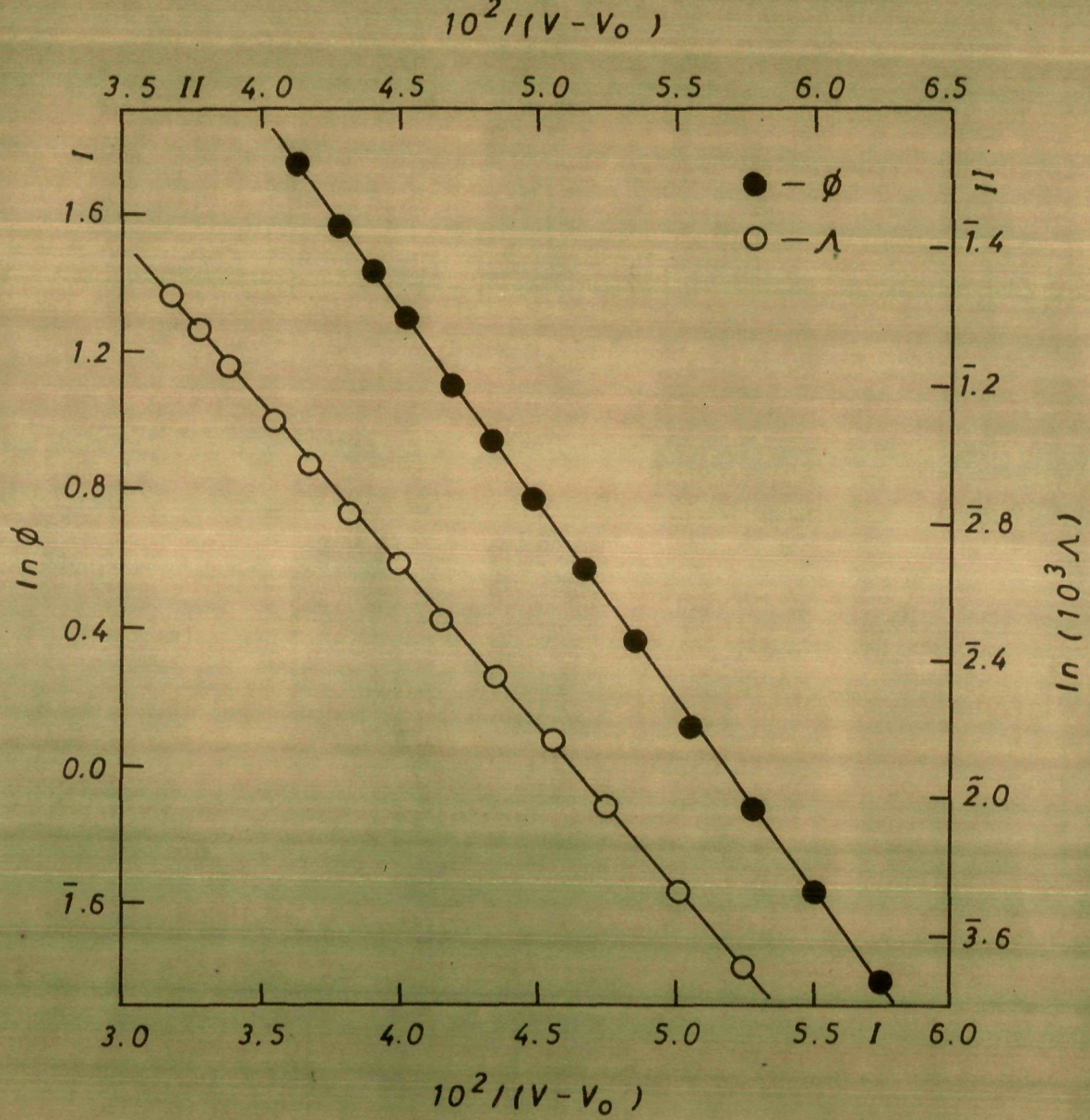

FIG. 2 PLOTS OF ln ϕ AND ln Λ VS. $1/(V-V_o)$ FOR TBABr + $PdCl_2$ MOLTEN SALT SYSTEM

TABLE III. Parameters of the VTF and the CEM Equations for different temperature regions

$A_\phi/\sqrt{A_\phi}$	k_ϕ	$T_{o,\phi}$	Std dev in ln ϕ	$A_\Lambda/\sqrt{A_\Lambda}$	k_Λ	$T_{o,\Lambda}$	Std dev in ln Λ
			VTF (353 - 413)[1]				
7942.20	700.0	249.0	0.05	437.38	600.0	247.0	0.05
			VTF (353 - 383)[2]				
6516.20	685.0	248.0	0.02	456.28	622.0	244.0	0.01
			CEM (353 - 413)[1]				
155.66	690.0	251.0	0.03	9.69	590.0	249.0	0.02
			CEM (353 - 383)[2]				
137.78	691.0	249.0	0.02	8.92	579.0	249.0	0.01

1. Parameters obtained considering all the data points of a given plot.
2. Parameters obtained considering only the non-linear region of the plot.

equation with non-Arrhenius fluidity data improves the standard deviation to 0.02 and improves the values of the parameters as well. Similar analyses were made with the conductance data as well. The above analyses were repeated using the CEK equation also. This type of data fit gives one an idea about the scanning of parameters from approximate values to accurate values. In such an analysis the decrease in the standard deviation is about 3.5% in the case of former equation while it is 1.6% in case of the latter. However, such fits do not involve significant change in the T_o values although a decrease of 1^o in the case of $T_{o(\phi)}$ and 3^o in that of $T_{o(\Lambda)}$ may be observed. Consequently, a gradual change in A and k values has also been observed. On the other hand, the data of Arrhenius region (398–413 K) for both fluidity and conductance were least-squares fitted to the two parameter equation of the type $\ln Y = A^*_{1Y} \pm E^*_Y/RT$ and the values of A^*_Y and E^*_Y for fluidity and conductance with the standard deviation are given in Table IV. The plots of $\ln \phi\, T^{1/2}$

TABLE IV. Parameters of Arrhenius Equation[a]

$A^*_{1\phi,\Lambda}$	$E^*_{\phi,\Lambda}$	Std dev in $\ln(\phi, \Lambda)$
6.1863	10.2593	0.009
(4.2083)	(8.3743)	(0.006)

a Parameters obtained from equivalent conductance data are given within parentheses.

and $\ln \Lambda T^{1/2}$ versus $1/(T-T_o)$ (Figure 3) and those of $\ln \phi$ and $\ln \Lambda$ versus $1/T$ $\ln T/T_o$ (Figure 4) signify the applicability of the VTF and the CEM equations, respectively.

The energies of activation were evaluated from the derivative, $\frac{\partial \ln Y}{\partial (1/T)}$, of the VTF equation and corrected by adding the term $\frac{1}{2}$ RT where R is the gas constant. The plots of E_{cor} for fluidity and conductance against $\left[T/(T-T_o)\right]^2$ (Figure 5) pass through the origin signifying the choice of accurate value of T_o, the glass transition temperature. A shift of $\pm 5^o$ from the T_o values will show the deviation into E_{cor} vs $\left[T/(T-T_o)\right]^2$ plots. Besides this the plots make the VTF equation more promising to evaluate the T_o values.

Recalling the earlier discussion on the temperature dependence of transport properties, which shows the non-Arrhenius nature in the region below the melting point of the parent solvent and that of the Arrhenius in the region above the melting point. This is further reinforced by examining the plots of η and Λ as a function of the reciprocal of free volume (Figure 6). It may be seen that with decrease in temperature the free volume decreases and the plots of η or Λ become increasingly more non-linear. As the free volume approaches zero the tendency of the η or Λ plots to acquire linearity becomes prominent. At this stage one may expect a zero slope of this plot which may

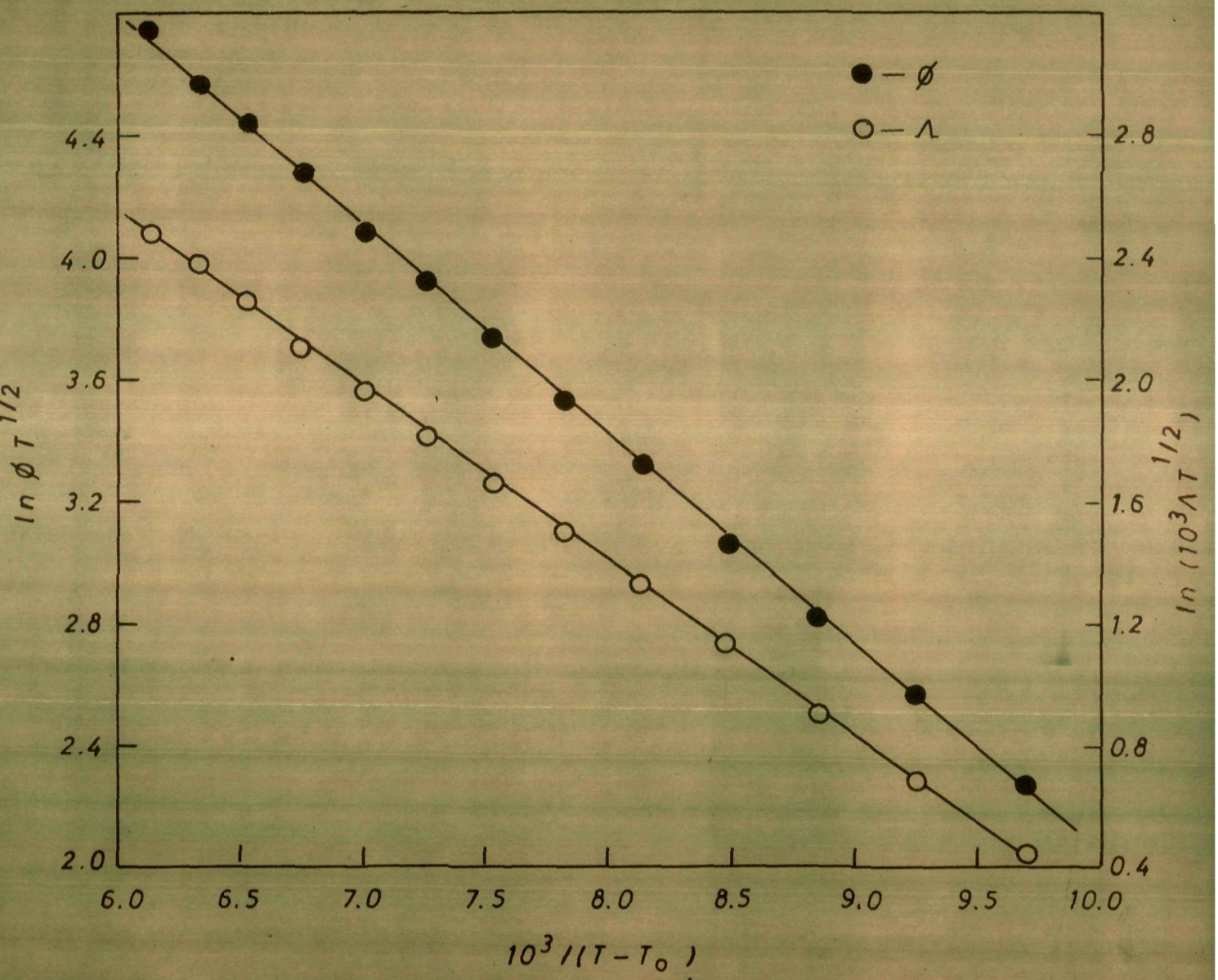

FIG. 3 PLOTS OF $\ln \emptyset T^{1/2}$ AND $\ln \Lambda T^{1/2}$ VS. $1/(T - T_o)$ FOR TBABr + $PdCl_2$ MOLTEN SALT SYSTEM

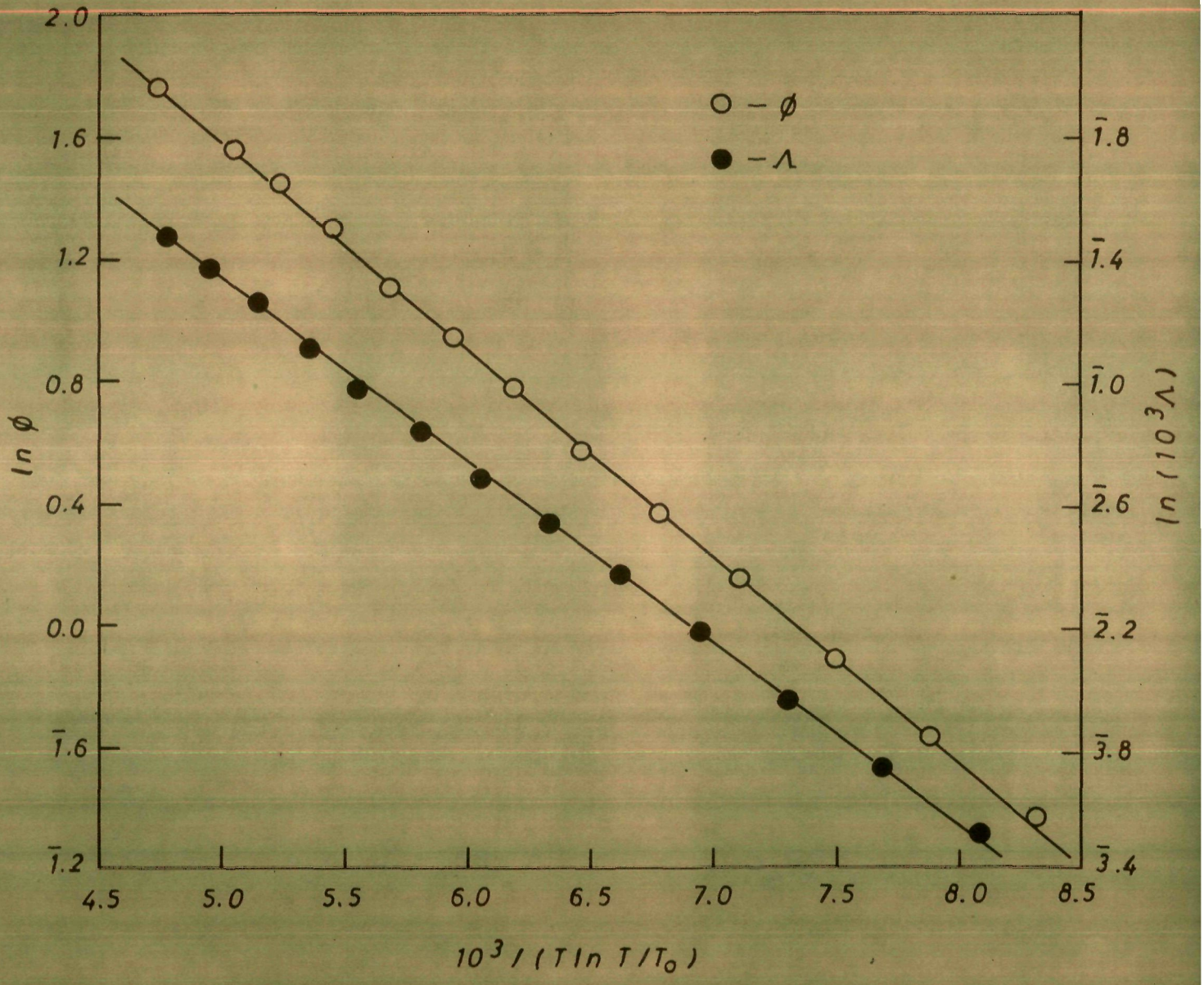

FIG. 4 PLOTS OF ln ϕ AND ln Λ VS. 1/ T ln T/T_0 FOR TBABr + $PdCl_2$ MOLTEN SALT SYSTEM

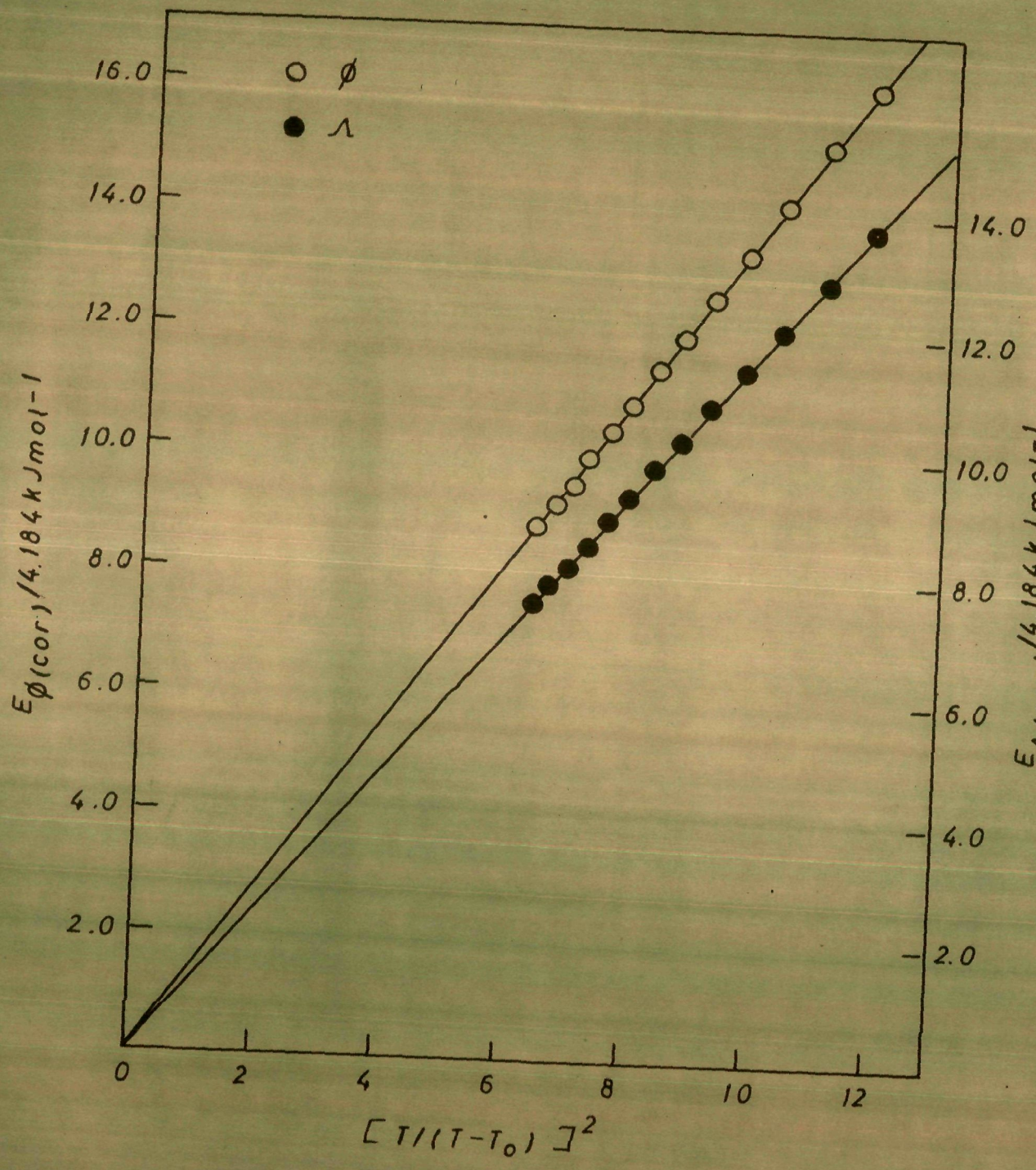

FIG. 5 PLOTS OF E_{cor} VS. $[T/(T-T_o)]^2$ FOR TBABr + $PdCl_2$ MOLTEN SALT SYSTEM

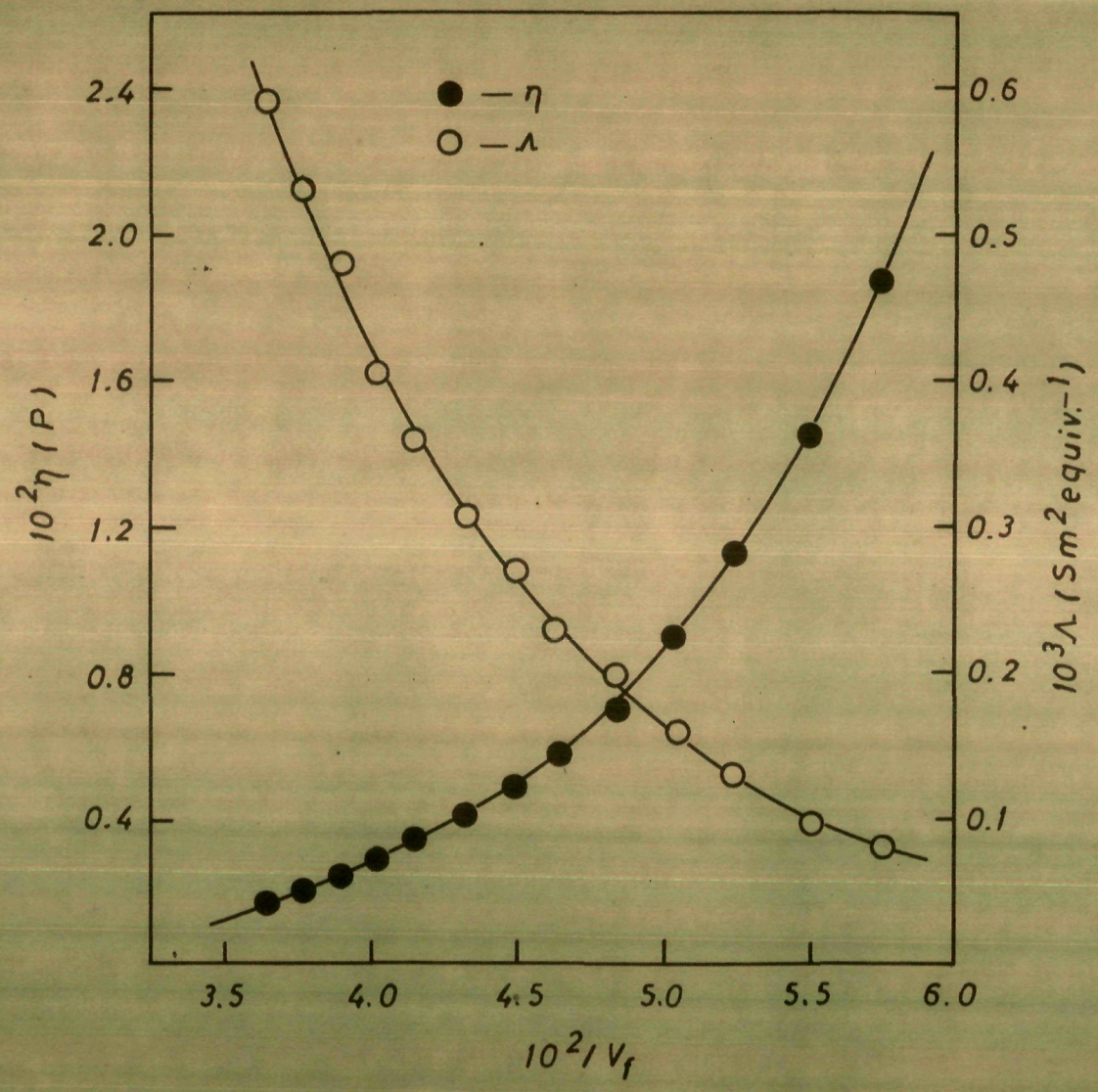

FIG. 6 PLOTS OF VISCOSITY AND EQUIVALENT CONDUCTANCE AS A FUNCTION OF RECIPROCAL OF FREE VOLUME FOR TBABr + $PdCl_2$ MOLTON SALT SYSTEM

be considered as the emergence of a new phase of zero mobility possessing a very high viscosity of the order of 10^{13} poise. Therefore, one may imagine the existence of three regions in a single temperature dependent property viz., Arrhenius, above the melting point of the solvent, non-Arrhenius below the melting point of the solvent and again Arrhenius near the glass transition temperature, T_o. This idea is further emphasized by examining the parameters and the standard deviations computed in the case of non-linear equations. In view of these facts the applicability of the environmental relaxation model (ERM) was examined. Accordingly, the viscosity and the conductance data were least-squares fitted to the five parameter ERM equation and the best-fit parameters are listed in Table V.

TABLE V. Parameters of Equations (11 and 12)[a]

$(C_\infty A)_{\eta,\Lambda}$	$E_{\eta,\Lambda}$	$(1/2)C_o$	T_o	ϵ_o	Std dev in $\ln(\eta,\Lambda)$
0.3840×10^{-2}	2.6295	2.505	250.0	3.185	0.020
(0.0183)	(3.4938)	(1.8688)	(250.0)	(4.000)	(0.020)

a Parameters obtained from equivalent conductance data are given within parentheses.

Comparison of energies of activation computed from different models

The energies of activation for viscosity and con-

ductance computed from the derivatives of the three parameter VTF and the CHM equations, and the five parameter ERM equation. In addition to the above derivatives, the energies of activation are also obtained from the experimental plots of $\ln \eta$ and $\ln \Lambda$ (tangent values) versus 1/T (Figure 7). These values are listed in Table VI.

It is clear from Table VI that the energies of activation in the Arrhenius region, i.e., at higher temperature are found to be independent of the model used. In the lower temperature region, however, the E_γ values differ significantly as the non-Arrhenius nature dominates. This may be attributed to the cohesive interaction of the component species of the system under study. On decreasing the temperature (Figure 7) the coulombic forces are expected to increase while the free volume decreases. These factors appear to be responsible for the non-linear behaviour of the system under discussion. However, the values of energies of activation obtained from the derivative of the ERM equation are in reasonably good agreement with those obtained from the experimental values (i.e., tangent values). It is because of the fact that the five parameter equation considers both the Arrhenius and the non-Arrhenius regions On the basis of this fact one can suggest that the ERM equation is more effectively applicable to explain the non-linear temperature dependence of the transport properties in such systems.

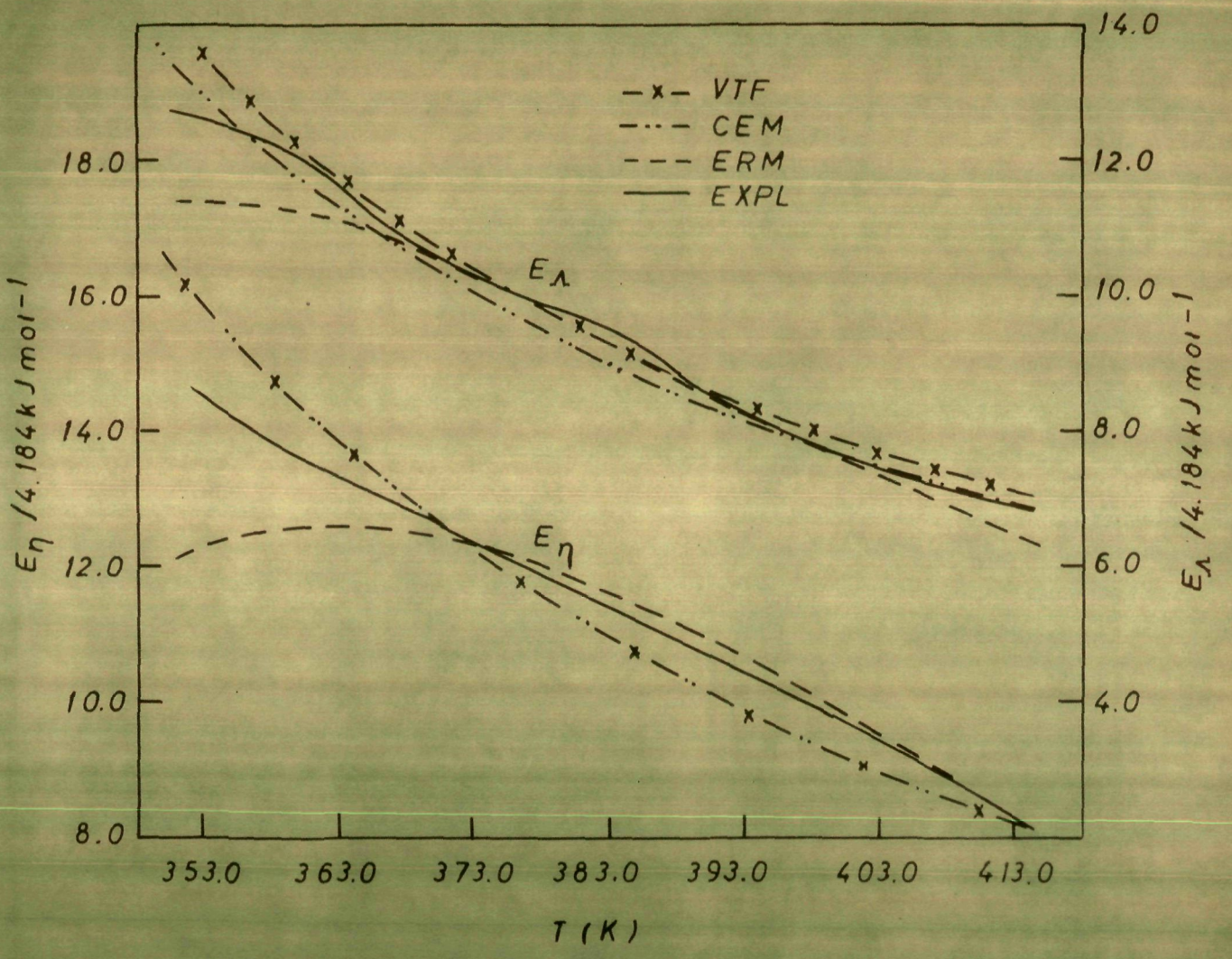

FIG. 7 PLOTS OF ENERGIES OF ACTIVATION AS A FUNCTION OF TEMPERATURE FOR TBABr + $PdCl_2$ MOLTEN SALT SYSTEM

TABLE VI. Energies of Activation (E_Y/4.184 kJ mol^{-1}) computed through different models

	VTF		CEM		KRF		Experimental (Tangent value)	
T K	E_η	E_Λ	E_η	E_Λ	E_η	E_Λ	E_η	E_Λ
353.0	15.75 (16.10)	13.42 (13.77)	15.83	12.92	12.27	11.42	14.50	12.61
358.0	14.71 (15.07)	12.53 (12.89)	14.75	12.08	12.48	11.30	13.87	12.33
363.0	13.71 (14.14)	11.73 (12.09)	13.80	11.32	12.56	11.06	13.34	11.56
368.0	12.97 (13.33)	11.04 (11.41)	12.96	10.65	12.50	10.71	12.88	10.78
373.0	12.23 (12.60)	10.41 (10.78)	12.21	10.05	12.31	10.29	12.44	10.40
378.0	11.58 (11.96)	9.85 (10.22)	11.54	9.51	12.01	9.81	11.88	9.91
383.0	10.99 (11.37)	9.34 (9.72)	10.93	9.02	11.61	9.30	11.56	9.57

(continued)

TABLE VI. (continued)

	VTF		CEM		KRM		Experimental (Tangent value)	
T K	E_η	E_Λ	E_η	E_Λ	E_η	E_Λ	E_η	E_Λ
388.0	10.45 (10.84)	8.88 (9.27)	10.38	8.58	11.13	8.78	10.79	8.83
393.0	9.97 (10.36)	8.46 (8.85)	9.89	8.18	10.60	8.27	10.40	8.32
398.0	9.52 (9.92)	8.08 (8.48)	9.43	7.81	10.01	7.77	9.91	7.97
403.0	9.11 (9.51)	7.73 (8.13)	9.02	7.47	9.46	7.31	9.63	7.70
408.0	8.74 (9.15)	7.41 (7.82)	8.64	7.16	8.88	6.88	---	---
413.0	8.39 (8.80)	7.12 (7.53)	8.29	6.88	8.32	6.49	...	...

Corrected energies of activation are given within parentheses.

APPENDIX

A. Calculation of Activation Energy

(i) From Vogel-Tammann-Fulcher Equation

The Arrhenius equation can be written as

$$Y\ (= \phi \text{ or } \Lambda) = A_Y \exp\left[-E_Y/RT\right]$$

or

$$\ln Y = \ln A_Y - E_Y/RT \qquad (1)$$

On differentiation with respect to inverse temperature T^{-1}

$$\frac{d \ln Y}{d(1/T)} = -E_Y/R \qquad (2)$$

The VTF equation for fluidity, ϕ and equivalent conductance, Λ is given as

$$Y = A_Y T^{-1/2} \exp\left[-k_Y/(T - T_o)\right]$$

or

$$\ln Y = \ln A_Y - 1/2 \ln T - k_Y/(T - T_o) \qquad (3)$$

$$\frac{d \ln Y}{d(1/T)} = \left[\frac{1}{2T} - k_Y/(T - T_o)^2\right] T^2 \qquad (4)$$

Comparing equation (2) and (4)

$$E_Y = R\left[k_Y/(T - T_o)^2 - \frac{1}{2T}\right] T^2 \qquad (5)$$

The corrected activation energy may be written as

$$E_{cor} = E_Y + \tfrac{1}{2}RT = Rk_Y\left[T/(T - T_o)\right]^2 \qquad (6)$$

(ii) <u>From Configurational Entropy Model</u>

The equation based on this model can be written as

$$\ln Y\ (= \phi \text{ or } \Lambda) = \ln \bar{A}_Y - k_Y/[T \ln (T/T_o)] \qquad (7)$$

Therefore,

$$\frac{d \ln Y}{d(1/T)} = -k_Y \left[\left\{1 + \ln (T/T_o)\right\}/\left\{\ln (T/T_o)\right\}^2\right] \qquad (8)$$

Comparing equation (2) and (6), we obtain

$$E_Y = Rk_Y\left[\left\{1 + \ln (T/T_o)\right\}/\left\{\ln (T/T_o)\right\}^2\right] \qquad (9)$$

At T/T_o = constant, c, equation (7) may become on differentiation with T^{-1}

$$\frac{d \ln Y}{d(1/T)} = -k_Y/\ln c \qquad (10)$$

Therefore, E_Y at constant $T/T_o = c$ may be written as

$$E_Y = Rk_Y/\ln T/T_o \qquad (11)$$

(iii) Calculation of apparent activation energy from KRM equation

The equation for viscosity based on KRM may be written as

$$\ln \eta = \ln (C_{\infty} A)_{\eta} + \left\{ \bar{E}_{\eta} + (1/2) \epsilon_{o\eta} \left[T_o^4 / (T_o^4 + \epsilon_{o\eta}^2 (T - T_o)^4) \right]^{3/2} \right\} / RT \quad (12)$$

$$\frac{\partial \ln \eta}{\partial x} = \frac{\bar{E}_{\eta}}{R} + (1/2) \frac{\epsilon_{o\eta}}{R} \left[u + x \frac{du}{dx} \right] \quad (13)$$

where $x = 1/T$, and

$$u = \left[\frac{T_o^4}{T_o^4 + \epsilon_{o\eta}^2 (T - T_o)^4} \right]^{3/2} = \left[\frac{T_o^4 x^4}{T_o^4 x^4 + \epsilon_{o\eta}^2 (1 - T_o x)^4} \right]^{3/2} \quad (14)$$

Therefore,

$$\frac{dm}{dx} = \frac{3}{2}\left[\frac{T_o^4x^4}{T_o^4x^4 + \epsilon_{o\eta}^2(1 - T_ox)^4}\right]^{1/2}$$

$$\left[\frac{\left\{T_o^4x^4 + \epsilon_{o\eta}^2(1 - T_ox)^4\right\} 4T_o^4x^3 - T_o^4x^4\left\{4T_o^4x^3 + 4\epsilon_{o\eta}^2(1 - T_ox)^3(-T)\right\}}{\left\{T_o^4x^4 + \epsilon_{o\eta}^2(1 - T_ox)^4\right\}^2}\right]$$

$$= \frac{3}{2}\left[\frac{T_o^4x^4}{T_o^4x^4 + \epsilon_{o\eta}^2(1 - T_ox)^4}\right]^{1/2}$$

$$\left[\frac{4\,T_o^4x^3}{T_o^4x^4 + \epsilon_{o\eta}^2(1 - T_ox)^4} - \frac{4T_o^4x^4\left\{T_o^4x^3 - T_o\epsilon_{o\eta}^2(1 - T_ox)^3\right\}}{\left\{T_o^4x^4 + \epsilon_{o\eta}^2(1 - T_ox)^4\right\}^2}\right]$$

(continued)

$$= \frac{3}{2}\left[\frac{T_o^4}{T_o^4 + \epsilon_{o\eta}^2 (T - T_o)^4}\right]^{1/2}$$

$$\left[\frac{4T_o^4 T^4}{T^3\left\{T_o^4 + \epsilon_{o\eta}^2 (T - T_o)^4\right\}} - \frac{4T_o^4 T^3\left\{T_o^4 - T_o \epsilon_{o\eta}^2 (T - T_o)^3\right\}}{T^4 T^3\left\{T_o^4 + \epsilon_{o\eta}^2 (T - T_o)^4\right\}^2}\right]$$

$$= \frac{3}{2}\left[\frac{T_o^4}{T_o^4 + \epsilon_{o\eta}^2 (T - T_o)^4}\right]^{3/2}\left[4T - \frac{4T\left\{T_o^4 - T_o \epsilon_{o\eta}^2 (T - T_o)^3\right\}}{T_o^4 + \epsilon_{o\eta}^2 (T - T_o)^4}\right]$$

$$= \frac{4 \times 3T}{2}\left[\frac{T_o^4}{T_o^4 + \epsilon_{o\eta}^2 (T - T_o)^4}\right]^{3/2}\left[\frac{T_o^4 + \epsilon_{o\eta}^2 (T - T_o)^4 - T_o^4 + \epsilon_{o\eta}^2 T_o (T - T_o)^3}{T_o^4 + \epsilon_{o\eta}^2 (T - T_o)^4}\right]$$

$$= 6T\left[\frac{T_o^4}{T_o^4 + \epsilon_{o\eta}^2 (T - T_o)^4}\right]^{3/2}\left[\frac{\epsilon_{o\eta}^2 (T - T_o)^3 (T - T_o + T_o)}{T_o^4 + \epsilon_{o\eta}^2 (T - T_o)^4}\right]$$

$$x\frac{du}{dx} = 6\left[\frac{T_o^4}{T_o^4 + \epsilon_{o\eta}^2 (T - T_o)^4}\right]^{3/2}\left[\frac{T \epsilon_{o\eta}^2 (T - T_o)^3}{T_o^4 + \epsilon_{o\eta}^2 (T - T_o)^4}\right] \qquad (15)$$

On substituting equations (14) and (15) in (13) we obtain

$$\frac{\partial \ln \eta}{\partial x} = \frac{\partial \ln \eta}{\partial (1/T)} = \frac{\bar{E}_\eta}{R} + \frac{c_{o\eta}}{2R} \left\{ \frac{T_o^4}{T_o^4 + \epsilon_{o\eta}^2 (T - T_o)^4} \right\}^{3/2} \left\{ 1 + \frac{6T \epsilon_{o\eta}^2 (T - T_o)^3}{T_o^4 + \epsilon_{o\eta}^2 (T - T_o)^4} \right\} \quad (16)$$

Comparing equation (2) with equation (16), we obtain

$$E_\eta = \bar{E}_\eta + \frac{c_{o\eta}}{2} \left[\frac{1}{1 + \epsilon_{o\eta}^2 (T/T_o - 1)^4} \right]^{3/2} \left[1 + \frac{6 \epsilon_{o\eta}^2 (T/T_o)(T/T_o - 1)^3}{1 + \epsilon_{o\eta}^2 (T/T_o - 1)^4} \right] \quad (17)$$

Similar expression can also be obtained for E_λ

REFERENCES

1. J.H. Hildebrand and G. Archer, Trans. Amer. Phil. Soc., 47, 1881 (1961).
2. D.W. Ridgway, "Interview with J.H. Hildebrand", J. Chem. Edu., 52, 46 (1975).
3. E.N. Andrade, Nature, 125, 309 (1930).
4. H. Eyring, J. Chem. Phys., 4, 283, (1936).
5. A.J. Batschinski, Z. Physik. Chem., 84, 643 (1913).
6. J.H. Hildebrand, Science, 174, 490 (1971).
7. A.K. Doolittle, J. Appl. Phys., 22, 1471 (1951).
8. M. Islam, M.R. Islam, B. Waris and Ismail M, J. Phys. Chem., 80, 291 (1976).
9. W. Naumann, Chem. Rev., 43, 219 (1948).
10. M.H. Cohen and D. Turnbull, J. Chem. Phys., 31, 1164 (1959).
11. G. Adams and J.H. Gibbs, J. Chem. Phys., 43, 139 (1965).
12. H. Vogel, Physik. Z., 22, 645 (1921).
13. A. Weiler, S. Blaser, and P.B. Macedo, J. Phys. Chem., 73, 4147 (1969).
14. A. Weiler, S. Blaser and P.B. Macedo, J. Chem. Phys., 53, 1258 (1970).
15. J.H. Simmons and P.B. Macedo, J. Chem. Phys., 54, 1325 (1971).
16. F.S. Howell, R.A. Bose, P.B. Macedo, and C.T. Moynihan, J. Phys. Chem., 78, 639 (1974).
17. A. Einstein, Ann. Physik, 19, 289 (1906); 34, 591 (1911).

18. G. Jones and M. Dole, J. Am. Chem. Soc., 51, 2950 (1929).

19. V.J. Vand, J. Phys. Colloid Chem., 52, 277 (1948); 52, 314 (1948).

20. D.G. Thomas, J. Colloid Sci., 20, 267 (1965).

21. S.P. Moulik, J. Phys. Chem., 72, 4682 (1968).

22. V.A. Bloomfield and K.K. Dewan, J. Phys. Chem., 75, 3113 (1971).

23. C.A. Angell, J. Phys. Chem., 70, 3988 (1966).

24. M. Islam and Ismail A, J. Phys. Chem., 80, 1929 (1976).

25. M. Islam, M.N. Islam, S. Ahmad and B. Waris, J. Am. Chem. Soc., 97, 3026 (1975).

26. M. Islam, M.A. Islam, S. Ahmad, and B. Waris, Appl. Spectrosc., 29, 68 (1975).

27. T. Moeller, "Inorganic Synthesis", Vol. V, McGraw-Hill, New York, N.Y. 1957, p. 153.

28. C. Tanford, "Physical Chemistry of Macromolecules", John Wiley and Sons, Inc., New York, N.Y., 1961, p. 329.

29. D.E. Goldsack and R. Franchetto, Can. J. Chem., 55, 1062 (1977).

30. J. O'M Bockris, J.A. Kitchener, S. Ignatowicz, and J.W. Tomlinson, Trans. Faraday Soc., 48, 75 (1952).

31. H.C. Gaur and S.K. Jain, Ind. J. Chem., 9, 860 (1971).

32. R.H. Ewell and H. Eyring, J. Chem. Phys., 5, 726 (1937).

33. L.D. Eicher and B.J. Zowlinski, J. Phys. Chem., 76, 3295 (1972).

34. C.A. Angell, J. Phys. Chem., 68, 1917 (1964).

35. N. Islam, A. Maroof, and Ismail K, Can. J. Chem., 57, No. 2 (1979).

36. C.T. Moynihan, C.A. Smalley, C.A. Angell, and E.J. Sare, J. Phys. Chem., 73, 2276 (1969).

37. C.A. Angell, J. Phys. Chem., 68, 1917 (1964).

38. C.A. Angell, J. Electrochem. Soc., 112, 1224 (1965).

39. N. Islam and Ismail K, J. Phys. Chem., 79, 2160 (1975).

40. N. Islam, K.P. Singh, and S. Kumar, J.C.S. Faraday Trans. I (in press).

41. N. Islam, S. Kumar, and K.P. Singh, Can. J. Chem., 56, 1231 (1978).

42. N. Islam and M.A. Islam, Ind. J. Chem., 12, 705 (1974).

43. S. Kumar, Doctoral Dissertation , A.M.U., Aligarh (India), 1977.

44. N. Islam and A. Ali, Can. J. Chem., 1979 (communicated).

45. G.P. Smith, C.H. Liu, and T.H. Griffiths, J. Am. Chem. Soc., 86, 4796 (1964).

46. G.P. Smith and S. von Winbush, J. Am. Chem. Soc., 88, 2127 (1966).

47. N. Islam, Aust. J. Chem., 26, 2371 (1973).

48. B.R. Sundheim and N. Islam, Appl. Spectrosc., 27, 285 (1973).

49. B.A. Sundheim and N. Islam, Appl. Spectrosc., 27, 394 (1973).

50. N. Islam, Applied Spectrosc., 28, 277 (1974).

51. N. Islam, B. Jamil and S.A.A. Naidi, Ind. J. Chem., 11, 266 (1973).

52. N. Islam and M.A. Islam, Z. Phys. Chem., 253, 340 (1973).